FINITE ELEMENT MODELLING OF PAPAYA FRUIT UNDER COMPRESSIVE LOADS

By

AINA ADEMOLA MICHAEL

Thesis Submitted to the School of Graduate Studies, Universiti Putra Malaysia, in Fulfilment of the Requirements for the Degree of Master of Science

January 2024

FK 2024 2

Abstract of thesis presented to the Senate of Universiti Putra Malaysia in fulfilment of the requirement for the degree of Master of Science

FINITE ELEMENT MODELLING OF PAPAYA FRUIT UNDER COMPRESSIVE LOADS

By

AINA ADEMOLA MICHAEL

January 2024

Chairman : Hazreen Haizi binti Harith, PhD
Faculty : Engineering

This thesis contributes to the improvement of postharvest practices and the reduction of damage during the handling of papaya fruits. Grading and sorting, critical postharvest tasks, can be performed more effectively using predictive models utilizing computer vision technology. Additionally, papaya fruits are highly susceptible to mechanical damage due to the loads imposed on them during harvesting, transportation, and packaging. Understanding the fruit's response to static and dynamic loads is vital to prevent postharvest losses due to mechanical damage. This study focuses on modelling the mass of papaya and its mechanical behaviour under compression loading to improve postharvest practices and minimise damage during handling.

Seven regression models were developed for mass modelling based on the fruit's geometric properties. The accuracy of the models for predicting papaya fruits' mass was evaluated using the coefficient of determination (R^2) and Root Mean Square Error (RMSE) metrics based on the testing dataset. Results indicate that the power model

(R^2=0.94, RMSE=87.72 g) and quadratic model (R^2=0.94, RMSE=88.21 g) had better performance compared to the linear model (R^2=0.91, RMSE=108.59 g) and S-curve model (R^2=0.82, RMSE=150.63 g) when mean diameter was employed as the sole predictor for mass estimation. While using the ordinary least square regression (OLS), linear Lasso (Least Absolute Shrinkage and Selection Operator) and SVR (Support Vector Regression) algorithm, the OLS outperforms other models with R^2 and RMSE values of 0.95 and 81.72 g, respectively, using multiple geometric variables as predictors. Conventionally, human operators sort and grade papaya fruits manually. However, this method is subjective and can be quite laborious. In contrast, the mass models developed in this study offer a more objective solution as they can be integrated with computer vision technologies to automate sorting and grading papayas based on their mass. This will enhance grading accuracy and likely reduce workload. Next, finite element modelling (FEM) was used to characterize the mechanical behaviour of papaya under compression. The steps include geometry modelling, material properties modelling, mesh creation, boundary conditions, loading, and analysis solutions. Three material models were used to simulate its mechanical response under compressive loads. The stress response by these models was compared with experimental data. The model with the smallest deviation from the experimental results was considered as the best model to represent papaya's mechanical behavior. Therefore, it was selected to was selected for simulating the mechanical response of papaya fruit under compression. Next, the stress responses under transverse and longitudinal compressive loads were compared. Lastly, a hypothesis was tested to evaluate the difference in the stress response of the geometry model created using laser scanning and sketching methods.

The comparison of material models' mechanical behaviour with its equivalent experimental data indicates that the viscoelastic model best captures the deformation behaviour of papaya fruit under compressive load. Therefore, the model was used to investigate the effect of loading direction on the fruit. The results show that loading in the transverse direction increases the susceptibility of the fruit to mechanical damage. Also, there was no significant difference in the stress response between the 3D models produced using scanning and sketching methods.

Overall, the comprehensive understanding gained from this research can enhance the handling, transportation, and design of systems involving papaya fruit. The findings contribute to the field of postharvest engineering and can be valuable for researchers, agriculturalists, and industries involved in fruit processing and distribution. Further studies could build upon this research by exploring additional factors and optimising material models to improve the accuracy of fruit mechanical simulations.

Keywords: Post-harvest loss, Mechanical Damage, Mechanical behavior, Mass model, Finite Element Modelling

SDG: GOAL 2: Zero Hunger

Abstrak tesis yang dikemukakan kepada Senat of Universiti Putra Malaysia sebagai memenuhi keperluan ijazah Master Sains

FINITE ELEMENT MODELLING OF PAPAYA FRUIT UNDER COMPRESSIVE LOADS

Oleh

AINA ADEMOLA MICHAEL

Januari 2024

Pengerusi : Hazreen Haizi binti Harith, PhD
Fakulti : Kejuruteraan

Tesis ini menyumbang kepada peningkatan amalan lepastuai dan pengurangan kerosakan dalam pengendalian buah betik. Penggredan dan pengisihan merupakan aktiviti lepastuai yang penting, dan boleh dilakukan dengan lebih berkesan melalui model ramalan yang menggunakan teknologi penglihatan komputer. Selain itu, buah betik sangat terdedah kepada kerosakan mekanikal akibat beban yang dikenakan ke atasnya semasa penuaian, pengangkutan, dan pembungkusan. Memahami tindak balas buah terhadap beban statik dan dinamik adalah penting untuk mengelakkan kerugian lepastuai akibat kerosakan mekanikal. Kajian ini memberi tumpuan kepada pemodelan jisim buah dan perilaku mekanikal buah dibawah beban mampatan untuk meningkatkan kualiti amalan lepastuai dan mengurangkan kerosakan semasa pengendalian.

Tujuh model regresi telah dibangunkan untuk pemodelan jisim berdasarkan sifat geometri buah. Ketepatan model untuk meramalkan jisim buah betik dinilai menggunakan pekali penentuan (R^2) dan metrik ralat punca min kuasa dua (RMSE)

berdasarkan data ujian. Keputusan menunjukkan bahawa model kuasa (R^2=0.94, RMSE=87.72 g) dan model kuadratik (R^2=0.94, RMSE=88.21 g) mempunyai prestasi yang lebih baik berbanding model linear (R^2=0.91, RMSE=108.59 g), dan model lengkung-S (R^2=0.82, RMSE=150.63 g) apabila diameter purata digunakan sebagai peramal jisim tunggal . Semasa menggunakan regresi *ordinary least square regression* (OLS), *linear Lasso* (*Least Absolute Shrinkage and Selection Operator*) and *Support Vector Regression* (SVR), OLS mengatasi model lain dengan nilai R^2 dan RMSE masing-masing sebanyak 0.95 dan 81.72 g, apabila menggunakan lebih dari satu pemboleh ubah sebagai peramal. Secara praktis, buah betik disusun dan digred secara manual oleh manusia. Walaubagaimanapun, kaedah ini adalah subjektif dan boleh membebankan. Sebaliknya, model jisim yang dibangunkan dalam kajian ini menawarkan penyelesaian yang lebih objektif dan cekap. Model ini boleh disepadukan dengan teknologi penglihatan komputer untuk mengautomasikan pengisihan dan penggredan betik berdasarkan jisim mereka. Ini bukan sahaja dapat meningkatkan ketepatan, ia juga dapat mengurangkan beban kerja.

Seterusnya, proses pemodelan unsur terhingga (FEM) melibatkan beberapa langkah, seperti pemodelan geometri, pemodelan sifat bahan, penciptaan model jaringan, keadaan sempadan, pemuatan, dan penyelesaian analisis.Tiga model bahan digunakan untuk mensimulasikan tindak balas mekanikal buah betik di bawah beban mampatan. Tindak balas tekanan hasil dari simulasi kesemua model ini dibandingkan dengan data eksperimen. Model dengan sisihan minimum dari hasil eksperimen dipilih sebagai model yang sesuai untuk mensimulasikan tindak balas mekanikal buah betik di bawah beban mampatan. Kemudian, tindak balas buah terhadap beban melintang dan membujur dibandingkan. Akhir sekali, hipotesis telah diuji untuk menilai perbezaan tindak balas tegasan yang dihasilkan oleh model geometri yang dibuat menggunakan kaedah pengimbasan laser dan kaedah lakaran.

Perbandingan antara simulasi model bahan dengan data eksperimen menunjukkan bahawa model *viscoelastic* merupakan model terbaik dalam menunjukkan perubahan bahan dan bentuk buah betik di bawah beban mampatan. Oleh itu, model *viscoelastic* digunakan untuk mengkaji kesan arah beban pada buah. Hasil kajian menunjukkan bahawa beban melintang lebih mudah mendedahkan buah kepada kerosakan. Di samping itu, tiada perbezaan signifikan didapati dalam tindak balas tegasan menggunakan model 3D yang dihasilkan melalui kaedah imbasan dan kaedah lakaran.

Secara keseluruhan, pemahaman komprehensif yang diperoleh daripada penyelidikan ini mampu meningkatkan cara pengendalian, cara pengangkutan, dan reka bentuk sistem yang melibatkan buah betik. Penemuan ini menyumbang kepada bidang kejuruteraan lepastuai dan berharga bagi penyelidik, ahli pertanian, dan industri yang terlibat dalam pemprosesan dan pengedaran buah-buahan. Kajian lanjut melibatkan penerokaan faktor lain dan mengoptimumkan model bahan bagi buah betik untuk meningkatkan ketepatan hasil simulasi mekanikalnya.

Kata Kunci: Kehilangan selepas tuaian, Kerosakan Mekanikal, Kelakuan mekanikal, Model Jisim, pemodelan unsur terhingga

SDG: MATLAMAT 2: Kelaparan Sifar

ACKNOWLEDGEMENTS

I extend my heartfelt gratitude to the Almighty God for granting me the strength, resilience, and perseverance to overcome all the challenges and complete this thesis.

I am deeply thankful to my supervisory committee for their invaluable guidance and support throughout this research journey.

I want to express my sincere appreciation to Dr Hazreen Haizi bt. Harith, who chaired my committee, and the esteemed members, Assoc. Prof. Ir. Dr. Norhashila bt. Hashim, and Dr Mohamad Firdza b. Mohamad Shukery, for their valuable insights and constructive feedback that significantly contributed to the improvement of my writing skill and other skills.

Thanks to the Department of Agricultural Engineering, particularly the Food and Process Lab technician and Biomaterial Lab for their technical assistance and support in conducting various experiments and analyses.

I am forever indebted to my family, especially my parents, for their unwavering guidance, abundant resources, and unconditional love and encouragement throughout my academic journey. I am also grateful to my colleagues and friends for their constant assistance and support, which played a crucial role in making this research a reality.

Finally, I appreciate all those who have contributed directly or indirectly to this thesis through their knowledge, encouragement, and well wishes. Your support has been invaluable, and I am deeply grateful for your contributions to my academic pursuits.

This thesis was submitted to the Senate of Universiti Putra Malaysia and has been accepted as fulfilment of the requirement for the degree of Master of Science. The members of the Supervisory Committee were as follows:

Hazreen Haizi binti Harith, PhD
Senior Lecturer
Faculty of Engineering
Universiti Putra Malaysia
(Chairman)

Norhashila binti Hashim, PhD
Associate Professor Ir.
Faculty of Engineering
Universiti Putra Malaysia
(Member)

Mohamad Firdza bin Mohamad Shukery, PhD
Senior Lecturer
Faculty of Engineering
Universiti Putra Malaysia
(Member)

ZALILAH MOHD SHARIFF, PhD
Professor and Dean
School of Graduate Studies
Universiti Putra Malaysia

Date: 11 July 2024

TABLE OF CONTENTS

			Page
ABSTRACT			i
ABSTRAK			iv
ACKNOWLEDGEMENTS			vii
APPROVAL			viii
DECLARATION			x
LIST OF TABLES			xiv
LIST OF FIGURES			xv
LIST OF APPENDICES			xvii

CHAPTER

1	**INTRODUCTION**			1
	1.1	Background		1
	1.2	Problem Statement		3
	1.3	Significance of Study		5
	1.4	Research Objectives		6
2	**LITERATURE REVIEW**			7
	2.1	Overview		7
	2.2	Papaya Production		7
	2.3	Postharvest Management of Papaya		9
	2.4	Postharvest Physiology of Papaya Fruit		10
	2.5	Postharvest Treatments		12
	2.6	Biomechanical Properties of Fruits		14
	2.7	Modelling Strategies		17
		2.7.1	Mechanistic or Physics Based Modelling	18
		2.7.2	Data-driven Modelling	19
		2.7.3	Multiscale Modelling	21
	2.8	Numerical Methods		23
		2.8.1	Discrete Element Method	24
		2.8.2	Finite Element Method	27
	2.9	Summary		44
3	**MATERIALS AND METHODS**			46
	3.1	Overview		46
		3.1.1	Sample Collection	48
	3.2	Mass Modelling		48
		3.2.1	Determination of Geometric Physical Properties	48
		3.2.2	Mass Model Development	51
		3.2.3	Mass Model Validation	53
	3.3	Mechanical Properties and Response of Papaya Fruit under Compression		54
		3.3.1	Characterizing Mechanical Properties of Papaya along its Longitudinal Axis	54
		3.3.2	Finite Element Modelling	59

4	**RESULTS AND DISCUSSION**	71
	4.1 Geometric Physical Properties of Papaya	71
	4.1.1 Mass Modelling	73
	4.2 Mechanical Properties of Papaya	76
	4.2.1 Elastic Modulus	76
	4.2.2 Viscoelastic Parameters	78
	4.3 Finite Element Analysis	82
	4.3.1 Finite Element Model Validation	82
	4.3.2 Model Applications	88
	4.3.3 Model Limitations	96
	4.4 Summary	97
5	**CONCLUSION AND FUTURE RECOMMENDATION**	99
	5.1 Conclusion	99
	5.2 Recommendation	100
REFERENCES		102
APPENDICES		116
BIODATA OF STUDENT		129
LIST OF PUBLICATIONS		130

LIST OF TABLES

Table		Page
1	Geometry modelling specification of different fruits	30
2	Material models used for different fruits and vegetables	32
3	Mass model equations	52
4	Simulation objectives and the corresponding setup	61
5	The parameters for elastic, elastic-plastic and viscoelastic material models of the bottom section of papaya fruit	67
6	Physical properties of papaya (n = 63)	72
7	Statistical parameters of single variable mass models for papaya fruits	75
8	Performance metrics of multiple variable mass models for papaya fruits	76
9	Maxwell viscoelastic parameters (E_0, Ee, E_1, E_2, E_3 are relaxation moduli; T_1, T_2, T_3 are relaxation time)	81
10	Comparison of Root Mean Square Error (RMSE) values for viscoelastic, elastic, and elastic-plastic material models equivalent stress response at different sample locations in the papaya fruit	84
11	Comparison metrics of different material models	85
12	T-test comparison of stress response of whole fruit compression stress (mpa) using sketched and scanned models	89
13	Whole fruit compression results (n=5)	91

LIST OF FIGURES

Figure		Page
1	The basic anatomy of fruit (a) papaya (b) mango	11
2	Schematic diagram of papaya postharvest management	13
3	Constitutive behaviour of fruit. (a) force–deformation behaviour of biomaterial; (b) the Maxwell model; (c) the Kelvin-Voigt model; (d) the generalized Maxwell model	16
4	Multiscale features of food materials	22
5	Finite element modelling procedure	28
6	Overall methodology workflow	47
7	The ripening index scale of the Eksotika papaya (Kwok & Liang, 2019)	48
8	An illustration of the axis: *a, b and c. a,* the longest axis measured along the longitudinal axis, *b* was measured as the axis perpendicular to *a*, and *c* was measured as the axis normal to *a* and *b*	49
9	An illustration sliced sample of papaya fruit for compression.	55
10	Compression and stress-relaxation tests setup	57
11	A representative stress-time curve of papaya along its longitudinal axis indicating the overstress and equilibrium region using equations 20 and 21	58
12	Finite element modelling flowchart	60
13	3D Solid modelling of papaya fruit. (a) – scanning of the fruit (b) – converting scanned model to solid model	63
14	Reversed engineering process of the scanned model	64
15	Creation process of the simplified geometry model. (a) tracing the fruit edge where the green line represents the traced profile (b) the resulting 3d solid model	65
16	Illustration of loading directions. (a) Transverse loading, (b) Longitudinal loading. The bottom plate remains static, while the upper plate is constrained to move only in the vertical or y-direction	70
17	Correlation coefficient matrix between geometric physical properties variables and mass	72

18 The average and standard deviation (n = 30) of (a) elastic modulus (b) failure load (c) failure strain (d) failure stress along the longitudinal axis. no significant difference ($p < 0.05$) was observed in all variables with respect to locations 78

19 Comparison of stress-strain relationships across various material models (elastic, elastic-plastic, viscoelastic) for the three sections (top, middle and bottom) in a papaya fruit. The experimental result from compression tests conducted on sliced samples on the bottom section (dashed line) is also included for comparison 85

20 Comparison of stress-strain relationships across various material models (elastic, elastic-plastic, viscoelastic) for whole papaya fruit. the experimental result from compression tests conducted on whole papaya fruit (dashed line) is also included for comparison 86

21 Stress distribution (MPa) of elastic model at 16 mm compression. maximum stress at contact point; minimum stress at opposite end 87

22 Stress distribution (MPa) of elastic-plastic model at 16 mm compression. maximum stress at contact point; minimum stress at opposite end 87

23 Stress distribution (MPa) of viscoelastic model at 16 mm compression. maximum stress at contact point; minimum stress at opposite end 88

24 Stress-strain relationship from fe simulation of papaya under compression using 3d geometry models produced by sketching and scanning methods. (a) Each plot represents the simulation response of the individual geometry model under the same loading condition. (b) The result of average stress for scanning and sketching methods is in figure (a), with error bars indicating the standard deviation 90

25 Variations in the papaya fruit model's von Mises stress distributions as a function of varying compression displacement in the longitudinal direction. (a) 4 mm displacement along the longitudinal direction; (b) 8 mm displacement along the longitudinal direction; (c) 16 mm displacement along the longitudinal direction 94

26 Variations in the papaya fruit model's von Mises stress distributions as a function of varying compression displacement in the transverse direction. (a) 4 mm displacement along the transverse direction; (b) 8 mm displacement along the transverse direction; (c) 16 mm displacement along the transverse direction 95

LIST OF APPENDICES

Appendix		Page
A	Statistical Analysis Code Snippet	116
B	Stack Damage Calculation	127
C	Geometry Modelling Methods Data	128

CHAPTER 1

INTRODUCTION

1.1 Background

Carica papaya is an herbaceous fruit belonging to the family of Caricaceae. It is believed to have originated from tropical and eastern central America, but it is widely grown in most tropical countries of the world. Around 98% of the total production of tropical fruits comes from developing countries, whereas developed countries account for 80% of the global import trade. Sarris & FAO (2003) reported that papaya is a part of the dominant tropical fruits produced worldwide. The Malaysia papaya production in 2021 was estimated at 60,884 metric postharvest and an estimated value of gross production value of 23 million USD (FAOSTAT, 2023)

Papaya is a fruit with a naturally short shelf but also suffers from postharvest quality losses due to overripening and mechanical injury that occurs during harvesting, field handling or transportation (Prasad & Paul, 2021). The physical, textural, or mechanical properties of fruits play a significant role in determining their economic value because consumer response to fruit purchase is predominantly influenced by sensory attributes, including taste, freshness, ripeness, and texture (Martinez-Romero et al., 2004). According to Sivakumar & Wall (2012) research, the retail quality of "Red Lady" papayas was primarily affected by a decrease in firmness and the occurrence of chilling injury when exposed to fluctuating temperatures during simulated transportation and handling. Fadiji et al. (2016) estimated that 30% – 40% of agricultural produce may be lost due to mechanical damage in the distribution chain between the grower and the consumer. Minimisation of postharvest losses will not only enable maximisation of profit but also reduce biological waste.

Several research works have been done to reduce postharvest losses of papaya. These research works were able to study the postharvest losses of papaya fruit from the perspective of biochemistry (Nian et al., 2022; Sew et al., 2015; Srimartpirom et al., 2023; Zhou et al., 2022) and physiology (Kechinski et al., 2012; Proulx et al., 2005).

However, to effectively optimise the postharvest handling process and reduce postharvest losses due to mechanical damage, it is crucial to have a comprehensive understanding of the biomechanics of fruits. The use of experimental methods has been the conventional way of studying the mechanical response of papaya. Fruits undergo dynamic or static loading, with the response measured using instrumentation (Sanchez et al., 2020; Vázquez García et al., 2013).

However, the advancement in computing power has provided us with novel and improved ways towards the reduction of postharvest losses through real-time monitoring and understanding of food (or fruit) physics at a level of detail that is not possible with experimentation alone (Datta, 2016; Defraeye et al., 2021; Shoji et al., 2022). The area of study responsible for this advancement is called computer-aided food engineering (CAFE), which deals with the application of computer software for analysis in the design and control of food products, processes, packaging, or equipment, from the molecular scale to that of an entire food plant (Datta et al., 2022). Advancements in the field of study have called for the application of digital twins in the postharvest process of fruits. A digital twin of a product is a virtual representation that includes all its fundamental properties, like geometry and materials properties. It closely simulates all relevant processes and their dynamics over the product's lifespan. Also, it is connected to the real product and its operations through sensor data, ideally updated in real-time (Defraeye et al., 2021).

The fundamental step towards a digital representation of the fruit is correctly representing the physical, mechanical, thermal, and other properties. The problem formulated across this property is resolved through a multiphysics approach (Erdogdu et al., 2022). Solutions to the equations that define a given physical problem may be either exact solutions or numerical estimates. Exact solutions are precise, but often limited in their applicability due to their reliance on simplified geometries and specific initial and boundary conditions. On the other hand, the latter are far more general, as they can be applicable in complex geometry (Datta, 2016; Erdogdu et al., 2022). Finite element techniques have evolved into one of the most versatile and potent frameworks for the numerical solution for partial differential equations (Clason, 2017; Rapp, 2017). The fundamental idea behind FEM is to divide complex computational geometry into discrete elements and find local solutions that satisfy the differential equation within the boundary of each element.

1.2 Problem Statement

Postharvest losses in papaya production accounts for a significant 30-40% of its total production (Sekeli et al., 2018). While lowering storage temperatures can extend papaya shelf life, mechanical damage during handling, such as bruising and cell wall rupture, accelerates fruit degradation, leading to increased losses. Fruits can be injured and damaged due to compressive forces from harvesters, mishandling during sorting and grading, and box overpacking (Opara & Fadiji, 2018).

Traditionally, human operators graded fruits through manual inspection, which is subjective and tedious (Riyadi et al., 2007). However, these processing systems have evolved to incorporate advanced technologies, such as computer vision and automation, to achieve accurate grading and sorting processes of fruits (Desai et al., 2023; Seema et al., 2015). Models to sort fruit into different grades have been reported for different fruits, but that of papaya has not been reported (Lorestani & Tabatabaeefar, 2006; Mahawar et al., 2019; Mansuri et al., 2022; Murakonda et al., 2022; Nyalala et al., 2019; Omid et al., 2010; Panda et al., 2020; Schulze et al., 2015) Therefore, this study addresses this gap by developing a mass model to automate the grading and sorting process of papaya.

Studies have been conducted on papaya fruit to assess its mechanical response to its multi-layered tissue (Zulkifli et al., 2021). However, the mechanical properties of fruits are affected by various factors such as size or shape, ripeness condition, density, and heterogeneity. In this study, the variation in mechanical properties of papaya fruit along its longitudinal axis will be determined.

Computer-aided food engineering offers a framework for monitoring, understanding, and optimising postharvest fruit handling processes. Precise 3D geometry and material properties data are crucial for physics-based modelling in this field (Datta, 2016; Defraeye et al., 2021). Different methods have been used in defining the geometry and material properties of fruits when using a physics-based approach to solve physical problems related to mechanical or thermodynamics (Fadiji et al., 2018; Puri & Anantheswaran, 1993; Zulkifli et al., 2020). However, fruit properties differ, making it difficult to assume that the material model defined for another fruit will accurately simulate the mechanical response of papaya. Therefore, this study seeks to determine the material model of papaya, of specific ripening stage, that reflects its mechanical response under compression when modelled as a homogeneous fruit (i.e., the skin-flesh difference is disregarded) using the finite element method.

1.3 Significance of Study

The reduction of postharvest losses will aid in achieving the sustainable development goal (SDG) two of zero hunger through food security and modelling approaches to digitise the postharvest management process.

Traditional experimental methods, while informative, may be time-consuming and expensive. Hence, computational simulations, particularly finite element modelling, offer a cost-effective and efficient means to explore the mechanical properties of papaya fruit and predict its deformation and stress distribution under compressive loads.

This study utilised experimental, statistical modelling, and numerical techniques (FEM) to characterise the physical and mechanical properties of papaya. It presents a model that can be used to predict the mass of papaya and simulation case studies to predict the fruit's mechanical behaviour when subjected to compressive loading. The findings of this research can prove advantageous to designers in design studies of harvesting and postharvest machinery. Additionally, this study is a foundation for implementing an advanced framework for digital twins.

1.4 Research Objectives

This study aims to develop a model for predicting papaya's mass and mechanical response during compression. This was accomplished through the following specific objectives:

1. To determine the geometric properties that model the mass of papaya.
2. To determine the variation in papaya's mechanical properties, i.e., the failure stress, failure strain, Young's Modulus, and viscoelastic parameters as a function of location along its longitudinal axis.
3. To determine the most suitable material model that represent the mechanical behaviour of papaya under compression.
4. To assess and compare the finite element modelling (FEM) stress responses between the scanned and sketched geometry models of papaya through hypothesis testing.

CHAPTER 2

LITERATURE REVIEW

2.1 Overview

This chapter delves into the origins of the Exotica papaya variety and its production in Malaysia. Additionally, pertinent literature on postharvest management, treatment strategies, and the biomechanical properties of the papaya fruit. This chapter also highlights the use of mechanistic (physics-based) and data-driven modelling strategies in fruit modelling. Finally, our discussion on numerical methods details the types of geometry modelling approaches, material models used for various fruits in the literature, and how loading conditions are modelled and applied to address postharvest problems.

2.2 Papaya Production

The world production of papaya in the past decade reached approximately 14 million tons with an approximate harvest area of 475 thousand hectares (FAOSTAT, 2022). Around 98% of the total production of tropical fruits comes from developing countries, whereas developed countries account for 80% of the global import trade. Sarris & FAO (2003) reported papaya as one of the dominant tropical fruits produced worldwide.

Papaya was first grown in Malaysia as a smallholder crop nationwide, with several commonly grown varieties, including Eksotika, Sekaki, Batu Arang, Sitiawan and Subang 6. While Eksotika is a self-pollinated inbred variety that has similar features to Sunrise Solo, it is notable for its larger fruit size. In 2022, Malaysia produced 54.8

thousand tons of papayas; however, the highest production of 83.8 thousand tons was recorded in 2017, with subsequent years showing a decline (FAOSTAT, 2023; Tridge, n.d.).

The introduction of the Eksotika variety transformed papaya farming from a smallholder crop to a plantation crop. Papaya plantations have emerged as a promising industry in Malaysia, with a significant contribution to the world's papaya export trading. Between 1993 and 2013, Malaysia exported over 37 thousand tons of papaya annually, making it the second-largest exporter globally, with an estimated export value of around RM100-120 million per year (Sekeli et al., 2018). Regarding value, papaya production rose significantly to $25 million in 2022 (IndexBox, n.d.).

Papaya production plays a vital role in Malaysia's economy, with the country producing 60,980 tons of fruit in the year 2021. Of this, around 68% was consumed by Malaysians or used for feed, while the rest was exported (MyPF, 2022).

Sekeli et al. (2018) gave a histological account of the Exotica papaya variety coming into existence through the backcross breeding program of the Malaysian Agricultural Research and Development Institute (MARDI). The backcross breeding was created through crossbreeding using Sunrise Solo, a variety originating from Hawaii with great taste but low yield and small fruit size, with Subang 6, a locally adapted variety with a larger fruit size. Kwok & Liang (2019) highlighted the following characteristics of Exotica papaya variety:

1. It is a variety of fruit with strong and resilient growth characteristics, capable of thriving in diverse soil types, provided that the drainage system is adequate.

2. It is a prolific bearer, capable of producing up to 60 tons of fruit per harvested area annually.

3. The fruit is relatively small to medium, weighing between 400-800 g and showing a vibrant orange-red flesh that exudes a pleasant aroma and high sugar content of 13-15◦Brix.

These alluring characteristics, including its high yield and appealing appearance, have made Eksotika a preferred variety for commercial cultivation and export, particularly in regions such as China, Hong Kong, Singapore, the Middle East, and Europe (Sew et al., 2015). A report indicates that postharvest losses of papaya can range from 40-60% at various growing regions, with factors such as improper harvesting, mishandling, improper storage, packaging, transportation, and diseases contributing to these losses (Prasad & Paul, 2021). Another study on Papaya var. Taiwan 786 showed a total postharvest loss of 25.49%, which included field level loss, transit loss, ripening loss, and retail level loss (Gajanana et al., 2010).

2.3 Postharvest Management of Papaya

Papayas are susceptible to losses due to over-ripening, mechanical damage, microbial attack, and decay, which often result from poor harvesting techniques, rough handling, inadequate packaging, and transportation conditions. Maintaining the quality and safety of papayas during transport from the farm to the market relies heavily on good postharvest handling practices. Losses must be minimised for farmers to reap the benefits of their papaya production (Savary et al., 2012; Sawicka, 2019). As consumer demand for high-quality fruits and vegetables continues to rise, it is becoming increasingly important to implement good postharvest handling practices throughout the entire supply chain to ensure the quality of papayas.

2.4 Postharvest Physiology of Papaya Fruit

Papaya fruit moisture content ranged from 85 to 91%. It is prone to water loss and shrivelling under low humidity after harvest (Ali et al., 2011). Paull (1993) quantified papaya's threshold level (an indicator of shelf-life termination) as 10% physiological loss in weight. According to Proulx et al. (2005), a papaya's texture turns rubbery and low gloss when it loses roughly 8% of its weight, rendering the fruit unmarketable.

The pericarp of a fruit comprises three layers that vary in their chemical composition and thickness (Cerri & Reale, 2020). These layers are the exocarp, mesocarp, and endocarp, as shown in Figure 1. The exocarp layer is covered with an extracellular hydrophobic layer called the cuticle. The cuticle is one of the micro-structural components of the fruit exocarp and is instrumental in maintaining the fruit's physiological state. It primarily comprises cutin and cuticular waxes, forming a protective barrier against infections and uncontrolled water loss through transpiration (Rios et al., 2015). During the postharvest period, the cuticle is responsible for preserving the fruit quality by regulating water and gas exchange, preventing rapid deterioration, and maintaining the fruit's optimal physiological state (Bargel & Neinhuis, 2005). The cuticle must remain intact throughout the entire growth and development, harvesting, and storage processes to produce high-quality fruits with an adequate shelf life (Fernández-Muñoz et al., 2022). The cuticle membrane's elasticity, which determines its stiffness, is affected by various factors such as temperature, relative humidity, and chemical composition (Tsubaki et al., 2012). The study by

Matas et al. (2004) shows that tomatoes' cuticular membranes are isotropic and exhibit viscoelastic behaviour with an initial elastic response. The elastic behaviour is primarily influenced by the accumulation of polysaccharides and flavonoids in the cutin matrix. In contrast, the viscoelastic behaviour is attributed to the cutin matrix's low elastic modulus and high strain values (Dominguez et al., 2009). The stiffness and strength of cuticular membranes varied inversely with temperature and relative humidity (Matas et al., 2005); this leads to cracking in the presence of high relative humidity, as well as high fruit temperature (Li et al., 2018; Matas et al., 2005; Rios et al., 2015).

Furthermore, the arrangement of the cell walls, water content, and the presence of pectin, cellulose, and hemicellulose affect the mechanical properties of fruits (Li et al., 2013). Other factors that affect the mechanical properties of papaya fruit include its shape, size, density, cultivar and maturity or ripeness index (Wang, 2004).

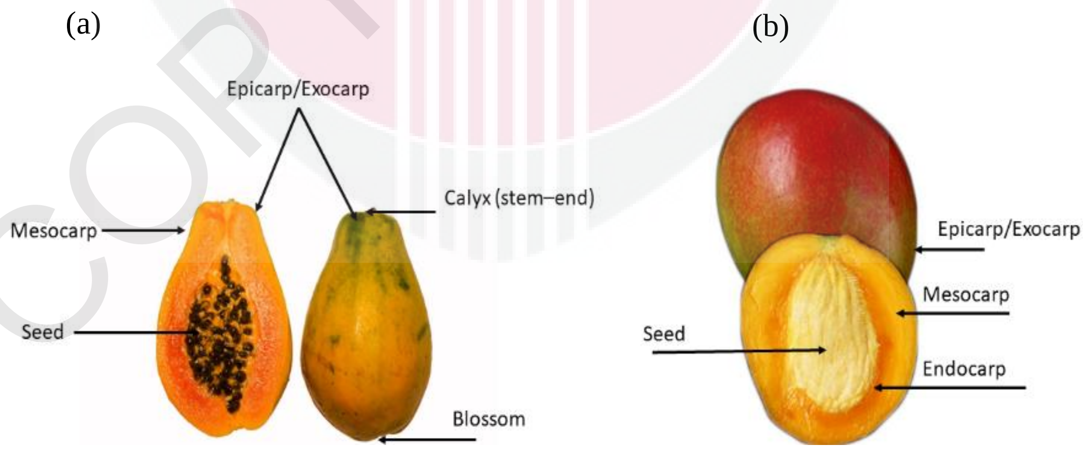

Figure 1 : The basic anatomy of fruit (a) papaya (b) mango

2.5 Postharvest Treatments

Postharvest losses in papaya can be due to fungi infection at the pre-harvest or harvest stage, which becomes active during storage (as the fruit ripens) even if they were previously dormant (Prusky et al., 2013). These diseases manifest as visible symptoms such as lesions and off-odours, rendering the fruit inedible and resulting in losses of 20-40% (Savary et al., 2012). Figure 2 describes postharvest treatments for controlling postharvest diseases (Kwok & Liang, 2019; Prasad & Paul, 2021).

Sanitising treatments are performed to eliminate microorganisms from the surface of fruits. These treatments target potential human pathogens such as coliforms and the microorganisms that cause postharvest diseases such as anthracnose or soft rots (Kwok & Liang, 2019).

Heat treatments are one of the methods used for disinfection of tropical fruits, primarily due to the effectiveness of heat in killing fungi and insects, its ease of application, and avoiding the issue of chemical residues (Srimartpirom et al., 2023). In addition to heat treatments, several other disinfection treatments used include vapour heat treatment, ozonated water with heat treatment (Terao et al., 2019), a combination of hot water treatment and chitosan coating (Vilaplana et al., 2020; Zhou et al., 2022), and honey coating (Maringgal et al., 2020).

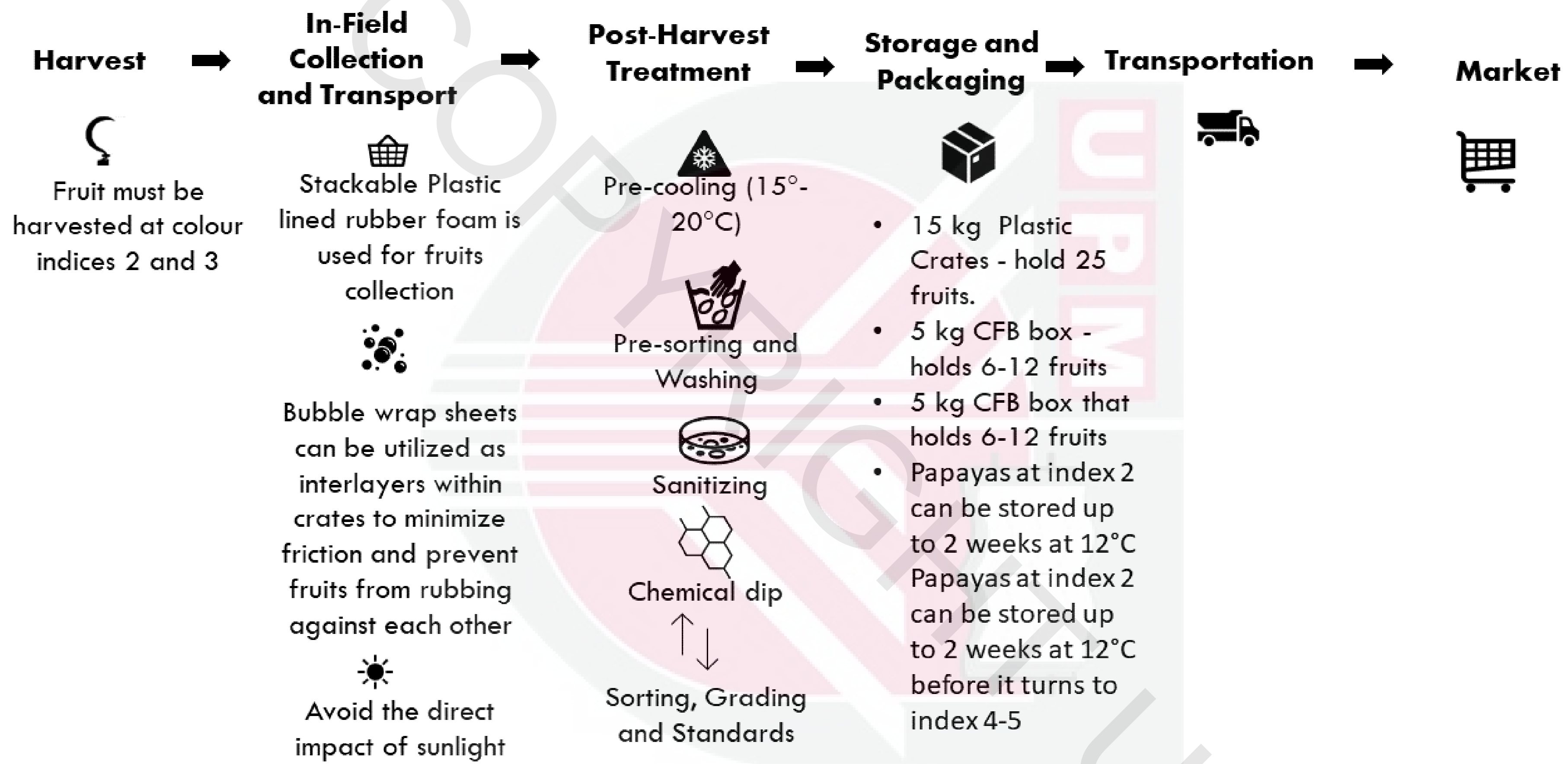

Figure 2 : Schematic diagram of papaya postharvest management

2.6 Biomechanical Properties of Fruits

The use of machines has become a notable tool in man's civilisation; this has transformed our daily activities, including how we cultivate, process, store and transport our food. The agricultural industry has grown from using crude tools to using autonomous machines (robots) in agricultural processes. However, the interaction of machines with fresh produce may cause damage to the produce due to the indiscriminate application of force. Therefore, fresh produce must be handled to minimise damage, which can be done effectively through modelling instead of trial and error.

Mechanical damage is caused by excessive load application on fruits that causes a rupture in the fruit cell wall. The load applied can either be compressive, impact, or vibration loads. The relationship between an external load acting on a specific fruit material and the resulting deformation behaviour is defined by the rheology of the fruit. The rheology of fruits is classified into elastic, plastic, and viscoelastic models. However, this behaviour has been combined to reflect the real behaviour of fruit material. Zhao et al. (2019) highlighted that the material models used to describe fruit behaviour during numerical studies include the linear elastic model, the nonlinear elastic model, the linear viscoelastic model, the nonlinear viscoelastic model, and the elastic-plastic model.

The elastic-plastic model is based on the theory of plasticity. The theory of plasticity is concerned with materials that initially deform elastically but permanently deform plastically upon reaching yield stress. The yield stress is considered the point for the initial damage to the fruit, as shown in Figure 3(a) (Celik et al., 2017). The linear elastic model is simple and incapable of capturing the irreversible deformation in fruit when overloaded. The area under the force–deformation curve from zero deformation to failure was directly determined as the deformation energy (Salarikia et al., 2017). The viscoelastic model describes the material behaviour as a function of load, deformation and time. The viscoelastic material model aims to capture this behaviour by accounting for both instantaneous elastic and time-dependent viscous deformation. This model idealised that the materials may deform under stress (load) and remain deformed even after the stress is removed. The simplest viscoelastic material model is the Maxwell model, which consists of a spring and dashpot in series (Figure 3(b)). The spring represents the elastic deformation, while the dashpot represents the viscous deformation. When stress is applied to the material, the spring and dashpot deform, resulting in an instantaneous elastic deformation and a time-dependent viscous deformation. The amount of deformation in the spring and dashpot is determined by the material's elastic modulus and viscosity, respectively. On the other hand, the Kelvin-Voigt model (Figure 3(c)) consists of a spring and dashpot in parallel, with the spring representing the elastic deformation and the dashpot representing the viscous deformation. This model is beneficial for modelling materials that exhibit creep behaviour, where deformation increases over time under constant stress. Biological tissues that exhibit complex viscoelastic behaviour are represented using the Prony series or the generalised Maxwell model, and multiple springs and dashpots are used in parallel and in series to capture the material's behaviour over a range of time scales. Stress relaxation or creep analysis experiment data are fitted with the viscoelastic model to obtain the required input parameters for the FEM simulation. Further discussion about modelling strategies and numerical modelling will be discussed in sections 2.6 and 2.7, respectively.

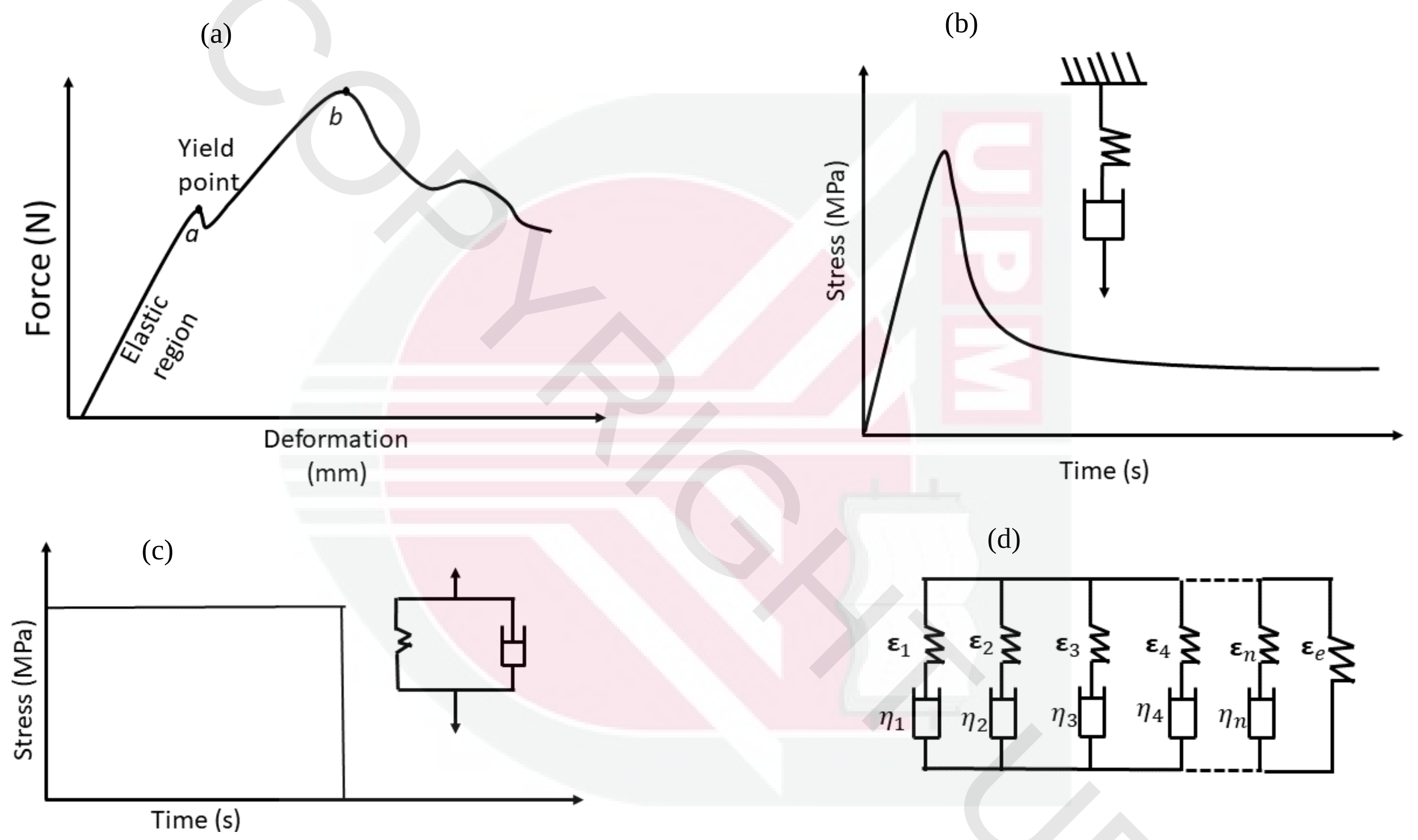

Figure 3 : Constitutive behaviour of fruit. (a) force–deformation behaviour of biomaterial; (b) the Maxwell model; (c) the Kelvin-Voigt model; (d) the generalized Maxwell model

Notably, the biomechanics of fruits after harvest extends beyond the load-deformation behaviour but also includes the influence of environmental conditions, i.e., relative humidity and temperature (An et al., 2022; Arendse et al., 2014; Celik et al., 2021). Proulx et al. (2005) reported that the 20˚C storage temperature of papaya fruit accelerates water loss, which causes the papaya fruit to shrivel, soften, and ultimately reduce shelf life to only two days after harvest. Azene et al. (2014) also reported how packaging material influences papaya fruit characteristics such as weight loss and textural and chemical properties. The author concluded that papaya fruits packaged in HDPE bags in an evaporatively cooled storage maintain better fresh weight and chemical composition during 21 days of storage.

2.7 Modelling Strategies

Modelling encompasses capturing a physical or biological system's fundamental characteristics and relationships and subsequently expressing them through a mathematical or computational framework. A model can either be deductive or inductive. Deductive models involve using a comprehensive mathematical framework that facilitates the generation of predictions regarding a system. If these predictions do not align with empirical observations (experiment), then the very validity of the model may be called into question. In contrast, an inductive model employs statistical techniques to derive a prediction from a collection of observations, and the success of this prediction is assessed by comparing it with previously unseen data. Hence, in the context of a biological system, deductive models are often used as coupled non-linear differential equations (Coveney & Fowler, 2005). This approach adopts a mechanistic stance, elucidating the interrelations between variables based on underlying physical processes. Notably, physics principles govern this modelling strategy: motion of rigid body or deformation with fundamental principles such as the conservation of energy, momentum, and mass, coupled with constitutive equations that elucidate the behaviour of the material under study. Nonetheless, the role of data-driven modelling strategies (inductive modelling) cannot be trivialised; the details of these modelling strategies are discussed in the following subsections.

2.7.1 Mechanistic or Physics Based Modelling

Mechanistic or physics-based modelling offers a rigorous approach to comprehending the intricate physical processes during fruit handling. Unlike empirical models that rely solely on experimental data, mechanistic models aim to elucidate the underlying physics governing fruit behaviour when subjected to various physical quantities such as mechanical stresses and hygrothermal conditions experienced during supply chains. This modelling approach enables a better understanding of how multiple factors affect fruit postharvest losses. For instance, orange quality metrics were modelled in relation to the effects of pre-harvest biological variability and variations in hygrothermal conditions in supply chain operation between shipments (Onwude et al., 2022). Zulkifli et al. (2021) modelled how the ripening stage of papaya fruit impacts its deformation behaviours.

Numerous mechanistic models have been developed to simulate and predict mechanical damage in fruit postharvest handling. These models vary in complexity and specificity, addressing issues ranging from impact or compressive forces during postharvest handling to the effects of temperature variation during transport and storage (Shoji et al., 2022; Miraei Ashtiani et al., 2019a; Salarikia et al., 2017; Ho et al., 2009; Van Zeebroeck et al., 2006). The validation of mechanistic models is an indispensable step in ensuring their reliability and accuracy. Experimental data obtained through controlled tests and field observations are used to corroborate model predictions. Successfully validated models offer practical utility in optimising postharvest handling processes.

While mechanistic modelling holds immense promise, it has challenges and limitations. These models often require extensive data inputs and computational resources (Datta et al., 2022; Erdogdu et al., 2022). Moreover, they rely on simplifying assumptions that may not fully capture the complexity and variability of real-world scenarios (Defraeye et al., 2021; Onwude et al., 2022). Striking a balance between model accuracy and computational feasibility remains challenging in this modelling strategy (Hertog, 2016). The numerical analysis approach typically used in the mechanistic model was discussed in section 2.7.

2.7.2 Data-Driven Modelling

The data-driven modelling approach is based on analysing and processing available data relating a physical measurement to postharvest loss or damage to identify patterns, correlations, and predictive relationships. These models are advantageous when the underlying physical mechanisms may be challenging to describe their physics fully. Data-driven models complement mechanistic approaches by directly providing practical, empirical solutions from observations. The effectiveness of data-driven models hinges on selecting relevant data inputs and variables. In the context of mechanical damage, these might include data on handling equipment parameters (e.g., conveyor belt speed, sorting mechanisms), fruit properties (e.g., firmness, shape, size), environmental conditions (e.g., temperature, humidity), and historical records of mechanical damage incidents. Accurate and comprehensive data inputs are essential for these models' robustness and predictive power.

Data-driven models vary in complexity, from simple regression analyses (Abedi & Ahmadi, 2013; Komarnicki et al., 2017; Wang et al., 2019) to more sophisticated machine learning algorithms such as neural networks, support vector machines, and random forests (Melesse et al., 2022). The approach has been applied in various contexts, such as reducing bruising during sorting and improving packaging for transportation (Fadiji, Coetzee, Chen, et al., 2016; Fadiji et al., 2017; Opara & Fadiji, 2018).

One of the areas in which data-driven strategies have received much attention is in elucidating the physical properties of fruits and vegetables, such as mass, density, sphericity, surface area, volume, etc. Researchers have used relationships between the geometric physical properties and the mass to develop mathematical models to predict fruit mass. Khoshnam et al. (2007) recommended a non-linear regression model using a single variable (minor diameter) as a suitable model for predicting the mass of pomegranate. A similar non-linear equation with different coefficient values using the geometric mean diameter (predictor) was recommended for kinnow mandarin mass (Mahawar et al., 2019). (Mansuri et al., 2022) concluded that the linear support vector machine (SVM) model outperformed other methods in modelling the mass and volume of the apple ber fruit by validating the developed model using the fruit's projected area. In the case of lime fruit, a linear equation was used to predict the mass based on minor diameter (Miraei Ashtiani et al., 2014). Image processing and mathematical modelling provide an efficient way of determining the physical properties of fruit (Seyedabadi et al., 2011). These data-driven models have proven to be efficient during sorting and grading of fruits to reduce postharvest losses (Mansuri et al., 2022; Nyalala et al., 2019; Seema et al., 2015)

2.7.3 Multiscale Modelling

The hierarchical structure of food encompasses various features that range from the molecular scale up to the food plant scale (Cáez-Ramirez et al., 2015; Ho et al., 2013; Li & Thomas, 2016). Ho et al. (2013) reviewed and gave an overview of a scale reference defining the multiscale properties of food material, as annotated in Figure 4. The mesoscale refers to a scale between micro and macro scales. It is relevant to the mechanical properties of fruits because it relates to the structure and arrangement of cells and tissues within the fruit, which can affect its overall mechanical behaviour. Meanwhile, the macro-scale pertains to the observable mechanical properties of the fruit, such as its firmness, elasticity, and toughness (Li & Thomas, 2016).

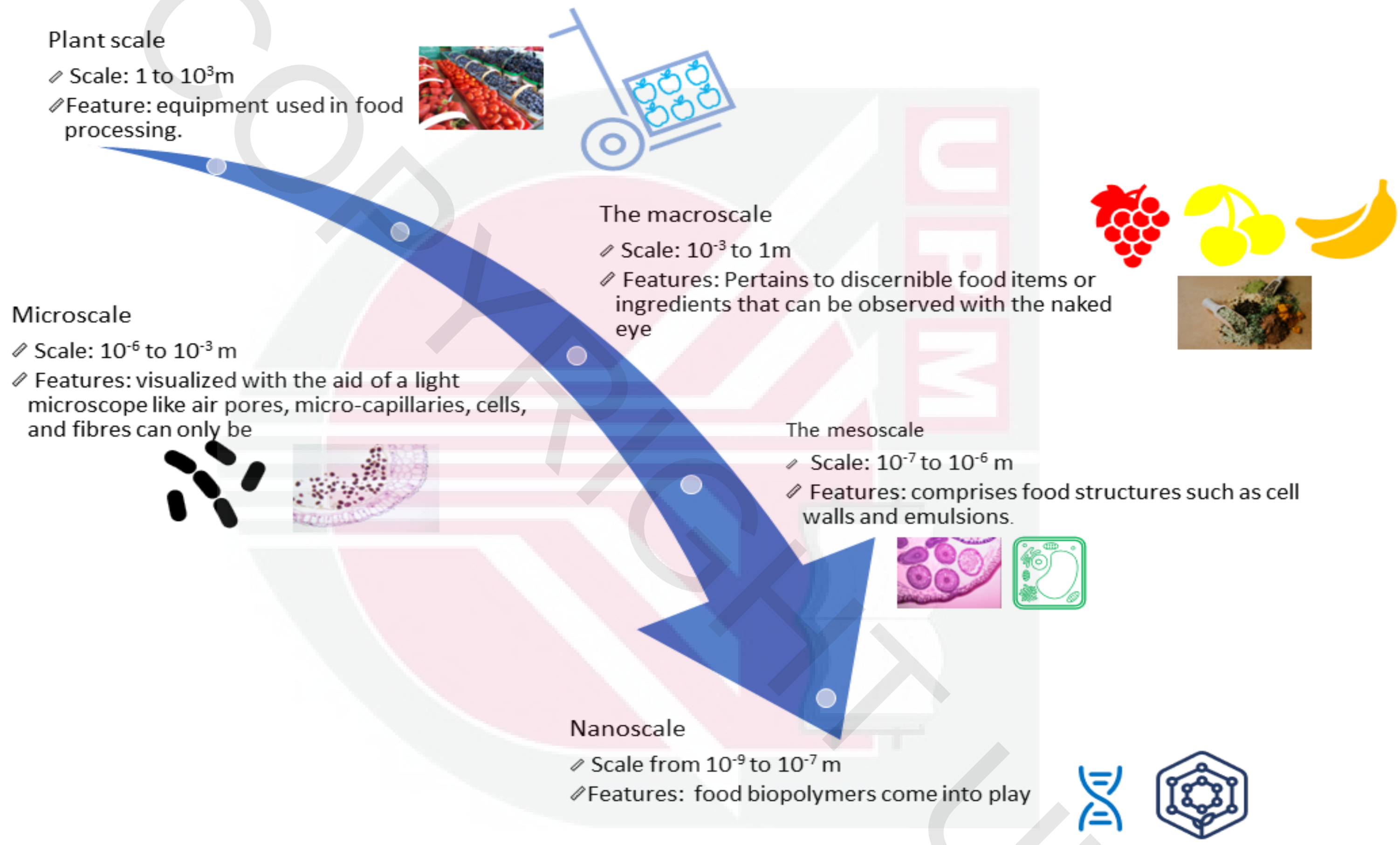

Figure 4 : Multiscale features of food materials

The interconnectivity of living things (invariably plant base material) structure from cellular level to organs/tissue shows that the behaviour of a cell, in response to any stimuli, can be used to predict the behaviour of the overall system. This basic understanding is why multiscale modelling has received attention from different research works describing the mechanical behaviour of fruits (Ho et al., 2013).

A multiscale model consists of interconnected models that describe the material properties of the fruit (or plant material) at various spatial scales (macroscale, mesoscale, microscale). However, one of the drawbacks of this strategy in numerical studies is the computational cost. To overcome this limitation, Ghysels et al. (2010) introduced the particle method to simulate the microscopic aspect, which includes modelling the cell fluid as viscoelastic using smoothed particle hydrodynamics (SPH), while the material properties of the macroscopic domain were not explicitly defined but computed using the microscopic model in small subdomains, called representative volume elements (RVEs). The multiscale modelling of mechanical properties can help us comprehend the dynamic behaviour of biological material (Horbens et al., 2015). However, there is limited literature on using the multiscale approach to model fruits and vegetables, possibly due to computational intensity and resource requirements.

2.8 Numerical Methods

Numerical models for solving fruit stress problems have received much attention in the past decade due to increased computational power (Fadiji et al., 2018). The approach has been used for modelling mechanical responses of fruits under static (Li et al., 2021; Li & Wang, 2016; Stopa et al., 2019; Zulkifli et al., 2021; Liu et al., 2023) and dynamic loading (Du et al., 2019; Nikara et al., 2020). This is because the numerical method can handle complex geometry and boundary conditions. The finite element method (FEM) and discrete element method (DEM) are the major numerical approaches commonly used in solving problems related to stress analysis in agricultural (food) engineering.

2.8.1 Discrete Element Method

The discrete element method (DEM) is a method in which discrete particles interact with each other and with other surfaces during an explicit dynamic simulation. The technique is an excellent tool for comprehending the interaction of fresh produce with materials used during postharvest handling. For example, fruit-to-fruit impact and fruit-to-container impact during transportation (Wang et al., 2022). An experimental methodology is used to determine material properties such as particle density, particle stiffness, particle-wall friction coefficient and particle-particle and particle-wall restitution coefficient (González-Montellano et al., 2011)..

Geometry is an essential factor in the accuracy of DEM; using more realistic geometric properties will enhance the modelled dynamics of the particles at both the single-particle and bulk levels (Scheffler et al., 2018). Another study also found that increasing the number of apple spheres used to model a drop test increased the accuracy of the result with the drawback of increased computational time (Kafashan et al., 2021). Describing the forces acting on particles in contact in the discrete element method is necessary. The forces between the two particles are split into normal and tangential components.

The elastic contact force model applies when deformation is reversible and unaffected by the deformation rate. On the other hand, viscoelastic contact deformation is reversible but dependent on the deformation rate. Plastic contact, however, causes permanent deformation in the body. When two colliding bodies behave completely elastically, the only source of energy dissipation is the action of elastic waves propagating through the material (Dintwa et al., 2008).

The theoretical background of the viscoelastic contact force model, where the energy is dissipated through viscous loss, was discussed by Ahmadi et al. (2012) and Scheffler et al. (2018). Nonlinear viscoelastic contact force was described by different authors (Hunt & Crossley, 1975; Kuwabara & Kono, 1987; Brilliantov et al., 1996a, 1996b). The linear spring dashpot model with spring and damper in parallel is the simplest model for viscoelastic behaviour (Ahmadi et al., 2012). The linear elastic behaviour of a fruit can be described by Equation 1.

$$F = k\delta + c\dot{\delta} \qquad \text{Equation 1}$$

Where F represents the force applied to the fruit, k is the elastic constant or stiffness of the fruit, which measures how much force is needed to deform the fruit. δ is the deformation of the fruit, such as how much it has been compressed. c is the damping coefficient, which is related to the deformation rate. $\dot{\delta}$ represents the rate of change of deformation or how quickly the fruit is deformed.

However, the nonlinear viscoelastic behaviour of fruit can be described using Kuwabara and Kono model given by Equation 2

$$F_n = K_n \delta_n^{3/2} + \frac{3}{2} C_n K_n \delta_n^{1/2} \dot{\delta}_n \quad \text{Equation 2}$$

Where F_n is the normal contact force in N, K_n is the normal elastic constant in N/m$^{3/2}$, C_n is the normal damping constant in s, δ_n is normal deformation in m and $\dot{\delta}_n$ Normal deformation rate in m/s.

Where K_n is the Hertzian contact stiffness (N m$^{-3/2}$) (Ahmadi et al., 2016), which can be expressed as by Equation 3

$$\boldsymbol{K_n} = \frac{\boldsymbol{4}}{\boldsymbol{3}} \sqrt{\boldsymbol{R^*}} \boldsymbol{E^*} \quad \text{Equation 3}$$

Where E^* is the effective elastic modulus of impacting bodies, E_1 and E_2 (Pa) are the apparent elastic moduli of the two impacting bodies and v_1 , v_1 are the Poisson' s ratios of the two bodies as given in Equation 4 (Ahmadi et al., 2016).

$$E^* = \left(\frac{(1 - v_1^2)}{E_1} + \frac{(1 - v_2^2)}{E_2}\right)^{-1} \quad \text{Equation 4}$$

The Kuwabara and Kono model has been used to describe the normal contact force of apple for discrete element modelling (Scheffler et al., 2018). A similar model (Hunt & Crossley, 1975; Lankarani & Nikravesh, 1990) has also been used to describe impact force and the deformation at a given instant for the entire period of litchi impact (S. Zhang et al., 2021).

Since impacts between bodies of diverse material characteristics can be accounted for, the relationship between mechanical damage and peak contact force is best suited for application in DEM (Van Zeebroeck et al., 2006). The amount of bruising seen in apples was discovered to have an excellent linear correlation with the peak force (Scheffler et al., 2018).

2.8.2 Finite Element Method

The finite Element Method (FEM) treats a bulk particulate system as a continuum; this contrasts with the DEM, which considers a system as a collection of discrete entities.

The choice between FEM and DEM for numerical analysis depends on the nature of the problem. If the problem involves a system of discrete particles, DEM might be a better choice, for example, the collision of fruits in a bin during transport. On the other hand, for problems involving complex geometries and boundary conditions, FEM might be a more suitable approach (Mansuri et al., 2022; Murakonda et al., 2022).

The general procedure for solving FEM has been grouped into pre-processing, solver, and post-processing stages (Fadiji et al., 2018; Rashvand et al., 2022; Zulkifli et al., 2020). The pre-processing stage is reportedly where more than 70% of analysis efforts are invested (Fadiji et al., 2018). The pre-processing stage involves geometry modelling of the fruit, material modelling (constitutive modelling), discretisation and boundary conditions as shown in Figure 5. The modelling of the mechanical response of fruits under different loading conditions and its applications in determining fruit internal quality and harvest optimisations through modal analysis was discussed in the following subsection.

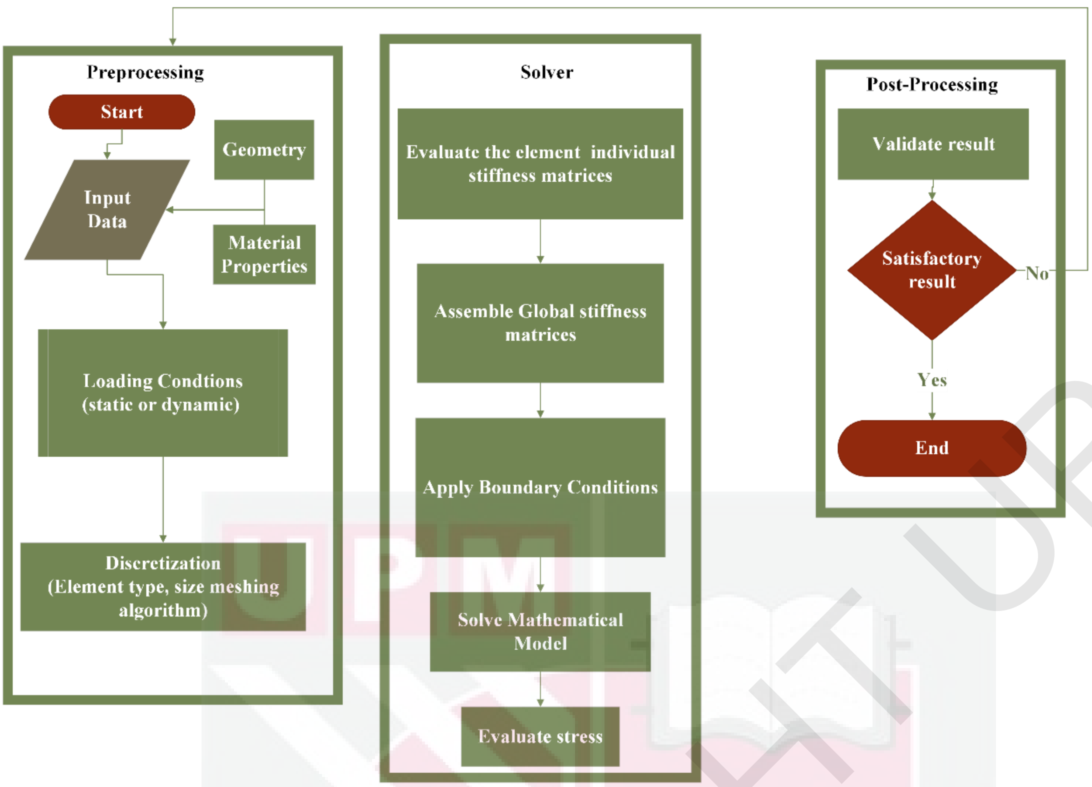

Figure 5 : Finite element modelling procedure

2.8.2.1 Geometry Modelling

Geometry modelling is an initial step in the pre-processing phase of finite element modelling. The geometry of the finite element model can be represented in either 3D or 2D form. However, using 2D geometry in fruit finite element modelling has become less common due to the absence of axial symmetry in loading conditions (Ahmadi et al., 2016). Preference is now given to 3D models, which better reflect the real-world scenario (Dintwa et al., 2008) and enhance accuracy (Celik, Rennie, et al., 2017). Recent studies have witnessed the rising popularity of 3D fruit models created through reverse engineering techniques employing laser scanning technology and parametric CAD software. This trend can be attributed to such technology's increased availability and affordability. Achieving an accurate representation of fruit geometry is critical, encompassing the shape and the size, significantly influencing elastic wave energy

(Dintwa et al., 2008). Moreover, geometry plays a vital role in various rheological investigations, covering structural deformation, flow analysis, heat, and mass transfer, as well as comprehensive examinations of aerodynamic and hydrodynamic behaviours (Sahin & Sumnu, 2006).

While a reverse-engineered 3D model excels in capturing intricate fruit geometry, including surface contours, irregularities, and fine features, a simplified CAD model may offer a more straightforward representation utilising basic geometric shapes or simplified surfaces. Table 1 gives the geometry specifications of different fruits used in the literature.

Table 1 : Geometry modelling specification of different fruits

S/N	Fruit Sample	Geometry Model	The method used for generating models	Reference
1	Apple	3D	Not specified	(Ahmadi et al., 2016)
2	Apple	3D	Reverse engineering technique	(Celik et al., 2011)
3	Apple	3D	Expanding 2D meshes using Mentat software	(Dintwa et al., 2008)
4	Pears	3D	Reverse engineering technique	(Celik, 2017)
5	kiwifruit	3D	Reverse engineering technique	(Dongdong Du et al., 2019)
6	Lycium barbarum L	3D	Reverse engineering technique	(Zhao et al., 2019)
7	'Pink Lady' apple	3D	Reverse engineering technique	(Celik et al., 2021)
8	Pear	3D	Not specified	(Yousefi et al., 2016)
9	Pear	3D	Reverse engineering technique	(Salarikia et al., 2017)
10	Artificial fruit	3D	Spherical CAD model	(Cerruto et al., 2015)
11	Apple	3D	Spherical CAD model	(Szyjewicz et al., 2021)
12	Pecan fruit	3D	Reverse engineering technique	(Celik et al., 2017)
13	Peach	3D	CAD model	(Kabas & Vladut, 2015)
14	Kiwifruit	3D	Reverse engineering technique	(D. Du et al., 2019)
15	Apple	3D	Spherical CAD model	(Pascoal-Faria & Alves, 2017)
16	Olive	3D	Reverse engineering technique	(Rashvand et al., 2021)
17	Orange	3D	CAD model	(Gharaghani & Maghsoudi, 2018)
18	Tomato	3D	Spherical CAD model	(Kabas et al., 2008)

2.8.2.2 Material Models

Another crucial consideration in finite element modelling is the choice of constitutive or material model, as it directly impacts both the accuracy and computational efficiency of the model (Dintwa et al., 2008; Gao et al., 2018; Zulkifli et al., 2020). Different material mechanical models, such as the linear elastic model, the nonlinear elastic model, the linear viscoelastic model, the nonlinear viscoelastic model, and the elastic-plastic model, can represent fruit materials (Zhao et al., 2019).

One of the factors for material model selection is the loading condition (Dintwa et al., 2008). Celik (2017) also stated that the elastic-plastic model was used in modelling the deformation of pear under impact load to reflect reality and characterise the permanent deformation of the fruit. When fruit is in storage, fruit experiences static or quasi-static loading; in this condition, viscoelastic models have been reported to model the mechanical response of the fruits (Kim et al., 2008; Shahgholi et al., 2020). The advantage of the finite element method over analytical method is that the material properties of individual elements can vary, allowing computations to be conducted for the anisotropic behaviour of the fruit. The peel or flesh can be defined as an elastic material, and the core and cortex are viscoelastic, as in the case of an apple (Ahmadi et al., 2016). Table 2 summarises different material models and their parameters' value for different fruits and vegetables in literature.

Table 2 : Material models used for different fruits and vegetables

S/N	Fruit Sample	Material Model	Parameters			Reference
			Variations in fruit material properties	Density	Elastic Properties	
1	Apple	Viscoelastic	Heterogenous properties in fruit parts	Skin/ Cortex /Core 840 Kg/m^3	Skin Elastic modulus E = 12MPa, poison's ratio v = 0.35; Core/Cortex - Elastic modulus E = 5MPa, v= 0.35. Core/Cortex Shear stress relaxation function - G_o = 0.15MPa, β = 1/800 s	(Ahmadi et al., 2016)
2	Apple	Elastic	Homogenous properties in fruit parts	0.796 g/cm^3	E = 1.512 Nmm^{-2}, poison's ratio v=0.384	(Celik et al., 2011)
3	Apple	Viscoelastic	Heterogenous properties in fruit parts	Skin/ Core/Cortex = 840 Kg/m^3	Skin Elastic modulus E = 12, MPa, poison's ratio v = 0.35 Core/Cortex Elastic modulus E =5MPa, v = 0.35. Shear stress relaxation function: G^1 = 0.15 MPa, τ^s_1 = 1 s, G^2 = 0.1 MPa, τ^s_2 = 800 s; and for the bulk modulus relaxation function: K^1 = 1.3 MPa, τ^b_1 = 0.4 s, K_2 = 0.2 MPa, τ^b_2 = 150 s	(Dintwa et al., 2008)
4	Pears	Elastic-plastic	Homogenous properties in fruit parts		Elastic Modulus E= 3.248MPa, Poisson's ratio v= 0.427, Bio-yield stress = 0.3MPa, Tensile Stress = 0.309MPa	(Celik, 2017)
5	kiwifruit	Elastic-Plastic	Heterogenous properties in fruit parts and ripeness	1.112 g/cm^3	Elastic Modulus E= 2.389 MPa, Poisson's ratio v= 0.427, Bio-yield stress = 0.467 MPa, Tangent modulus = 1.368MPa	(Dongdong Du et al., 2019)
6	Lycium barbarum L	Elastic-plastic	Homogenous properties in fruit parts	895 kg/m^3	Elastic Modulus E=0.05MPa, Poisson's ratio v= 0.39, plastic stress = 0.0142MPa	(Zhao et al., 2019)
7	'Pink Lady' apple	Anisotropic Elastic-plastic	Homogenous properties in fruit parts	855.55 Kg/m^3	Elastic Modulus E=4.175MPa, poison's ratio v=0.27, Bio-yield stress = 0.385 MPa	(Celik et al., 2021)
8	Pear	Elastic	Homogenous properties in fruit parts but the variation with ripeness	0.91, 0.97, 1.12 gml^{-1} unripe, ripe, and overripe respectively	Elastic modulus 8.74, 6.46, 2.64 MPa unripe, ripe, and overripe respectively	(Yousefi et al., 2016)

Table 2 : Continued

S/N	Fruit Sample	Material Model	Parameters			Reference
			Variations in fruit material properties	**Density**	**Elastic Properties**	
9	Pear	Elastic-plastic	Homogenous properties in fruit parts	0.91 g/cm3	Elastic modulus = 1.693 $N/mm^{2.}$ failure stress = 0.798 N/mm^2, failure strain = 0.275, and Poisson's ratio = 0.410	(Salarikia et al., 2017)
			Variations in fruit material properties	Density	Elastic Properties	
10	Artificial fruit	Elastic	Homogenous properties in fruit parts	900, 1000 and 1100 Kg/m^3	Elastic modulus = 0.5, 1.5, 2.5 and 3.5 MPa, Poisson's ratio = 0.27	(Cerruto et al., 2015)
11	Apple	Elastic-plastic	Model as a crushable foam material		Elastic modulus (E) = 4.069 MPa, Poisson's ratio (ν) = 0.32	(Szyjewicz et al., 2021)
12	Pecan fruit	orthotropic Perfectly brittle and elastic-plastic (bilinear strain hardening)	Heterogenous properties in fruit parts	Shell (1100 Kgm^{-3}), Kernel (1150 Kgm^{-3})	Elastic Modulus Shell= Orientation (X-122.220MPa, Y-47.614MPa, Z-34.251MPa); Elastic Modulus kernel = 3.881 MPa. Poisson's ratio = 0.3 (Shell), 0.4 (Kernel); Damage Failure = Orientation (X- 5.045 Y-2.530MPa, Z-1.710 MPa),	(Celik et al., 2017)
13	Peach	Elastic (Hertz theory)	Homogenous properties in fruit parts but the variation with ripeness	968.11 g/mm^3	Elastic modulus= 0.89Nmm^{-2}, Poisson ratio = 0.29	(Kabas & Vladut, 2015)
14	Kiwifruit	Elastic-plastic	Heterogenous properties in fruit parts and ripeness	Flesh -1.112 gcm^{-3}, skin - 0.996 gcm^{-3}	Flesh-Elastic Modulus E= 2.389 MPa, Poisson's ratio ρ= 0.40, Bio yield stress = 0.467 MPa, Tangent modulus = 1.369 MPa. Skin-Elastic Modulus E= 12.04 MPa, Poisson's ratio ν= 0.30,	(D. Du et al., 2019)

Table 2 : Continued

S/N	Fruit Sample	Material Model	Parameters			Reference
			Variations in fruit material properties	**Density**	**Elastic Properties**	
15	Apple	Elastic-plastic	Homogenous properties in fruit parts	900 Kgm^{-3}	Elastic Modulus E = 2.0 MPa, Yield Stress =0.4MPa, Failure Stress = 0.4 MPa, Poisson's ratio v= 0.33	(Pascoal-Faria & Alves, 2017)
16	Olive	viscoelastic	Homogenous properties in fruit parts but the variation with ripeness	-	Ripped- Elastic Modulus E = 0.32MPa, Yield Stress =0.11 MPa, Poisson's ratio v 0.28	(Rashvand et al., 2021)
17	Orange	Elastic (Hertz theory)	Homogenous properties in fruit parts	0.837 Kgm^{-3}	Elastic Modulus E = 0.5846 MPa, Poisson's ratio v= 0.2412	(Gharaghani & Maghsoudi, 2018)
18	Tomato	Elastic-plastic	Homogenous properties in fruit parts	795 Kg m^{-3}	Elastic Modulus E = 0.281 MPa, tangent modulus = 0.105 MPa, Poisson's ratio ρ= 0.335	(Kabas et al., 2008)

2.8.2.3 Discretization

When utilising the finite element method (FEM) for engineering problem-solving, the domain is discretised into elements, with the properties of the problem dictating its dimension (Madenci & Guven, 2015). The choice of element type and size are crucial parameters that influence the quality of a finite element model (Celik, 2017; Celik et al., 2021). Optimal mesh settings are essential to ensure simulation accuracy while minimising computation time (Li et al., 2017). The most used elements for solid fruit modelling are tetrahedral and hexahedral (Rashvand et al., 2022; Zulkifli et al., 2020). Different element types were employed to mesh different parts of the fruit in cases where material model specification was needed for distinct tissues (Li et al., 2017). For instance, tetrahedral elements were used to mesh the kiwifruit fruit's flesh, while triangular elements were used for the skin (Du, Wang, Wang Yao et al., 2019). Conducting a mesh sensitivity check is another metric to determine the appropriate element size. Celik et al. (2017) accomplished this by running an impact scenario with varied element sizes and examining the influence of these sizes (from coarse to finer) on the equivalent stress values. Mesh quality was also evaluated using a skewness metric in the finite element model (Celik et al., 2021). Additionally, the energy activity summary from explicit dynamics simulations can be utilised to assess the accuracy of simulation results (Celik, 2017; Du, Wang, Wang, Yao, et al., 2019; Rashvand et al., 2021). This summary includes an evaluation of kinetic, internal (absorbed), contact, and hourglassing/hourglass energy. Hourglassing refers to false deformation in a finite element model caused by zero-energy degrees of freedom when hex/quad meshes alter volume or strain. It is recommended that the hourglassing energy activity does not exceed 5-10% of the internal energy in an adequately conducted finite element analysis (Celik, 2017).

2.8.2.4 Loading Conditions

2.8.2.4.1 Compressive Loading

Fruits are packed in plastic crates, corrugated fibreboard (CFB) boxes and bulk bins. Compression is inevitable as the fruit at the container's bottom will experience compressive forces. If the compression stress exceeds a threshold of yield stress, compression damage can occur immediately. Internal damage to fruits occurs before apparent defects can be seen on the fruit exocarp (Miraei Ashtiani et al., 2019). Using the finite element method, the point at which internal damage occurs can be studied to avoid such damage.

The boundary condition of compression simulation involves the compression of the sample product between two rigid plates. Zero displacement and rotation are applied in all directions to the lower plate while the upper plate compresses the sample in the Y-direction (Li et al., 2017; Miraei Ashtiani et al., 2019).

The results of compression simulation are usually presented as the equivalent stress using the von Mises failure criterion. According to the von Mises criterion, yielding happens when the shear strain energy reaches a certain threshold Francis (2016), which has always been used to estimate the yield behaviour of materials. In the finite element modelling of fruits, the composition of elements whose stress was higher than the bio-yield stress was referred to as the bruised region (Celik et al., 2021). The internal damage volume of tomato was also calculated using Equation 1 (Li et al., 2017).

$$IDV = \sum_{i=1}^{8} \frac{1}{8} \times i \times N_{ic} \times L_{cell}^{3} \qquad \text{Equation 5}$$

Where IDV is the internal damage volume, i is the number of yielded integration points in the cell element, L_{cell} is the edge size of the cell elements, and N_{ic} is the number of cell elements with i yielded integration points.

Finite element modelling has been applied in determining the maximum number of fruits stacked on each other to cause damage to the fruit at the bottom of the packaging box. Miraei Ashtiani et al. (2019) reported that an optimal number of 30 grapefruits can be placed inside a single package in a lateral position to avoid fruit damage. Eight pineapples can be stacked safely in a single package in a transverse loading direction (Liu et al., 202(H. The research by Zheng et al. (2021) recommends minimising blueberry damage; the compression should be kept under 3.15 N, one layer stacking, and fruit should be placed in the vertical direction.

2.8.2.4.2 Impact Loading

The mechanical response of agricultural products produced under impact loads has been studied by several researchers using experimental procedures: drop test (Celik et al., 2021; Komarnicki et al., 2017; Stopa et al., 2018) and pendulum impact method (Wang, 2004; Zhang et al., 2021). The primary limitation of these methods is their inability to provide sufficient information to guide process and equipment design (Dintwa et al., 2008). FEM, on the other hand, is an effective tool in the investigation of fruit mechanical behaviour under different loading conditions. It provides a quick way to understand fruit deformation, which helps design optimal harvest and postharvest handling equipment and strategies that prevent and minimise fruit damage (Celik, 2017b; Celik et al., 2021). For example, various fruit drop height harvest scenarios on a catching surface with different impact angles can be simulated to investigate fruit damage. Salarikia et al. (2017) investigated a pear's stress/strain distribution in a drop scenario, measuring the overall contact force between the fruit and the impact material and evaluating the effect of impact surface material and drop orientation.

Investigating fruit deformation behaviour under impact loading, the boundary condition is usually constructed with two fruits in a collision or a single fruit colliding with a rigid surface. In the model where two fruits are in a collision, one of the fruits is held fixed. In contrast, the second fruit collides with it at a prescribed initial velocity (Ahmadi et al., 2016) or under gravity with a defined drop height (Celik, 2017b; Celik et al., 2021; Du, Wang, Wang, Yao, et al., 2019). Frictional contacts are defined between the rigid surface and fruit model (Celik, 2017; Celik et al., 2021). Fruit loading conditions associated with drop heights, contact surface and impact orientations are considered to influence fruit deformation behaviour (Celik et al., 2021; Du, Wang, Wang, & Yao, 2019; Yousefi et al., 2016).

To analyse the result of the model, damage to the fruit body was described from the simulation result as the stress regions beyond the yield stress point (Celik, 2017; Celik et al., 2021; Dongdong Du et al., 2019; Yousefi et al., 2016). Contact force and Von Mises stress results from different studies show a trend of increase with time until it reaches maximum value during the impact phase, then decrease to zero initial condition during the rebound phase (Celik, 2017; Celik et al., 2021; D. Du et al., 2019; Kabas et al., 2008; Salarikia et al., 2017; Yousefi et al., 2016). Reduction in displacement rates of impact and rebound phase is attributed to plastic deformation (permanent damage in fruit cells) (Du, Wang, Wang, & Yao, 2019). Empirical models to predict bruise rate and bruise susceptibility were also constructed in some studies using response surface methodology (RSM) by taking into account impact heights, impact orientations, and impact surfaces from simulation results as factors (Zhao et al., 2019)

Different parameters have been used to compare simulation and experimental results; some studies validated the output of FEM by comparing the initial velocity, maximum deformed length and contact time of impact and rebound phase of the simulation impact process and high-speed camera recording images (Celik, 2017b; Celik et al., 2017; Du, Wang, Wang, & Yao, 2019; Du, Wang, Wang, Yao, et al., 2019). Gharaghani & Maghsoudi (2018) validate FEM simulation results with an experimental drop test by comparing contact force measured by the load cell attached to the contact surface. Other studies validated FEM models by comparison with previous research (Ahmadi et al., 2016; Rashvand et al., 2021; Salarikia et al., 2017; Yousefi et al., 2016). Du et al. (2019) compared initial velocity errors between simulation and measurement, which was less than 5 %; minimum and maximum errors for maximum deformed length were 3.4 % and 19.0 %, respectively, while contact time was -3.3 % and 11.9 % and in terms of bruise volume with lowest and highest errors of 3.8 and 17.1 %. The lowest and the highest errors between the predicted and observed bruised areas were 0.00 and 60.53%, respectively, for pear impact (Yousefi et al., 2016). Gharaghani and Maghsoudi (2018) reported a 1.93 % and 0.24 % difference in contact forces and a 4 % and 0.38 % difference in everyday stresses for dropping heights of 2 and 3 metres, respectively. The differences between experimental and simulation-based results can vary depending on the FEA setup conditions (material properties, fruit ripening conditions, variety, moisture, harvest, and assumptions used) and the unpredictability of the physical environment conditions encountered during the experiments. (Ahmadi et al., 2016; Celik et al., 2021; Szyjewicz et al., 2021).

FE modelling of fruits under impact loads has been used to optimise design parameters of harvest and postharvest tools such as catching surface and packaging surface to avoid mechanical damage (Celik et al., 2021; Hernández & Bellés, 2003; Rashvand et al., 2021; Yousefi et al., 2016). It has also been used in sensitivity analysis of input parameters used for discrete element modelling of fruits (Dintwa et al., 2008) and prediction of impact damage of strawberries under varying temperatures (An et al., 2022)

2.8.2.5 Modal Analysis

Modal analysis of fruits entails the investigation of their natural frequencies and corresponding mode shapes. This encompasses the determination of the vibrational characteristics of a fruit, such as its resonant frequencies and the patterns of vibration associated with each frequency.

FEM can be applied to perform a modal analysis of fruits. The process is similar to the general procedure of developing the model of the fruit. The fruit modelled as a 3D geometry is discretised, and material properties, such as density and stiffness, are assigned to these elements. The equations of motion are then solved numerically to determine the fruit's natural frequencies and mode shapes, as described below.

The displacement at any point in an element $u(\xi, t)$ can be expressed in terms of the nodal displacement $q^e(t)$ as:

$$u(\xi, t) = N^e(\xi).\mathrm{q}^e(t) \quad \text{Equation 6}$$

Where $N^e(\xi)$ is the shape function matrix.

The dynamic motion of the fruit can be expressed using Newton's second law:

$$F(t) = M\ddot{q}(t) + C\dot{q}(t) + Kq(t) \quad \text{Equation 7}$$

Assuming the system is not damped, the undamped vibration can be expressed as

$$F(t) = M\ddot{q}(t) + Kq(t) \quad \text{Equation 8}$$

where M is the mass matrix, C is the damped matrix, K is the stiffness matrix, q(t), $\dot{q}(t)$ and $\ddot{q}(t)$ is the displacement, velocity and acceleration vectors, and t is the time. In FE modal analysis, if free vibration is assumed, no force is applied, and correspondingly, F(t)=0. For a linear system, this vibration will be harmonic in the form:

$$q_i(t) = \phi_i \, .sin\omega_i t \quad \text{Equation 9}$$

Where ϕ_i is the eigenvector representing the ith natural frequency, ω_i is the ith natural angular frequency and t is the time.

By substituting Equation 9 into 8,

$$(K - \omega_i^2 M)\phi_i = 0 \quad \text{Equation 10}$$

For a non-trivial solution this corresponds to the following equation

$$det(K - \omega_i^2 M) = 0 \qquad \text{Equation 11}$$

Equation 6 represents an eigenvalue problem that can be solved for n values of ω^2 (eigenvalues) and n eigenvectors, where n is the number of all the degrees of freedom (DOFs). This eigenvalue problem is solved by using the Finite element method program.

Modal analysis using FEM is instrumental in understanding the dynamic response of fruits to external forces or vibrations, which can help in applications such as designs and optimisation of harvest equipment; and evaluating the quality and ripeness of fruits.

2.8.2.5.1 Fruit Internal Quality

The vibration characteristics of fruits are influenced by their mechanical and structural properties, such as density and elasticity, which are related to firmness. The firmness of pear fruit was measured using an index f_2m^2, where f_2 is the second resonant frequency, and m is the mass of the fruit (Finney, 1971). The author found that the firmness index is correlated with Young’s modulus and the shear modulus of the fruit tissue.

Chen & Baerdemaeker's (1993) investigation on the modal analysis of apples and pineapple firmness using the finite element method concluded that the firmness index $f^2m^{2/3}$ is more accurate in estimating the elastic modulus of both fruits and also, the geometry of the fruits will affect the mode shapes.

Recently, Abbaszadeh et al. (2014) and Namdari Gharaghani et al. (2020) used FEM for modal analysis of apples and oranges, respectively; they evaluated the elasticity of the fruits. Hence, the authors were able to predict the ripeness of the fruit since the elasticity of the fruit decreases as it ripens. Additionally, FEM was also used to determine the optimum locations for excitation and detecting output vibrations based on the fruit mode shapes (Abbaszadeh et al., 2014; Chen & Baerdemaeker, 1993; Namdari Gharaghani et al., 2020).

2.8.2.5.2 Harvest Optimization

Mechanised harvesting employs bulk and selective technologies (Bu et al., 2021). Selective harvesting involves a robotic harvester that uses sensors to locate the fruit and a robot arm to grasp it. In contrast, bulk technology detaches all the fruits from the tree by shaking it and collecting them with a pre-set device (a collector). A machine applies a vibrational movement to the tree trunk or canopy to achieve this, causing the fruit to detach from the branches. However, these methods are not without the downside of detachment efficiency (Gupta et al., 2016; Zhao et al., 2021), environmental complexities (Bloch et al., 2018), damage from robotic grasping (Bloch et al., 2018; Bu et al., 2020), damage because of impact on catching surface (Wang et al., 2019). The 3-D model of trees generated from CAD modelling software models the interaction of the stem, branches, fruit, and leaves (Fu et al., 2016; He et al., 2015; Niu et al., 2022; Tang et al., 2011).

In the boundary condition in tree vibration harvesting modelling, fixed support was defined at the root region, and the tree behaved like a cantilever (Fu et al., 2016). Mechanical harvesting is a complex phenomenon that involves the interaction between the machine and the tree, as well as interactions among the different parts of the tree, such as fruits, branches, and leaves. Therefore, some assumptions and generalisations must be made to efficiently model and simulate the physical phenomena. The geometry of the tree is usually simplified to save computational resources. Gupta et al. (2016) simplified the geometry of a citrus tree as a primary limb (branches originating from the primary limb) and a secondary limb (main scaffold branches originating from the trunk of the tree).

The complex variations in the physical and mechanical properties of fruit and trees affect the harvest process's computational modelling (Villibor et al., 2019). The stiffness of coffee stems was reported to vary with harvesting season, plant age, variety of coffee, and maturity stage (Coelho et al., 2015; Júnior et al., 2018). By improving the modelling process by considering these factors, Lúcio Santos et al. (2021) used a stochastic method to model macaw material properties by identifying three possible operating ranges to design macaw palm harvesting machines. The stochastic FEM was also used in determining the dynamic behaviour of macabre palm (Rangel et al., 2020) and coffee (Coelho et al., 2016).

2.9 Summary

In conclusion, studying papaya fruits' physical and mechanical properties provides an efficient strategy for minimising postharvest losses.

This chapter discussed a literature review of postharvest treatment, detailing how papaya fruit's physiology, biochemistry and biomechanics affect its economic and shelf life. The review of the physiological characteristics of fruits gave an understanding of how water content, cellular arrangement, structure, maturity index, and heterogeneity of fruits affect their mechanical properties. The mechanical properties of papaya have been reported without specific relation to longitudinal location (Sanchez et al., 2020; Zulkifli et al., 2021). Therefore, this study aims to determine if variation exists in papaya's mechanical properties along its longitudinal axis.

Also, the chapter highlights the mechanistic (or physics-based) and data-driven modelling strategies used in fruit modelling. Mass modelling using a data-driven approach provides us with a model that can be applied with a computer vision system, which can be used in sorting and grading fruit, as discussed in section 2.6.2. However, there is no published literature on the mass model of papaya fruit, which necessitates the objective of developing a mass model of papaya fruit.

Furthermore, the discussion on the finite element method (section 2.7.2) as a type of numerical method highlights the kinds of geometry modelling approach, material models used for different fruits in literature and how loading conditions are modelled and applied to solve postharvest problems. It is worth noting that the accuracy of an FE model depends on the preprocessing stage. Therefore, this study aimed to determine the suitability of different material models in the FE modelling of papaya under compressive loads.

It is essential to study the mechanical response of papaya fruit under compressive loads because compression is inevitable for the fruit located at the bottom of the packaging materials (plastic crates, corrugated fibreboard (CFB) box and bulk bins).

CHAPTER 3

MATERIALS AND METHODS

3.1 Overview

The methodology of this study was developed to achieve the objectives stated in Chapter 1. Figure 6 describes the overall workflow. The workflow of the physical properties' measurement describes the process of mass modelling of papaya fruit, which relates to objective 1, while objectives 2 and 3 workflows are described under the workflow of the mechanical response of papaya fruit. Section 3.2 covers the material and methods used in the mass modelling of papaya fruit, while Section 3.3 expounds on the mechanical response of papaya fruit.

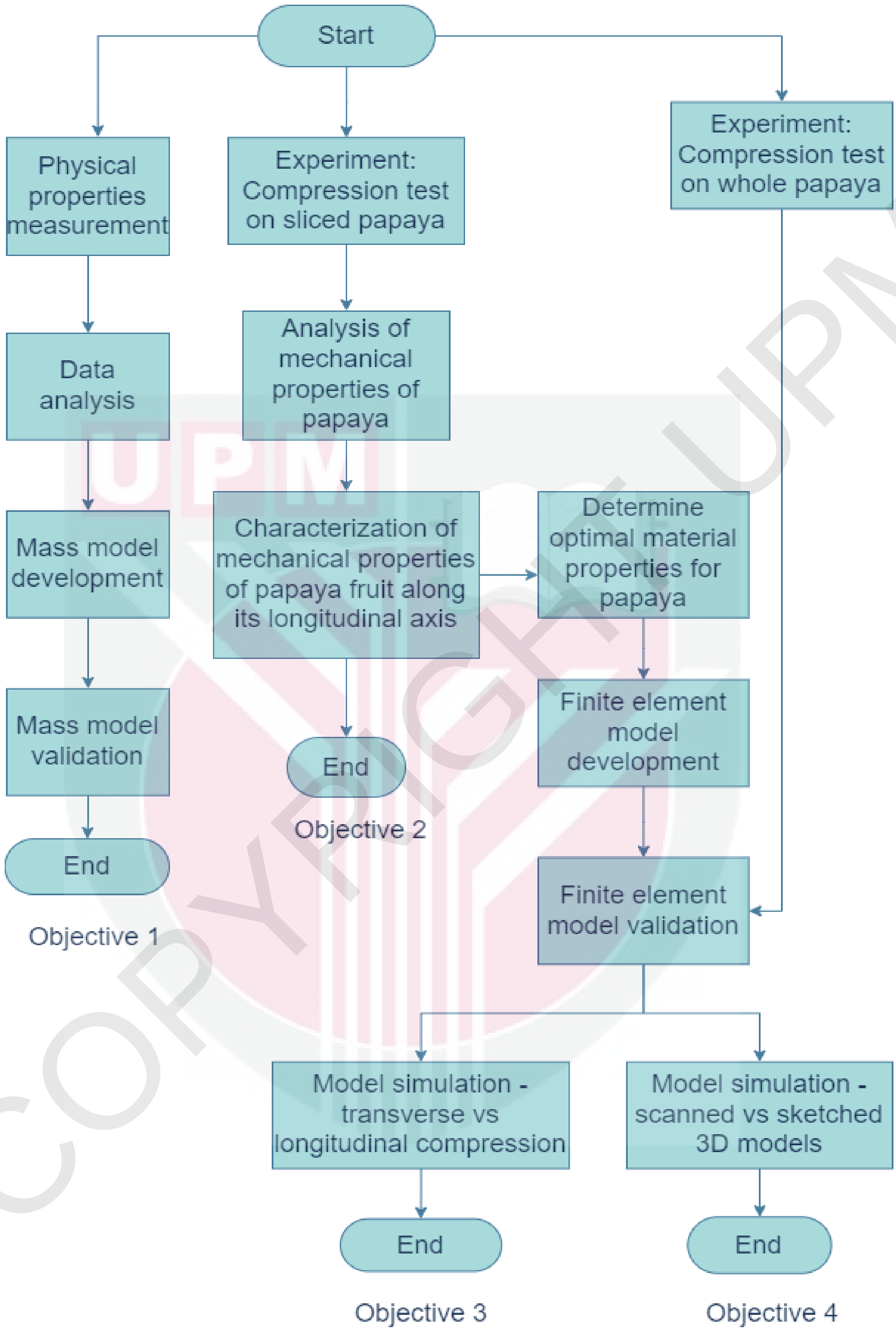

Figure 6 : Overall methodology workflow

3.1.1 Sample Collection

For this study, all *Carica papaya* ("Exotica" variety) fruits were purchased from the local market in Seri-Kembangan, Selangor, Malaysia. The fruits used in the experiment were at ripeness index 2, as determined using the standard colour chart (Figure 7) that Kwok & Liang (2019) developed. The ripeness index two was used because papaya fruits harvested at this stage are optimum for export and long-distance transportation (Barragán-Iglesias et al., 2018; Sekeli et al., 2018).

Figure 7 : The ripening index scale of the Eksotika papaya (Kwok & Liang, 2019)

3.2 Mass Modelling

This section describes the methods used to measure the geometric physical properties of papaya, a descriptive statistic of the parameters measured, and the procedure used in developing the model to predict its mass.

3.2.1 Determination of Geometric Physical Properties

Measurements were conducted on 63 fruits to determine their physical properties (Mansuri et al., 2022; Murakonda et al., 2022; Panda & Sethy, 2017). The sample size of 63 was the largest number of available fruits with a ripeness index of 2 during the experiment. A normality test was performed to verify that this sample size accurately represents the population. Three axial length measurements and mass were measured, and the mean diameter, volume, sphericity, and projected area were calculated. The axial lengths of each fruit were measured along three orthogonal axes, as depicted in Figure 8. A digital calliper was used to take precise measurements, with a sensitivity of ±0.05 mm.

$$Mean\ Diameter\ (\mathrm{D_0}) = \sqrt[3]{\mathrm{a} \times \mathrm{b} \times \mathrm{c}} \qquad \text{Equation 12}$$

$$Sphericity = \frac{\sqrt[3]{a \times b \times c}}{a} \qquad \text{Equation 13}$$

Figure 8 : An illustration of the axis: *a, b and c. a,* the longest axis measured along the longitudinal axis, *b* was measured as the axis perpendicular to *a*, and *c* was measured as the axis normal to *a* and *b*

The fruit's geometric mean diameter (D_0) and the sphericity were calculated using Equation (12) and Equation (13), respectively (Mohsenin, 1970; Sahu, 2018).

The surface area (S) measures the total area that the fruit's exterior occupies. It was derived from the mean geometric dimension described in Equation (14) (Meisami-asl et al., 2009; Mirzabe et al., 2013; Topuz et al., 2005).

$$S = \pi \times D_0^2 \qquad \text{Equation 14}$$

The projected area, a two-dimensional measurement obtained by projecting the three-dimensional object onto an arbitrary plane, plays a crucial role in modelling the mass (Mahawar et al., 2019; Mansuri et al., 2022). This parameter was computed using Equation (15) (Burubai et al., 2007; Mirzabe et al., 2013). The surface area considers all the exterior surfaces of a three-dimensional object. The projected area is a two-dimensional representation of that object.

$$P_a = \left(\frac{\pi ab}{4}\right) \qquad \text{Equation 15}$$

3.2.1.1 Descriptive Analysis of the Physical Properties of Papaya

A descriptive statistical analysis was conducted on the physical properties data, including mass, axial length dimensions, mean diameter, surface area, sphericity, and projected area. The mean, standard deviation, maximum, and minimum values were calculated to summarise and understand the characteristics of the data.

A Shapiro-Wilk normality test was also conducted to determine whether the sample data was representative. The null hypothesis of the test postulates that the distribution of the sample is normally distributed. So, if the p-value is greater than the chosen significance level (0.05), then the null hypothesis is not rejected, and we can assume that the data is normally distributed. If the p-value is less than the significance level, then the null hypothesis is rejected, indicating that the data does not follow a normal distribution (Ghasemi & Zahediasl, 2012). The calculated p-value for this test was 0.98765, suggesting that the distribution is normal.

A correlation analysis used the Pearson product-moment correlation coefficient to describe the relationship between mass and other variables. A correlation coefficient quantifies the strength and direction of the linear relationship between two variables (i.e. X and Y), as shown in Equation 16 ($-1 \leq r \leq 1$).

$$\boldsymbol{r} = \frac{\sum_{i=1}^{n}(X_i - \bar{X})(Y_i - \bar{Y})}{\sqrt{\sum_{i=1}^{n}(X_i - \bar{X})^2 \sum_{i=1}^{n}(Y_i - \bar{Y})^2}} \qquad \text{Equation 16}$$

Where: $\boldsymbol{n}$ is the number of observations, X_i and Y_i are the individual sample points and $\bar{X}$ and $\bar{Y}$ are the means for all X_i and Y_i respectively.

3.2.2 Mass Model Development

Mass modelling of fruits was carried out using seven regression models: linear, quadratic, S-curve, power, and three multiple variable models. These models are frequently emphasised in the existing literature as the most prevalent models for fruits (Khoshnam et al., 2007; Lorestani & Tabatabaeefar, 2006; Mahawar et al., 2019; Mansuri et al., 2022). The total number of samples used for the mass modelling was 63 to ensure uniformity of ripeness, and the data was split into 70% and 30% for model calibration and validation, respectively. First, the models were calibrated by determining the coefficients in each model using the curve fitting method. Once the models were defined, model validation was performed by comparing the predicted mass to the measured mass, i.e., the ground truth. All data analyses were carried out in Jupyter notebook (Anaconda 4.10.1; Python version: 3.8.8). Python libraries such as NumPy, Pandas, Matplotlib, SciPy, and Sklearn were used in the analysis (Refer to Appendix A for the code snippet of the analysis).

3.2.2.1 Model Calibration: Mass Models Using Single Variable as Predictor

The empirical models to predict papaya mass were linear, quadratic, S-curve, and power models (Table 3). Each model has two or three coefficients to be calibrated. We employed the linear regression curve fitting method for the linear equation and the non-linear regression curve fitting process for the remaining three non-linear equations using the calibration dataset to determine the models' coefficients (Mahawar et al., 2019; Mansuri et al., 2022).

Table 3 : Mass model equations

Regression Model	Equation
Linear	$M = \alpha + \beta X$
Quadratic	$M = \alpha + \beta X + \gamma X^2$
S-curve	$M = \alpha + (\frac{\beta}{X})$
Power	$M = \alpha X^{\gamma}$

Where M is mass (g), X is the variable used as the predictor of mass, and α, β, and γ are model coefficients.

3.2.2.2 Model Calibration for Mass Modelling Using Multiple Variables as Predictors

Due to the irregular shape of papaya, multiple predictors may lead to a more precise mass prediction. Three distinct modelling techniques were employed using the calibration data to model papaya mass. These techniques include ordinary least squares (OLS), last absolute shrinkage and selection operator (Lasso), and support vector regression (SVR). OLS utilises a linear equation to predict mass based on predictor variables. Lasso regression, on the other hand, modifies the cost function of regular linear regression to produce fewer overfitting models. While SVR avoids overfitting and uses a smaller number of training samples (Pedregosa et al., 2011). The multiple variable models (OLS, linear Lasso and SVR) were developed using all variables: three axial measurements, mean diameter, surface area, sphericity, and projected area to provide a robust model. Moreover, the mass of a fruit is typically influenced by several factors (Mansuri et al., 2022; Murakonda et al., 2022).

3.2.3 Mass Model Validation

Once the coefficients were established for all mass models, the predicted mass for each fruit within the validation dataset was computed across all seven models, encompassing four single-variable predictors and three multiple-variable predictors. Subsequently, the predicted mass was compared with the measured mass, facilitating a comparative analysis using the coefficient of determination (R^2) and root mean square error (RMSE) computed using Equations 17 and 18, respectively.

$$\boldsymbol{R^2} = \left[\frac{n\sum(m\ddot{m})-(\sum m)(\sum \ddot{m})}{\sqrt{[n\sum m^2-(m)^2][n\sum \ddot{m}^2-(\sum \ddot{m})^2]}}\right]^2 \qquad \text{Equation 17}$$

$$\boldsymbol{RMSE} = \sqrt{\frac{\sum_i^n (m-\ddot{m})^2}{n}} \qquad \text{Equation 18}$$

Where m is the measured mass and $\ddot{m}$ is the predicted mass.

The coefficient of determination (R^2) quantifies the extent to which the variation in the dependent variable (mass) can be explained by the independent variable(s). A higher R^2 value, approaching 1, signifies a strong fit of the model to the data, indicating its ability to predict the dependent variable effectively (Cheng et al., 2014;

Hahn, 1973). On the other hand, RMSE serves as another statistical metric to evaluate model performance, where a lower RMSE value closer to zero indicates a better fit of the model (Chai & Draxler, 2014; Sultan et al., 2018). Hence, it can be inferred that the optimal mass models for the investigated papaya species exhibit the highest R^2 and lowest RMSE values.

3.3 Mechanical Properties and Response of Papaya Fruit under Compression

The mechanical response of papaya fruit under compressive loading was investigated using experimental and finite element modelling methods. Section 3.3.1 described the methods used to investigate the variation in papaya's mechanical properties, i.e., the failure stress, failure strain, Young's Modulus, and viscoelastic parameters as a function of specimen location along its longitudinal axis. The results of the material properties in Section 3.3.1 were used as an input for defining the material properties of the finite element model of papaya (Section 3.3.2), aligning with objective 3. The technique involves the development of a finite element model to simulate the mechanical response of papaya fruit under compressive loading.

3.3.1 Characterizing Mechanical Properties of Papaya along its Longitudinal Axis

This section details the methods used in determining the mechanical properties of papaya, such as density, elastic modulus, failure stress, failure strain, and viscoelastic properties.

3.3.1.1 Sample Preparation

The papaya fruit used in this study section is the same as that described in section 3.1.1. Twenty (20) whole papaya fruits were randomly selected, and each fruit was divided along its longitudinal axis into three approximately equal sections: the top (stem end), middle, and bottom (blossom end), as illustrated in Figure 9. Then, each section was further sliced into cylindrical samples with a thickness of 30 mm. Since slices from each section of the fruit will give us more than 30 samples, we randomly selected 30 samples from each section (top, middle, and bottom), resulting in a set of 90 slices i.e. 30 slices by 3 sections. Two sets of samples were prepared for two tests: compression testing and stress-relaxation testing. The data from the compression test was used to determine the elastic and elastic-plastic material models, while the stress-relaxation test data was used for the viscoelastic material model.

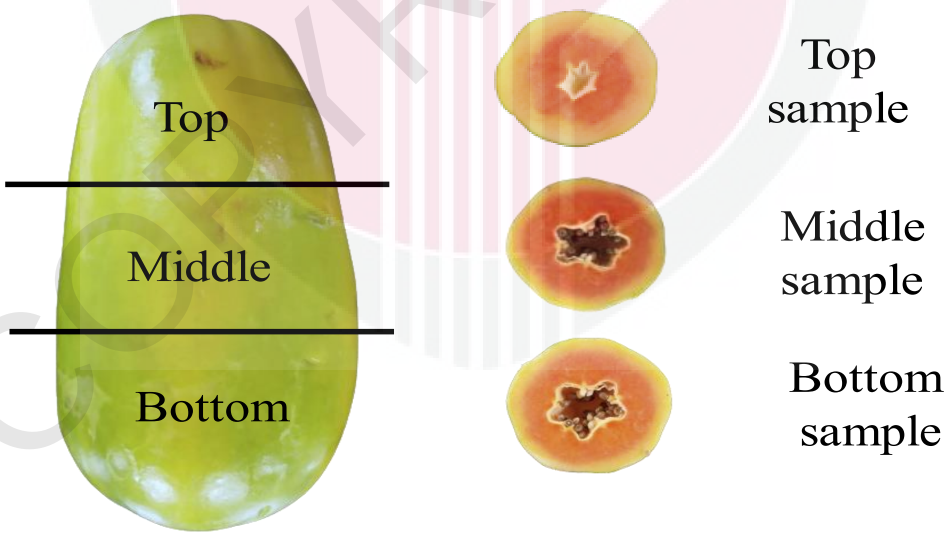

Figure 9 : An illustration sliced sample of papaya fruit for compression. Determination of Fruit Density

The volume of each whole papaya fruit was determined using the liquid displacement method. The mass (g) of the fruit was measured using a digital weighing balance (GF-10K, A&D, Japan) with a capacity of 1g –10 kg and an accuracy of ±0.01 g. The fruit density (D) was calculated using Equation 16.

$$\boldsymbol{\rho = \frac{M}{V}} \qquad \text{Equation 19}$$

Where M is the mass of the fruit (g), and V is the volume (cm^3).

3.3.1.2 Determination of Elastic Properties

The first set of cylindrical samples were laid horizontally and compressed with a compression platen of 150 mm diameter until failure (Figure 10). The ASAE S368.4 DEC2000 standard (ASAE, 2008) guided a compression speed of 10 mm/min. The stress and strain yield points of all samples for each section were averaged to obtain the stress and strain for each section.

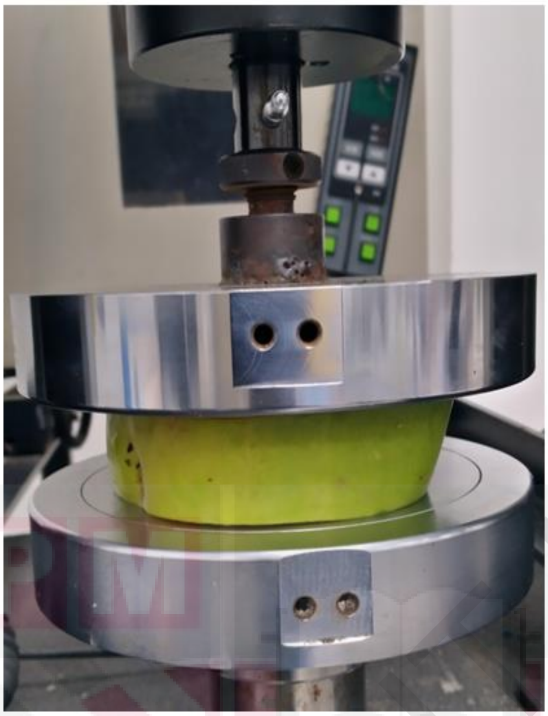

Figure 10 : Compression and stress-relaxation tests setup

3.3.1.3 Determination of Viscoelastic Properties

The stress relaxation test was carried out on the second set of cylindrical samples to determine the viscoelastic parameters using a test speed of 10 mm/min, with a hold time of 300 s (ASAE, 2008). The compression load, deformation, stress, and strain were recorded for this test. A hold time of 300s, at 20% strain was chosen to allow the stress curve to reach equilibrium without the total rupture of the sample, as shown in Figure 11. A time interval of 10s was used in the decimation. The relaxation parameters, relaxation moduli (E_e, E_1, E_2, E_3) and relaxation time (T_1, T_2, T_3) were determined by fitting the stress relaxation data to the three elements in the Maxwell model (Equations 20 and 21) using non-linear regression (Sanchez et al., 2020).

$$E(t) = E_e + E_1 e^{-t/T_1} + E_2 e^{-t/T_2} + E_3 e^{-t/T_3};\ \eta_i = E_i \times T_i \qquad \text{Equation 20}$$

$$\boldsymbol{\sigma(t) = \varepsilon_o E(t)} \qquad \text{Equation 21}$$

The relaxation function E(t) is the stress history per unit strain imposed, E_1, E_2 and E_3 are the relaxation moduli, and T_1, T_2, and T_3 are the relaxation time. η_i, E_i and T_i are the viscous coefficient, relaxation moduli and relaxation time of the i-th number of the Maxwell components respectively. E_e is the equilibrium moduli (Flügge, 1975). Equation 21 expresses the relationship between nominal stress $\boldsymbol{\sigma}(t)$ and strain $\boldsymbol{\varepsilon}_o$.

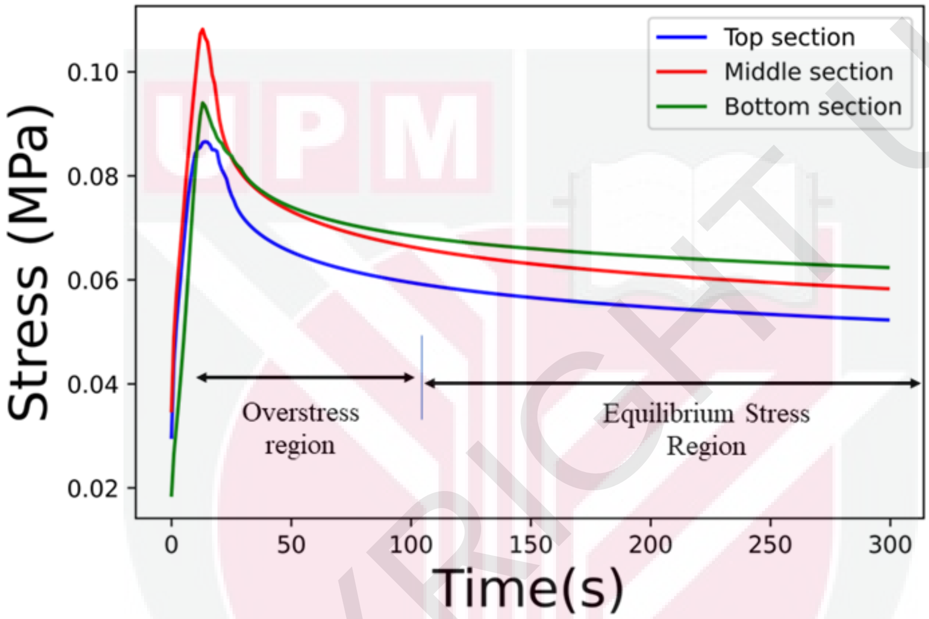

Figure 11 : A representative stress-time curve of papaya along its longitudinal axis indicating the overstress and equilibrium region using equations 20 and 21

3.3.1.4 Statistical Analysis: Analysis of Variance (ANOVA)

In order to ascertain the variations in the mechanical properties of a papaya fruit along its longitudinal axis, an analysis of variance (ANOVA) was conducted. The analysis specifically focused on the failure stress, failure strain, Young's modulus, and viscoelastic parameters to determine the mean differences among the three distinct sections of the fruit.

Following the ANOVA, a post-hoc test was performed specifically on the viscoelastic parameters. In all analyses, a significance level (P-value) < 0.05 was used. This threshold is a standard in many scientific studies, and it helps us ensure that the results obtained are not due to random chance but indicate a statistically significant difference.

3.3.2 Finite Element Modelling

3.3.2.1 Finite Element Model Setup

The finite element modelling of the mechanical response of papaya was set up using the multiphysics software ANSYS V.2023 R1. The static structural module of the module's software consists of the general workflow of solving finite element models, geometry, material properties, boundary conditions, loading conditions, and solutions to the model. The models were set up following the logical flow shown in Figure 12.

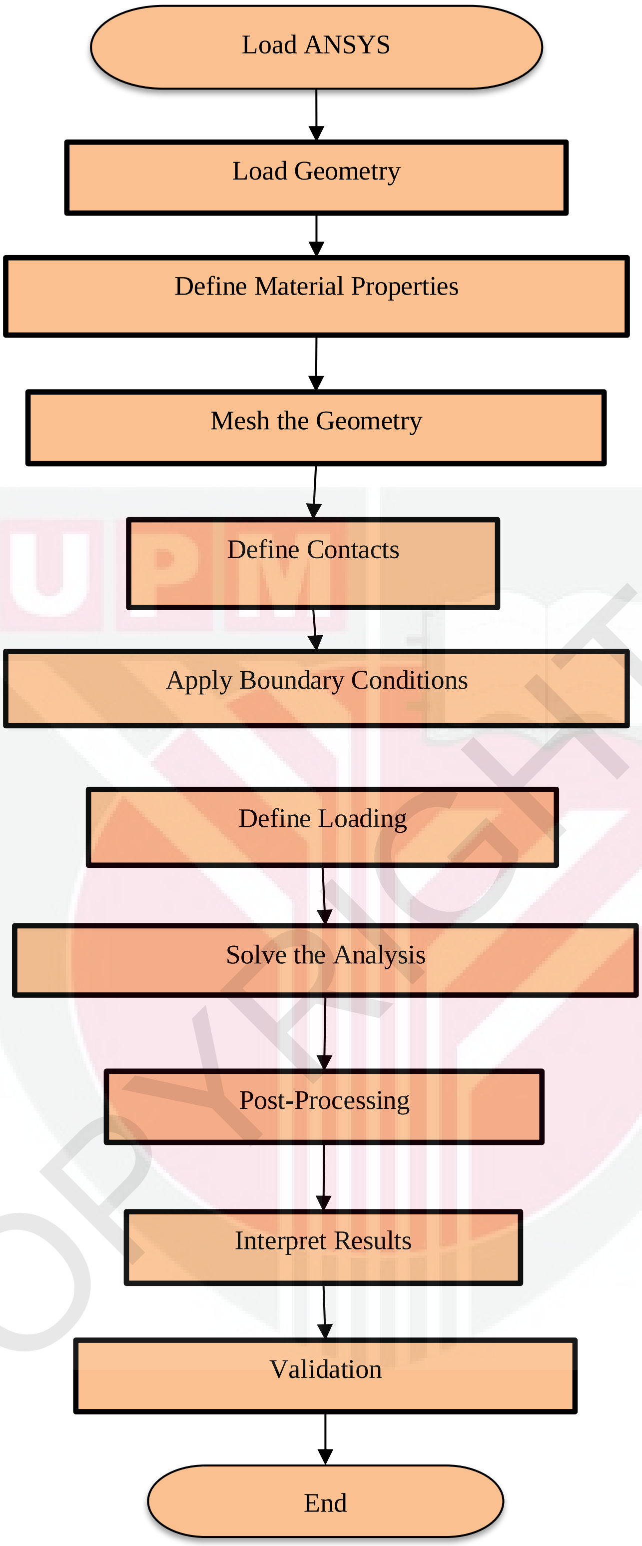

Figure 12 : Finite element modelling flowchart

Problem Formulation

In this study, finite element modelling was performed to investigate the difference in stress response of papaya under compression in two conditions:

1. When papaya is subjected to compression along its longitudinal and transverse directions.
2. When the papaya fruit model used is based on 3D scanned and sketched geometry.

The validation process for the FE model involved comparing its results with compression test data of the whole papaya fruit, which enabled the determination of the most suitable material model for subsequent FE simulations mentioned above. Table 4 presents the sequence of the key work carried out in this phase of the study.

Table 4 : Simulation objectives and the corresponding setup

Objective of simulation	Material Model	Geometry	Loading Condition
Determine the best materials model for papaya by comparing with sliced papaya experimental results, as part of the finite element model validation process	Elastic, Elastic-Plastic, and Viscoelastic model	Sliced papaya model	8 mm compression loading.
Determine the best materials model for papaya by comparing with whole papaya experimental results, as part of the finite element model validation process	Elastic, Elastic-Plastic, and Viscoelastic model	scanned models	8 mm compression loading.
Determine the best geometrical model for papaya using T-test mean comparison.	Viscoelastic model	scanned models, sketched models	16 mm longitudinal compression loading
Evaluate the differences in response due to transverse vs. longitudinal compression	Viscoelastic	Scanned models	4-, 8-, and 16-mm transverse and longitudinal loading respectively.

3.3.2.2 Geometry Models

The model's geometry must closely approximate the object to solve finite element problems more precisely. A conventional method for modelling is based on the presumption that agri-food products are uniform and symmetrical and that the objects being modelled are provided with standardised geometries such as cylinders, spheres, and cones (Anders et al., 2019). The decision whether to use simple or complex geometries in Finite Element Analysis (FEA) is critical, as each has advantages and disadvantages. Simple geometries, while computationally efficient and easier to work with, may not accurately represent the actual system, potentially resulting in errors. Complex geometries, despite their higher computational demand and meshing challenges, can provide a more accurate representation of the real system. However, the choice between simple and complex geometries ultimately depends on the specific requirements of the study, including the desired level of accuracy, available computational resources, and the complexity of the problem at hand (Anders et al., 2019; Umulis & Othmer, 2012; Zienkiewicz et al., 2013).

Geometry modelling is an essential task in food engineering, and it becomes more challenging and complex when dealing with irregularly shaped objects such as papaya (Goñi et al., 2007). The following subsections outlined the methods to generate papaya 3-D geometries: 3-D laser scanning and 2D sketching/outline.

3.3.2.2.1 3D Laser Scanning Method

Reverse engineering techniques were employed to obtain a geometry of the papaya fruit that can be converted into a solid model. The EinScan-SE V2 3D scanner from SHINING 3D Tech. Co., Ltd. Hangzhou, China (as illustrated in Figure 13a) was utilised for this purpose. The scanner performed eight scanning steps, capturing the complete surface of the fruit in both vertical and horizontal positions. Subsequently, the scanned surfaces were processed, aligned, re-meshed, and exported using the ExScan S software (v.3.1.3.0). To refine the scanned mesh further, Ansys SpaceClaim (V. 2022 R2) CAD software was employed to obtain a solid model (Figure 13b), which was later imported into Ansys Workbench for subsequent numerical analysis. Figure 14 illustrates the entire process, from 3D scanning to the final geometry model. This comprehensive methodology ensured the accurate representation of the papaya fruit's geometry, facilitating precise numerical simulations of its deformation behaviour.

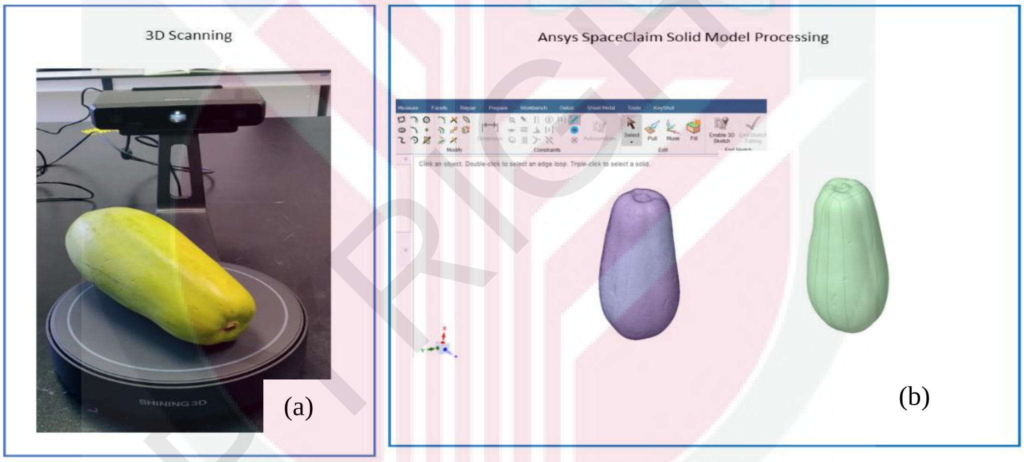

Figure 13 : 3D Solid modelling of papaya fruit. (a) – scanning of the fruit (b) – converting scanned model to solid model

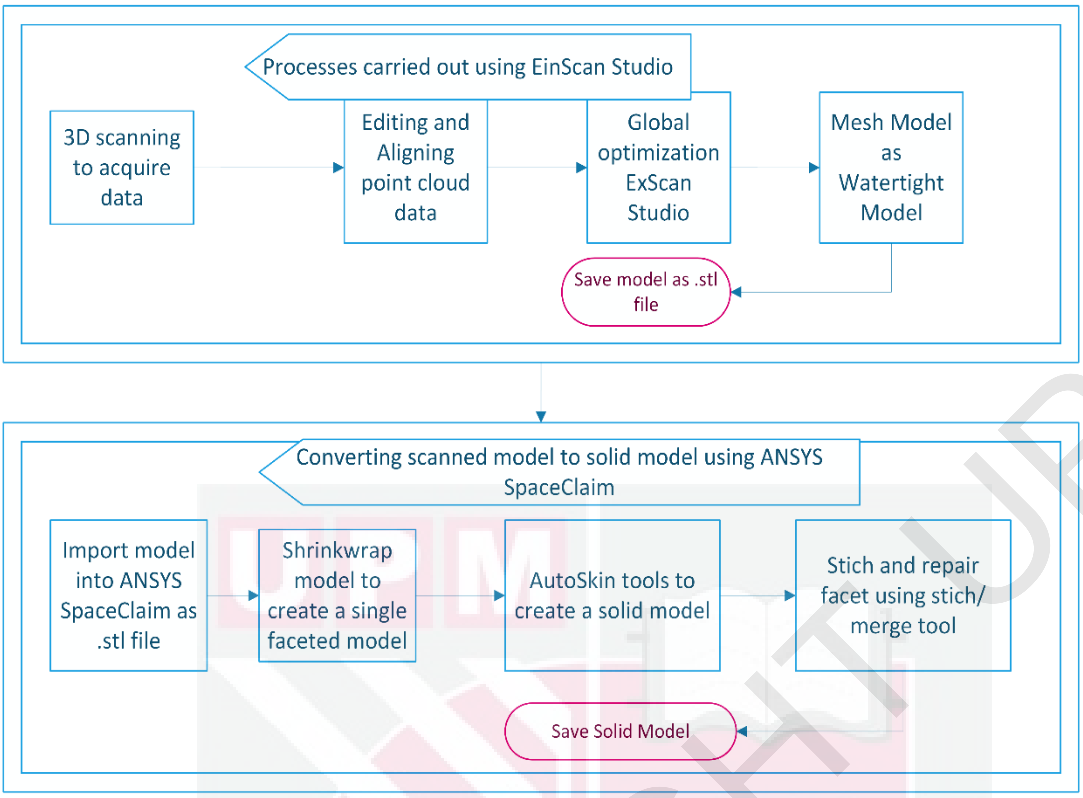

Figure 14 : Reversed engineering process of the scanned model

3.3.2.2.2 2D Sketching/Outline Method

A second 3D model was developed directly in ANSYS SpaceClaim software, by outlining the shape of papaya based on 2D images. A papaya fruit was selected and cut into half. Then, the cut surface was photographed using a smartphone camera with a 13 MP, f/1.8 specification. The image was loaded into ANSYS SpaceClaim, and a spline tool was utilised to trace the ¼ fruit's outer edge, resulting in an axisymmetric sketch of the fruit model (Figure 15(a)). The sketch was then appropriately scaled to match the geometric measurements of the scanned model. To obtain a 3D model based on the traced the profile, it was revolved 270° along the y-axis (Figure 15(b)).

The dissimilarity between Figure 15 (a) and (b) arises from the methods employed in the creation of the geometry model. Figure 15 (a) is a direct image cut from papaya fruit, preserving the natural contours of the fruit. In contrast, Figure 15 (b) is a digitally traced profile of the fruit and subsequently revolved 270° in ANSYS SpaceClaim, intended to depict an idealized version of the fruit's geometry for FE modelling purposes. This process reduces irregularities in the traced profile, leading to a more uniform shape in the modelled representation.

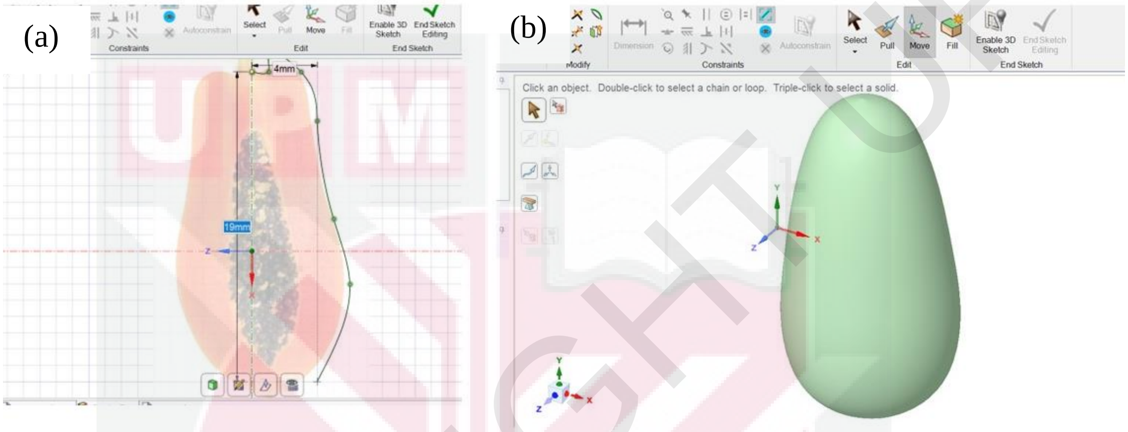

Figure 15 : Creation process of the simplified geometry model. (a) tracing the fruit edge where the green line represents the traced profile (b) the resulting 3d solid model

3.3.2.3 Defining the Material Properties of the Model

Next, the material properties were defined for the models. This study considered the papaya fruit model as a homogenous and isotropic material. Three different material models were employed: elastic, elastic-plastic, and viscoelastic. The parameters of each material model were determined through the experimental procedure described in Section 3.3.1. Specifically, the material properties of the bottom section of the papaya fruit were selected to define the material models of the finite element model based on the observations made in Objective 2 (refer to Section 4.2). These observations highlighted that the bottom section has a decreased resistance to damage, as demonstrated by its lower elastic modulus. This decision adopts a more cautious design strategy which adopts the material model for the area with the highest susceptibility to mechanical damage to ensure a safer design approach. The elastic model's parameters are density, elastic modulus, and Poisson's ratio. The elastic-plastic model incorporated parameters such as yield stress, tangent modulus, density, elastic modulus, and Poisson's ratio. Finally, the viscoelastic model was formulated with relative moduli and relaxation time in addition to the properties used in the elastic model. The relative moduli measure the ratio of the instantaneous modulus to the equilibrium modulus, while relaxation time measures the time required for the stress to decay to a certain fraction of its initial value. The stress relaxation test was used to obtain the stress-time data, as explained in section 3.3.1.4. The relaxation parameters, relaxation moduli (E_1, E_2, E_3) and relaxation time (T_1, T_2, T_3) were determined by fitting the stress relaxation data to the Maxwell model (Equations (20) and (21)) using non-linear regression. The instantaneous modulus E_0 is expressed by Equation (22), and the relative modulus β_i of each component of the Maxwell model is expressed by Equation (23).

$$\boldsymbol{E_o = E_e + E_1 + E_2 + E_3} \qquad \text{Equation 22}$$

$$\beta_i = \frac{E_i}{E_o} \qquad \text{Equation 23}$$

The Poisson's ratio, one of the input parameters for all the material models, was sourced from Zulkifli et al. (2021). Table 5 details the parameters defining the three material models, the parameters were extracted from the experiment carried out in Section 3.3.1.

Table 5 : The parameters for elastic, elastic-plastic and viscoelastic material models of the bottom section of papaya fruit

Material Model	Parameters						
	Density (kg/m^3)	Elastic Modulus (MPa)	Yield stress (MPa)	Tangent modulus (MPa)	Relative Moduli (MPa)	Relaxation time (s)	Poisson' s ratio
Elastic	990	0.50635	-	-	-	-	0.43
Elastic-Plastic	990	0.50635	0.06791	0.30931	-	-	0.43
Viscoelastic	990	0.50635	-	-	0.2688, 0.16711, 0.1547	1.77, 45.32, 103.83	0.43

3.3.2.4 Meshing of the 3D Models

A half-papaya model was employed throughout this investigation to optimise computational efficiency (Celik et al., 2021; Li et al., 2017). By utilising half-papaya, the computational resources needed were significantly reduced, and the analysis took advantage of the inherent symmetry along the sectioned plane. Before using the half-papaya model, whole papaya fruit was used for the simulation; the computational time per simulation took an average of 12 hours with error messages of incomplete calculation or convergence errors on a 2.5GHz 32GB memory Dell desktop tower. The half-papaya model significantly reduced this time due to the inherent symmetry along the sectioned plane, which optimised computational efficiency (the simulation time per simulation was reduced to less than 2 hours). The papaya fruit model was meshed using the path conforming algorithm and Tetrahedrons element type. Initially, a 10mm mesh size was assigned to the model. Subsequently, mesh convergence was checked on the stress response with each reduction in mesh size to ensure that further changes in mesh size would not affect the result. The reported results were carefully evaluated to ensure that changes in the response remained below 5% (Ansys Help Documentation, 2023).

3.3.2.5 Boundary Condition

To solve the finite element model correctly, appropriate boundary conditions are essential. In this study, fixed support was applied to the lower plate of the model setup, while the upper plate was permitted to move along the y-direction to compress the fruit model. The upper plate was constrained in other directions to prevent rigid body motion. Frictional contact was defined between the plates and the fruit model, where a frictional coefficient of 0.2 was assigned. The choice of the frictional coefficient value of 0.2 between the steel plates and the papaya model was determined based on the findings reported by Sahu (2018).

3.3.2.6 Finite Element Model Validation

To validate the simulation results, the outcomes obtained from the material models were compared with the results of the actual compression experiments.

The compression tests were performed on whole papaya fruits using a universal testing machine (10 kN INSTRON 5566, UK), operating at a speed of 10 mm/min. The testing procedure for all samples was terminated upon the appearance of a visible crack on the fruit.

The exact loading rate of 10mm/min was considered for both simulation and experiment (Liu et al., 2023; Miraei Ashtiani et al., 2019a; Sadrnia et al., 2008;

Seyedabadi et al., 2015). The Root Mean Square Error (RMSE) was used as a metric to evaluate the agreement between the simulated and experimental results.

$$RMSE = \sqrt{\frac{\sum_{i=1}^{N} \left(\sigma_{model} - \sigma_{exp}\right)^2}{N}} \qquad \text{Equation 24}$$

Where $RMSE$ is the root mean square error as a measure of accuracy, σ_{exp} is the stress at a particular deformation and σ_{model} is the average Von-Misses stress at the same compression deformation and N is the number of deformation points.

3.3.2.7 Simulation of Papaya under Longitudinal vs Transverse Compression

The fruit model was loaded in both longitudinal and transverse directions Figure 16. This was done to determine the susceptibility of papaya fruit to loading directions. Compression load was applied on the fruit model at multiple stages of 4 mm, 8 mm, and 16 mm deformations. The compression loading was stopped at 16 mm deformation since the experimental data of the whole fruit shows that the yield point was less than 16mm.

(a)

(b)

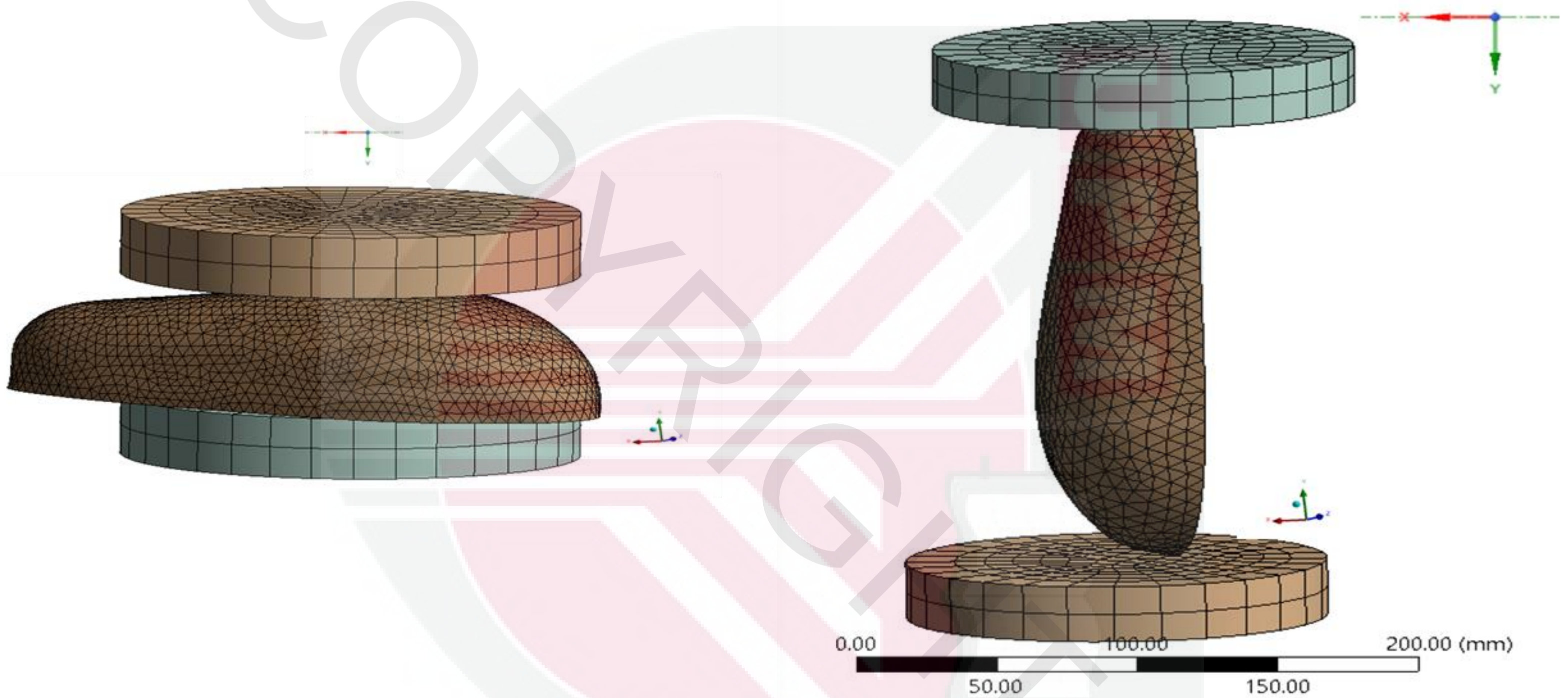

Figure 16 : Illustration of loading directions. (a) Transverse loading, (b) Longitudinal loading. The bottom plate remains static, while the upper plate is constrained to move only in the vertical or y-direction

CHAPTER 4

RESULTS AND DISCUSSION

4.1 Geometric Physical Properties of Papaya

The physical parameters significantly affect the design and development of postharvest handling machines (Mahawar et al., 2019). The descriptive statistical analysis of the geometric physical properties of the papaya samples is presented in Table 6.

The mass of the papaya samples (n= 63) exhibited considerable variation, ranging from 655.13 g to 2089.49 g, with an average value of 1298.68 ± 319.46 g. Regarding dimensional properties, the papayas' dimensions a, b, and c were 22.37 ± 1.97 cm, 10.50 ± 1.03 cm, and 8.93 ± 1.26 cm, respectively. Notably, the Exotica papaya variety demonstrated larger dimensions compared to the golden papaya variety. Specifically, the Exotica papaya's major dimension (length) measured 22.37 ± 1.97 cm, whereas the golden papaya had a major dimension of 13.83 ± 0.93 cm (Santos Pereira et al., 2018).

The p-values from the Shapiro-Wilk test were higher than 0.05, indicating that the parameters were distributed normally (Table 6). Figure 17 displays the correlation coefficients for the measured properties. Notably, mean diameter, projected area, and surface area exhibit strong correlations with mass, while sphericity exhibits a weak correlation with mass. This emphasises the close connection between mass, projected area, surface area, and mean diameter. Consequently, changes in these parameters will likely cause changes in papaya mass. On the other hand, Sphericity exhibits a very weak correlation with mass, indicating minimal influence on mass prediction.

Table 6 : Physical properties of papaya (n = 63)

Parameters	Mean	Standard deviation	Maximum	Minimum	Shapiro-Wilk statistics	p-value
Mass (g)	1298.684	319.459	2089.490	655.130	0.970	0.125
a (cm)	22.366	1.972	26.839	19.006	0.963	0.057
b (cm)	10.500	1.029	12.756	7.602	0.981	0.429
c (cm)	8.934	1.263	11.234	5.987	0.976	0.263
Mean diameter (cm)	12.777	1.194	15.367	9.761	0.968	0.101
Surface area, (cm^2)	517.313	95.737	741.869	299.306	0.967	0.092
Sphericity	0.572	0.039	0.667	0.478	0.993	0.984
Projected area, (cm^2)	185.032	28.429	254.130	121.991	0.981	0.442

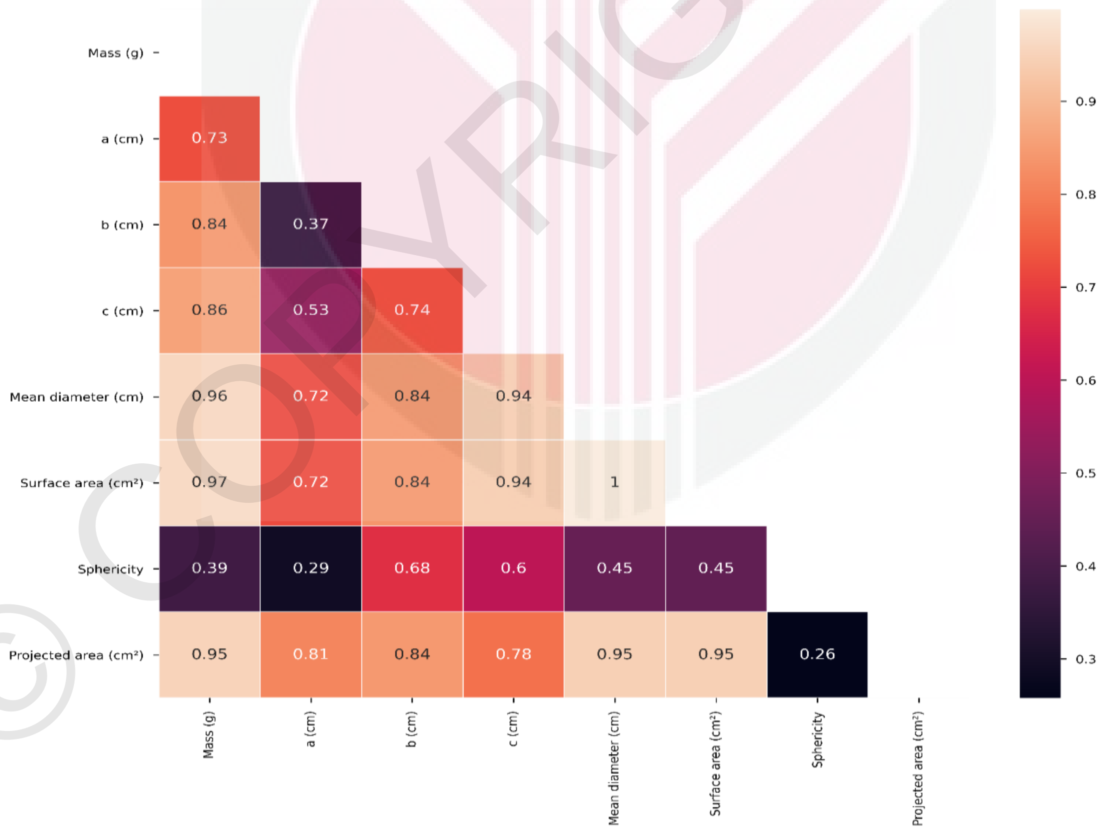

Figure 17 : Correlation coefficient matrix between geometric physical properties variables and mass

4.1.1 Mass Modelling

This section evaluated and discussed the results of the single-variable and multiple-variable mass modelling for papaya fruits. The developed mass models provide an objective and efficient solution. By integrating these models with computer vision technologies, we can automate the sorting and grading process based on papaya mass. This not only enhances accuracy but also significantly reduces the workload.

4.1.1.1 Single Variable Mass Modelling

The accuracy of the models was determined using the R^2 and RMSE values obtained by comparing the predicted and the measured mass of the validation dataset. Table 8 gives a detailed description of the developed model of papaya fruit mass using a single variable of the physical properties. When the mean diameter was utilised as the only predictor of the mass, the results indicate that the power model (R^2 = 0.940 and RMSE =87.724 g) outperforms the quadratic (R^2 = 0.939 and RMSE = 88.214 g), linear (R^2 = 0.908 and RMSE = 108.588 g) , and S-curve models (R^2 = 0. 823 and RMSE = 150.673 g). A similar outcome was observed when using surface area and projected area to develop the mass model, i.e., the power and quadratic model (R^2 = 0. 947 and RMSE = 82.28 g) demonstrates better performance than the linear (R^2 = 0.945 and RMSE = 84.267 g) and S-curve models (R^2 = 0. 885 and RMSE = 1521.557g). The single-variable mass modelling results confirmed the correlation analysis (Figure 17), whereby the mean diameter, surface area and projected area are reliable predictors for papaya mass. At the same time, sphericity is a poor predictor for papaya mass (Refer to Table 7).

The most suitable models for predicting the mass of fruits vary with the type of fruit and the variables employed in the model development. Single geometrical property as a predictor for the mass of uniform-shaped fruits, including tomatoes, pomegranates, mandarin oranges, and apples, have been reported in previous studies (Khoshnam et al., 2007; Mahawar et al., 2019; Mansuri et al., 2022; Murakonda et al., 2022; Nyalala et al., 2019). For irregular-shaped fruits, a similar outcome was reported for mangoes, where the power model with a combination of three axial lengths resulted in the best mass prediction (Spreer & Müller, 2011).

Table 7 : Statistical parameters of single variable mass models for papaya fruits

Model	Model Parameters	a	b	c	Mean Diameter	Surface Area	Sphericity	Projected Area
Linear	α	-1287.620	-1347.660	-594.276	-2101.410	-408.280	-583.155	-650.207
	β	114.732	250.335	209.812	265.121	3.281	3235.414	10.470
	R^2	0.535	0.708	0.797	0.908	0.931	0.064	0.945
	RMSE (g)	244.265	193.526	161.249	108.588	94.288	346.408	84.267
Quadratic	α	-4564.689	1577.122	2238.135	527.639	-162.878	9821.234	98.502
	β	405.604	-314.187	-429.326	-146.151	2.329	-32873.942	2.267
	γ	-6.412	27.009	35.458	15.973	0.001	31210.122	0.022
	R^2	0.529	0.720	0.816	0.939	0.939	0.095	0.947
	RMSE (g)	245.784	189.359	153.534	88.214	88.461	374.667	82.793
S-curve	α	3901.850	3798.692	3069.204	4662.445	2970.399	3066.25	3128.691
	β	-58300.212	-26216.265	-15722.211	-42846.407	-846442.054	-1025.086	-334039.909
	R^2	0.527	0.650	0.704	0.823	0.752	0.082	0.885
	RMSE (g)	246.193	211.839	194.913	150.673	178.265	343.084	121.557
Power Model	α	2.909	8.986	47.407	1.547	0.343	2930.631	0.454
	γ	1.957	2.105	1.502	2.633	1.316	1.503	1.521
	R^2	0.531	0.721	0.811	0.940	0.940	0.058	0.947
	RMSE (g)	245.274	189.132	155.552	87.724	87.724	347.514	82.284

Where α, β, and γ are model coefficients.

4.1.1.2 Multiple Variable Mass Modelling

Table 8 presents the results of the multiple variable models (OLS, linear Lasso and SVR) using all variables: three axial measurements, mean diameter, surface area, sphericity, and projected area. The OLS outperforms other models in predicting papaya's mass with R^2 and RMSE values of 0.9479 and 81.7232 g, respectively. Mansuri et al. (2022) reported that SVR had the best accuracy in predicting the mass of Ber apple using the projected area (R^2 = 0.968).

The study highlights the importance of considering a combination of physical properties for an accurate mass estimation. The optimal single-variable and multiple-variable mass models resulted in comparable performance, namely R^2 ~0.95 and RMSE of ~82 g. The single-variable mass model used the projected area as the predictor, combining two axial lengths, *a* and *b*.

Table 8 : Performance metrics of multiple variable mass models for papaya fruits

Model	**R^2**	**RMSE (g)**
OLS	0.9479	81.7232
Lasso	0.9440	84.6965
SVR	0.9464	82.8313

4.2 Mechanical Properties of Papaya

4.2.1 Elastic Modulus

The whole fruit was sectioned into three sections along its longitudinal axis. The elastic modulus was determined experimentally, and results show that it reduces from top to bottom, as shown in Figure 18(a). The elastic modulus of the top section has an average value of 0.5063 ± 0.19 MPa, the middle section has a value of 0.4242 ± 0.20

MPa, and the bottom section has a value of 0.39162 ± 0.19 MPa. From the comparison test, the difference in the means of the elastic modulus at different locations is insignificant at $P < 0.05$. Nevertheless, the decrease in elastic modulus indicates that the bottom end of the fruits is more delicate and susceptible to mechanical damage than the top region. Wang et al. (2019, 2020) also characterised the damage degree of litchi fruit as the change in elastic modulus.

The mean yield stress limit, also known as the failure stress of the top, middle and bottom locations in this study, was found to be 0.0679 ± 0.02 MPa, 0.0619 ± 0.02 MPa, and 0.0454 ± 0.01 MPa, respectively. Similarly, Zulkifli et al. (2021) reported a yield stress limit of 0.05 MPa for the exotic variety of papaya flesh tissue. Arrázola et al. (2021) also reported 0.0731 ± 0.0021 MPa for the stress yield limit of the Tainung F1 papaya.

The average force to cause failure on the top, middle and bottom sections was 459.96 ± 146.39 N, 522.09 ± 160.43 N, and 352.85 ± 149.36 N, respectively. The average force to cause a bio-yield in a non-climacteric fruit such as pomegranates ranges from 295.24 N to 162.64 N during harvest to five months of storage (Arendse et al., 2014). The bio-yield force of a woody apple was reported to be less than 5.9 kN (Murakonda et al., 2022). The mean failure force for a whole grapefruit was reported as 431.15 ± 21.09 N along the longitudinal axis (Miraei Ashtiani et al., 2019). The fruit failure of cantaloupe under compression was found to occur at 45 mm deformations or force equivalent of 730 N (Seyedabadi et al., 2015). Therefore, using the same postharvest handling process as with these other fruits will lead to losses because they have mechanical failure properties different from papaya.

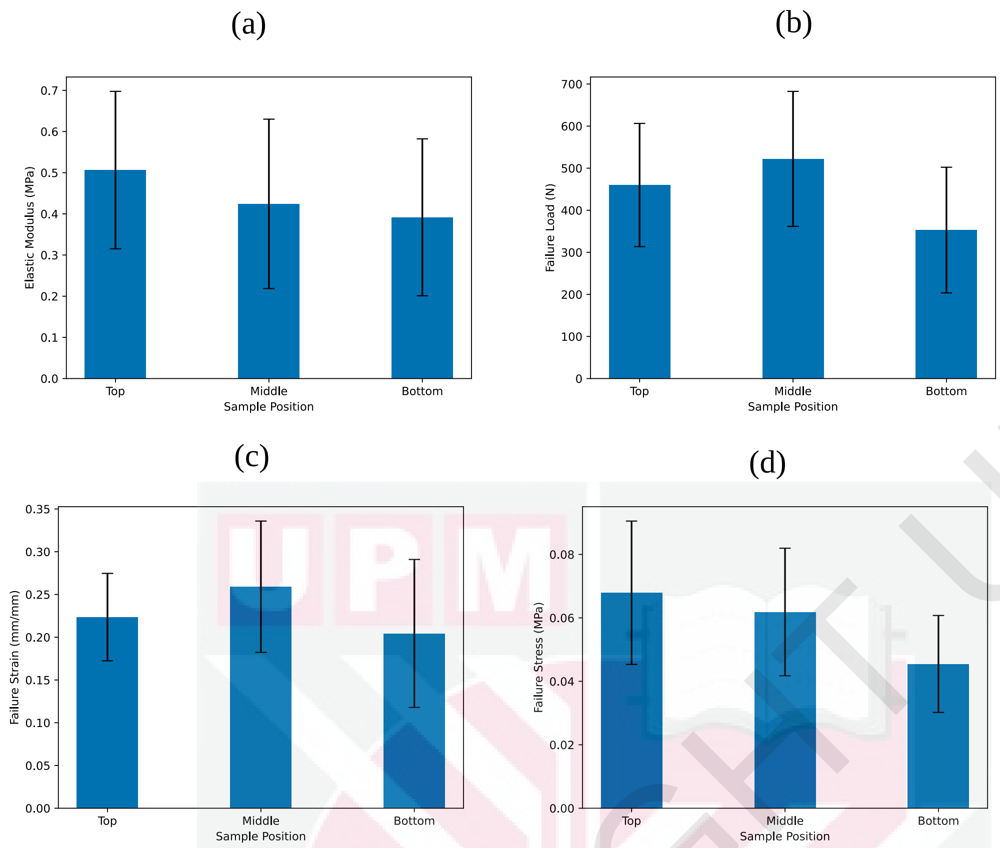

Figure 18 : The average and standard deviation (n = 30) of (a) elastic modulus (b) failure load (c) failure strain (d) failure stress along the longitudinal axis. no significant difference ($p < 0.05$) was observed in all variables with respect to locations

4.2.2 Viscoelastic Parameters

Fruit structure may be considered a multiscale continuity structure (Cáez-Ramirez et al., 2015; Ghysels et al., 2010; Ho et al., 2009). In the case of papaya tissue, its mechanical behaviour can be described using Maxwell elements (Sanchez et al., 2020). The ANOVA test results in Table 9 show that the locations along the longitudinal axis significantly influence the value of the spring component, i.e., the relaxation moduli (E_0, E_1, E_2, and E_3) ($p < 0.05$), but not the dashpot component, i.e., the relaxation time (T_1, T_2). However, the longitudinal location significantly influences one of the dashpot components, T_3 ($p < 0.05$).

The location along the longitudinal axis significantly influences relaxation moduli and one of the relaxation time, T_3 components in papaya. The instantaneous modulus (E_0) reduces along the longitudinal axis, ranging from 0.1078 ± 0.023 MPa, 0.1019 ± 0.003 MPa, and 0.1010 ± 0.002 MPa for the top, bottom, and middle sections. The first spring (E_1) and dashpot element (T_1) decrease along the longitudinal axis; this represents the deformation of the primary cell wall and the middle lamella (Karaman et al., 2016; Sanchez et al., 2020).

The components E_2, E_3, T_2, and T_3 reduced along the longitudinal axis. Yildiz et al. (2013) highlighted that these components are linked to cell structural features, and the magnitude of the relaxation moduli is directly proportional to the strength of the cell wall. Higher strength indicates that the wall has higher resistance to deformation. Since the top section of papaya fruit exhibits the highest relaxation moduli compared to the middle and bottom sections, it can be deduced that the top section cell walls is more resistant to deformation. The relaxation time (T_1) is when the force applied to the viscoelastic material dissipates to approximately 36.8% of the initial value (Mohsenin, 1970; Yildiz et al., 2013). The value of T_1 reduces along the longitudinal axis.

Chen (1994) described the components of the Maxwell model in relation to fruit tissue based on their time constants. T_1, as the short-time intercellular gases, can only sustain a load. T_2 as a medium time for the intercellular liquid flow. T_3 represents the cells as a whole and has a long relaxation time constant because fluids inside them move in and out slowly. As a result, when the fruit is subjected to a constant load, the stress on each tissue component changes over time. Overall, the result of the viscoelastic parameters implies that the tissue located at the bottom section of papaya behaves differently under mechanical load from those at the top and middle sections due to differences in the cell structure compositions.

Table 9 : Maxwell viscoelastic parameters (E_0, Ee, E_1, E_2, E_3 are relaxation moduli; T_1, T_2, T_3 are relaxation time)

	E_0(MPa)	E_e (MPa)	E_1(MPa)	E_2(MPa)	E_3(MPa)	T_1(s)	T_2(s)	T_3 (s)	η_1	η_2	η_3	R^2
Top	0.1078 ± 0.023^a	0.0422 ± 0.01334^a	0.03121 ± 0.0260^a	0.01801 ± 0.0062^a	0.0163 ± 0.0040^a	1.77 ± 1.067^a	45.31 ± 72.60^a	103.83 ± 47.84^a	0.07552 ± 0.144a	0.8707 ± 1.40^a	1.7342 ± 0.95^a	0.999 ± 0.0013^a
Middle	0.1019 ± 0.0034^a	0.04761 ± 0.0116^a	0.02293 ± 0.0071^{ab}	0.0155 ± 0.0036^{ab}	0.0158 ± 0.0041^a	1.7 ± 0.50^a	28.52 ± 40.99^a	117.53 ± 35.66^{ab}	0.0404 ± 0.021a	0.5357 ± 0.97^a	1.860627 ± 0.75^a	0.999 ± 0.0002^a
Bottom	0.101 ± 0.0019^a	0.05666 ± 0.008^b	0.016879 ± 0.0048^b	0.013967 ± 0.0018^b	0.01349 ± 0.0028^b	1.68 ± 0.44^a	15.45 ± 2.27^a	130.11 ± 12.63^b	0.0291 ± 0.013a	0.2160 ± 0.045^a	1.7596 ± 0.43^a	0.999 ± 0.0001^a
f-value	2.2742	11.3224	6.3047	6.1415	4.6153	0.0996	2.7698	3.7915	2.4849	3.0825	0.2340	2.8771
p-value	0.1097	0.00005	0.00291	0.00335	0.0128	0.9053	0.0689	0.0269	0.0899	0.0515	0.7918	0.0624

The values with the same letter indicate no significant difference, while different letters show significant differences ($p < 0.05$).

4.3 Finite Element Analysis

The result of the problem formulation discussed in section 3.3.2.2 was discussed in this section. The suitability of the material models concerning model validation was discussed, followed by the effect of the geometry modelling technique. Finally, the mechanical response of papaya fruit under different loading orientations and displacements was discussed.

4.3.1 Finite Element Model Validation

In this study, a comparison of three different constitutive behaviours, viscoelastic, elastic, and elastic-plastic, to study the effects of varying material models on the deformation behaviour of papaya. We used finite element analysis to simulate the compression of sliced and whole papaya samples and compared the results with experimental data (Tables 10 and 11).

Figures 19 and 20 shows the finite element model validation outcomes by comparing between the simulated and experimental stress-strain data for the sliced and whole fruit samples respectively. The results were presented up to 60% compressive strain, this focused on the most relevant range for the whole fruit's mechanical behaviour. This range was chosen because it encompasses the bioyield point, which is critical for understanding the fruit's structural integrity. The bioyield for the tested fruit is consistently less than 60%, hence the decision to present the data within this range. Additionally, Figures 21-23 depict the von Mises stress distribution of the finite element model following compression in the longitudinal direction to a vertical displacement of 16 mm.

The colour scale indicates the magnitude of stress in MPa. A distinct stress concentration is observed at the contact point between the compression plate and the fruit.

The elastic and elastic-plastic-model showed the worst fit with the experimental data for the bottom sliced section and whole papaya samples, with the highest RMSE values of 0.064 MPa, respectively. This implies that the elastic model and elastic-plastic is not suitable for simulating the deformation behaviour of papaya, as it ignores any nonlinear or time-dependent behaviour of the fruit.

The viscoelastic model showed the best fit with the experimental data for both the bottom sliced sample and whole papaya, with the lowest RMSE values of 0.015 MPa and 0.0001 MPa, respectively. This suggests that the viscoelastic model can account for the time-dependent properties of the papaya fruit but only for long-duration loading or dynamic conditions.

According to the linear elastic model, the papaya fruit will deform linearly when compressed and adhere to Hooke's law. Any nonlinear or time-dependent behaviour is ignored by this model (Liu et al., 2023). Arrázola et al. (2021) used an elastic material model in the modelling study for the deformation of Tainung F1 papaya; the authors reported a minimum and maximum percentage error of 2.5 % and 25.01 %, respectively. Yousefi et al. (2016) reported that the range of error, both minimum and maximum, in predicting the bruised area of a pear using an elastic model was determined to be 0.00 and -60.50%, respectively. The elastic-plastic material model captures the permanent deformation of a material at a high-impact load. Celik (2017) reported a relative error of less than 10% using the elastic-plastic model.

The viscoelastic has an RMS error of 0.0001 MPa for the whole fruit compression (equivalent of mean relative error of 12 %). The viscoelastic model can be considered suitable because it considers the time-dependent properties by incorporating both elastic and viscous characteristics. However, this might not be the case under impact load because only the viscoelastic material model's elastic properties will be the model's only apparent mechanical behaviour (Gao et al., 2018). Dintwa et al. (2008) reported a justification for this phenomenon. They reported that the relaxation time constants are substantially more significant than the collision time, thereby rendering it plausible that the colliding material may not have sufficient time to undergo the stress relaxation effect. The viscoelastic model is more appropriate for simulating long-duration loading or dynamic conditions because it provides better predictions of the papaya's behaviour over time.

Table 10 : Comparison of Root Mean Square Error (RMSE) values for viscoelastic, elastic, and elastic-plastic material models equivalent stress response at different sample locations in the papaya fruit

Material Sample Locations	Viscoelastic RMSE (MPa)	Elastic RMSE (MPa)	Elastic-Plastic RMSE (MPa)
Top	0.006	0.064	0.035
Middle	0.006	0.043	0.043
Bottom	0.015	0.064	0.064

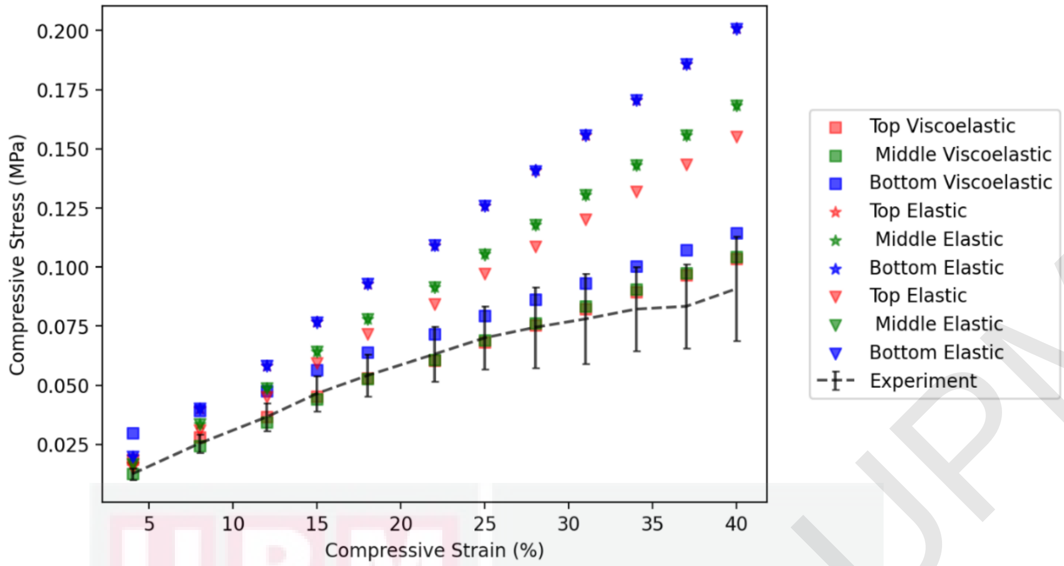

Figure 19 : Comparison of stress-strain relationships across various material models (elastic, elastic-plastic, viscoelastic) for the three sections (top, middle and bottom) in a papaya fruit. The experimental result from compression tests conducted on sliced samples on the bottom section (dashed line) is also included for comparison

Table 11 : Comparison metrics of different material models

Comparison Metrics	Viscoelastic	Elastic	Elastic-Plastic
RMSE (MPa)	0.0001	0.0064	0.0064
Mean Relative Error (RE) (%)	12.06	67.26	67.17
Maximum RE (%)	0.65	6.73	7.22
Minimum RE (%)	19.01	112.80	112.75

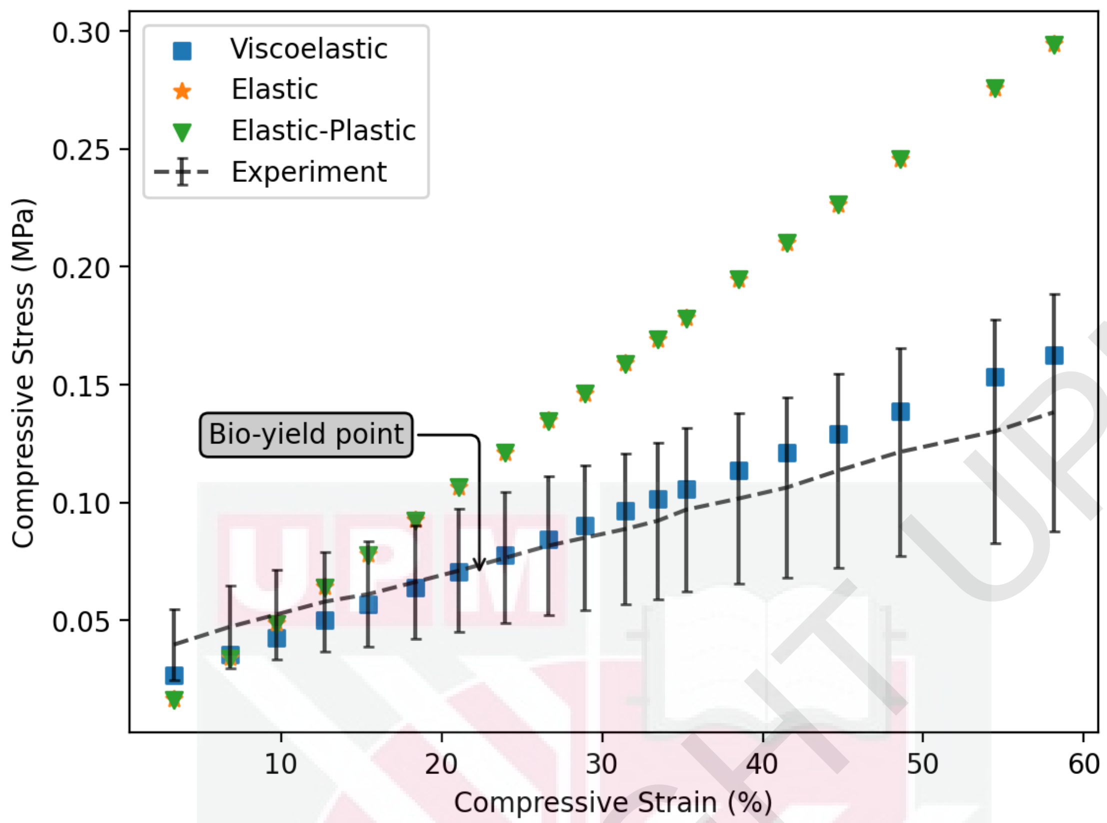

Figure 20 : Comparison of stress-strain relationships across various material models (elastic, elastic-plastic, viscoelastic) for whole papaya fruit. the experimental result from compression tests conducted on whole papaya fruit (dashed line) is also included for comparison

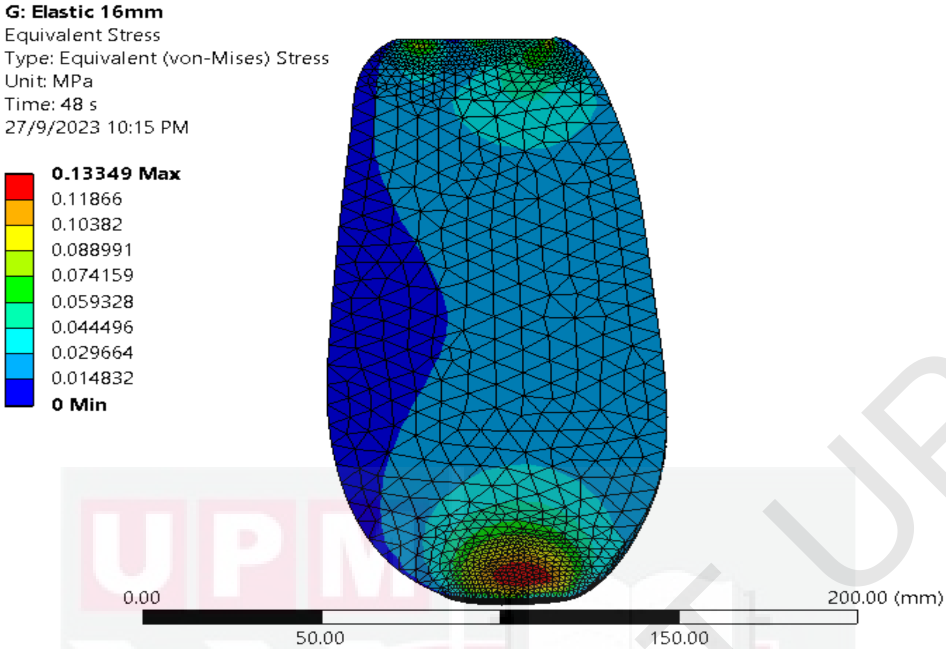

Figure 21 : Stress distribution (MPa) of elastic model at 16 mm compression. maximum stress at contact point; minimum stress at opposite end

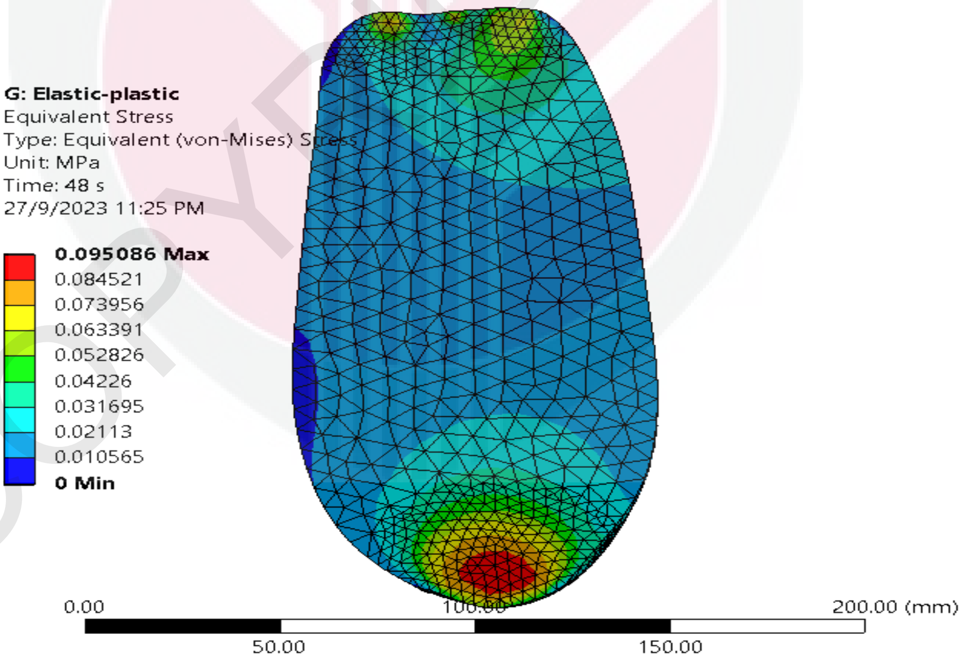

Figure 22 : Stress distribution (MPa) of elastic-plastic model at 16 mm compression. maximum stress at contact point; minimum stress at opposite end

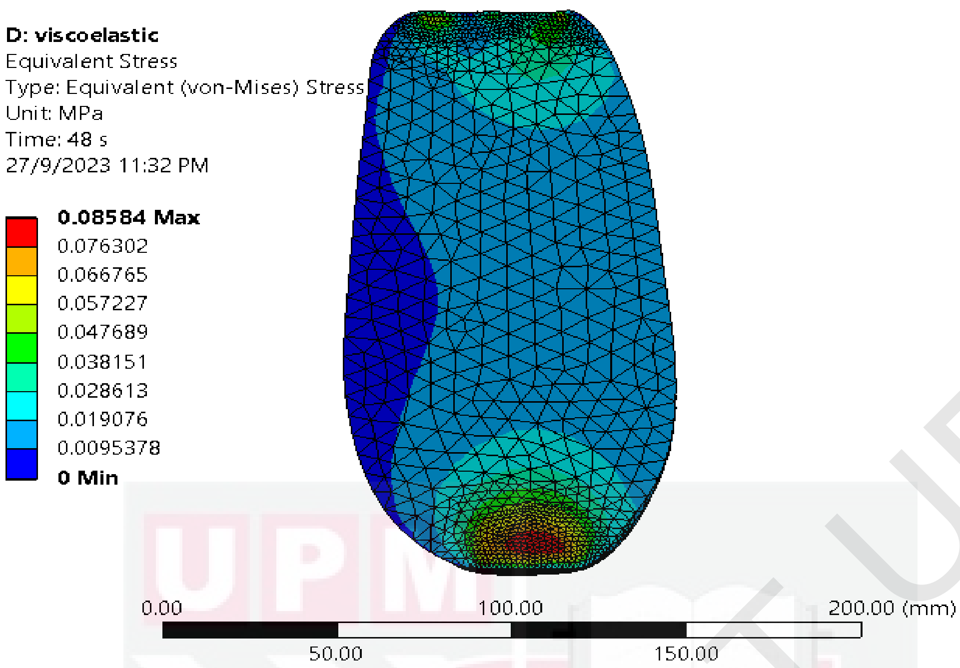

Figure 23 : Stress distribution (MPa) of viscoelastic model at 16 mm compression. maximum stress at contact point; minimum stress at opposite end

4.3.2 Model Applications

4.3.2.1 Geometry Modelling

The viscoelastic material model, as discussed in section 4.3.1, is more suitable for the FE model of papaya. Therefore, the FE model was applied to determine the difference in simulation results when a laser scanning and 2D sketching method was used to generate geometry for the model. Figure 24 shows the stress-strain relationship of the scanned and sketched model.

A t-test for paired two samples was used to determine the significant difference between 19 observations and the stress results of the two models. The null hypothesis states that no significant difference exists between the means of the scanned and the sketched model. In contrast, the alternate hypothesis states that a significant difference exists between the means of the scanned and the sketched model at the significance level (α) $\leq$ 0.05. The analysis (Table 12) shows that the t-statistic is less than the critical t-value, and the p-value is more significant than α. Therefore, the test fails to reject the null hypothesis; this shows there is no significant difference between the means of scanned and sketched models.

The result of this study agrees with Anders et al. (2019) that the volume estimation using numerical modelling of a 3D scanned model and simplified cucumber model did not differ significantly.

Table 12 : T-test comparison of stress response of whole fruit compression stress (mpa) using sketched and scanned models

	Scanned model	***Sketched model***
Mean (MPa)	0.1099	0.1094
Variance (MPa)	0.0026	0.0025
Observations	19	19
Pearson Correlation	1	
Hypothesised Mean Difference	0	
df	18	
t Stat	1.6011	
P(T<=t) one-tail	0.0634	
t Critical one-tail	1.7341	
P(T<=t) two-tail	0.1268	
t Critical two-tail	2.1009	

(a)

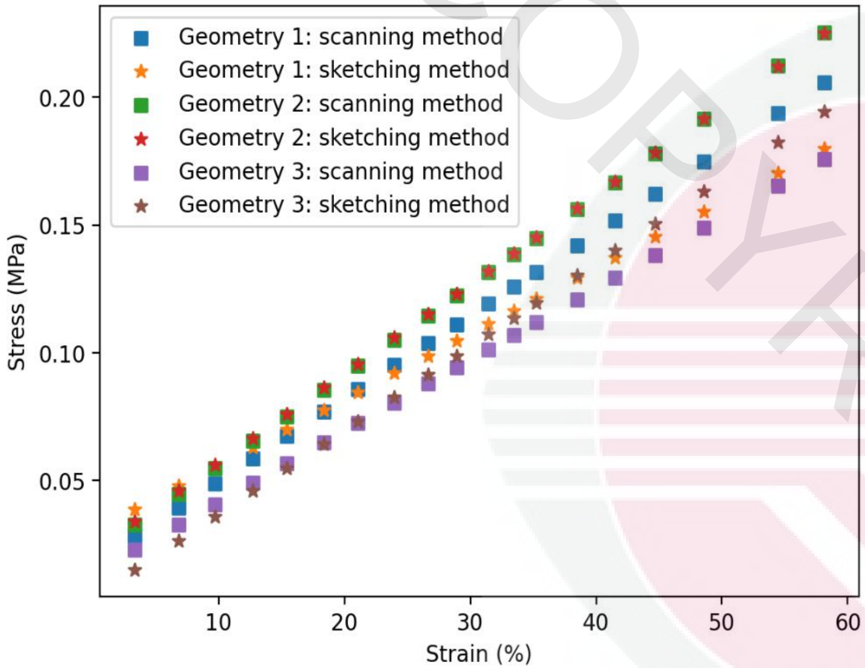

(b)

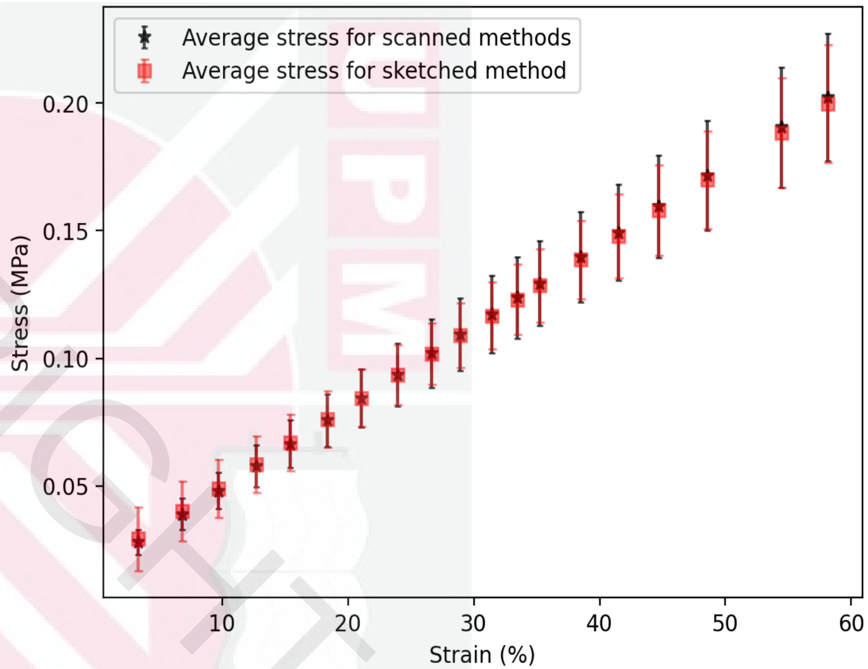

Figure 24 : Stress-strain relationship from fe simulation of papaya under compression using 3d geometry models produced by sketching and scanning methods. (a) Each plot represents the simulation response of the individual geometry model under the same loading condition. (b) The result of average stress for scanning and sketching methods is in figure (a), with error bars indicating the standard deviation

4.3.2.2 Effect of Loading Direction on Stress Distribution

The simulation results for the maximum von Mises stress distribution in the papaya fruit under longitudinal and transverse compression loading are shown in Figure 25. These figures demonstrate that the maximum stress is observed at the contact region between the fruit model and the lower platen. As the deformation increases, the stress distribution in the fruit widens from the contact region of both platens towards the centroid.

When considering longitudinal compression loading as shown in Figure 25, the maximum stress is initially 0.058 MPa at 4 mm compression, which is smaller than the yield stress of 0.0616 ± 0.024 MPa from the experimental test (Table 13). At 4 mm deformation, it is not likely to cause damage to the fruit. However, as the deformation increases to 8mm, the maximum stress reaches 0.0733 MPa (Figure 25(b)), which exceeds the yield stress, indicating that damage to the fruit may occur. As the deformation increases further to 16 mm, the damaged area increases towards the centroid of the fruit, indicating more extensive and severe fruit damage.

Table 13 : Whole fruit compression results (n=5)

Statistics	Modulus (MPa)	Compressive load at Yield (N)	Compressive Stress at Yield (MPa)	Compressive strain at Yield (mm/mm)
Standard Deviation	0.26755	24.56967	0.00241	0.096
Mean	0.26139	628.87717	0.06161	1.83
Maximum	0.72126	646.25055	0.06331	1.90

Similarly, more considerable stresses were observed at the contact region in the case of transverse compression loading (Figure 26). The von Mises stress increases from 0.0348 to 0.1629 MPa in the fruit tissue as deformation increases from 4 mm to 16 mm (Figure 26 (d), (e) and (f)). The FEM simulation results show that the yield stress is reached below the 8 mm displacement in some areas of the fruit tissue. As compression increases, more areas reach the yield stress, increasing the extent and severity of fruit damage.

These results are in line with previous simulation studies on other fruits like watermelon, grapefruit, kiwifruit, pineapple, and Rosa roxburghii, where an increase in deformation along the loading direction results in increased stress in the fruit tissue and potential damage (Sadrnia et al., 2008; Miraei Ashtiani et al., 2019; Liu et al., 2023; Seyedabadi et al., 2015; Lang et al., 2022; Tian et al., 2017).

Various studies have used the Finite Element Method (FEM) to analyse the optimal number of fruits that can be placed in a single package to avoid compression damage during packaging and transportation. For example, placing not more than 30 grapefruits in the transverse position was recommended to prevent fruit damage (Miraei Ashtiani et al., 2019). For pineapples, it was suggested that eight pineapples can safely be stacked in a transverse loading direction (Liu et al., 2023). In the case of blueberries, to reduce damage, compression should be kept under 3.15 N, with one layer stacking, and the fruit should be placed in the longitudinal direction (Zheng et al., 2021).

For papaya packaging, the present FEM model suggests that papayas should be positioned in their longitudinal axis, in the direction of the stem-calyx axis, and stacking more than 37 papaya fruits on top of each other could lead to excessive force and internal bruising of the fruit (Refer to Appendix B for more detail). Adhering to the recommended stacking limit is crucial to preserving papaya quality during packaging and transportation, especially when fruits are packed in bulk bins. This highlights the importance of proper handling and packaging strategies to minimise fruit damage and ensure the delivery of high-quality fruits to consumers.

(a)
(b)
(c)

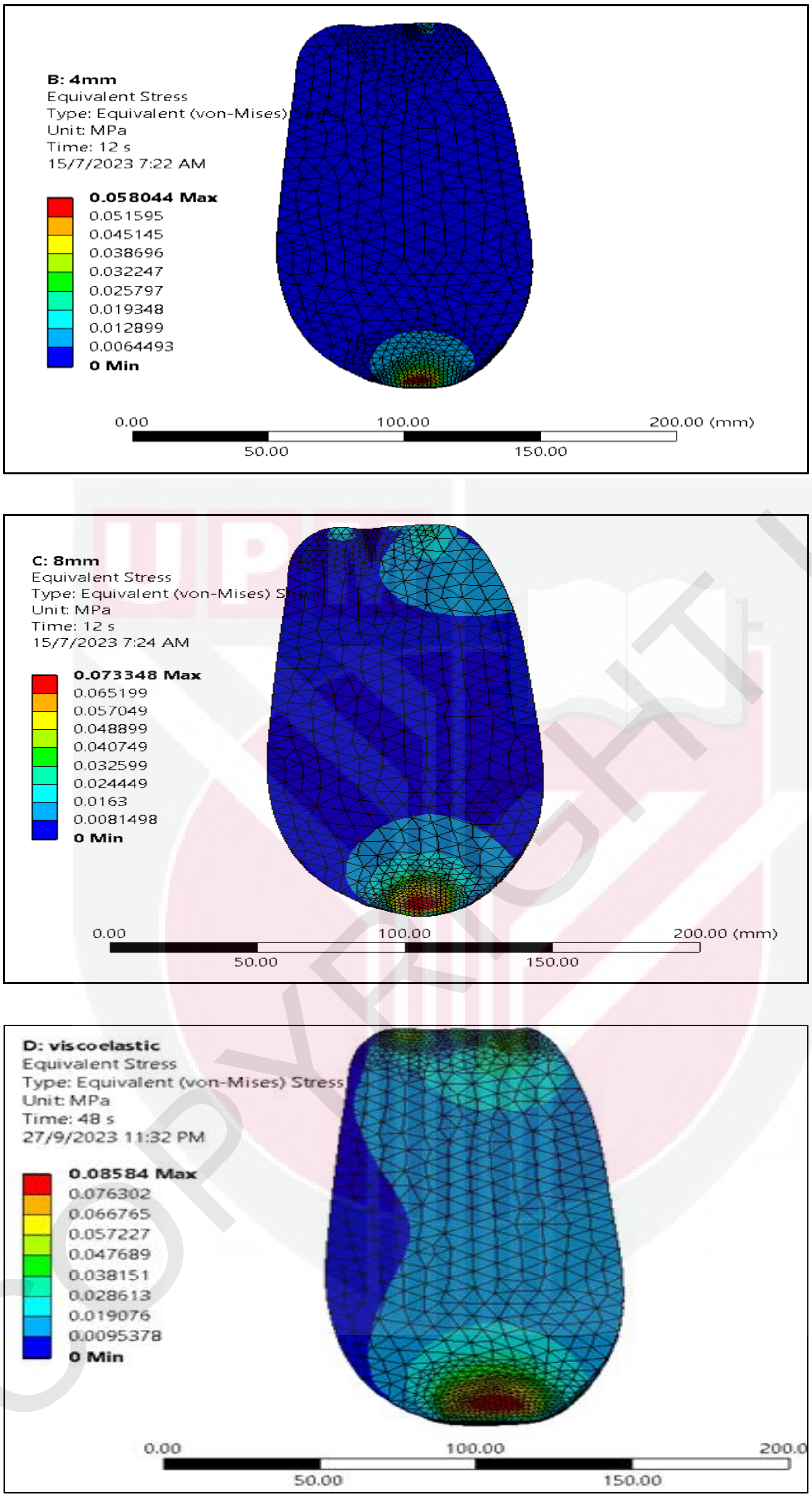

Figure 25 : Variations in the papaya fruit model's von Mises stress distributions as a function of varying compression displacement in the longitudinal direction. (a) 4 mm displacement along the longitudinal direction; (b) 8 mm displacement along the longitudinal direction; (c) 16 mm displacement along the longitudinal direction

(a)

(b)

(c)

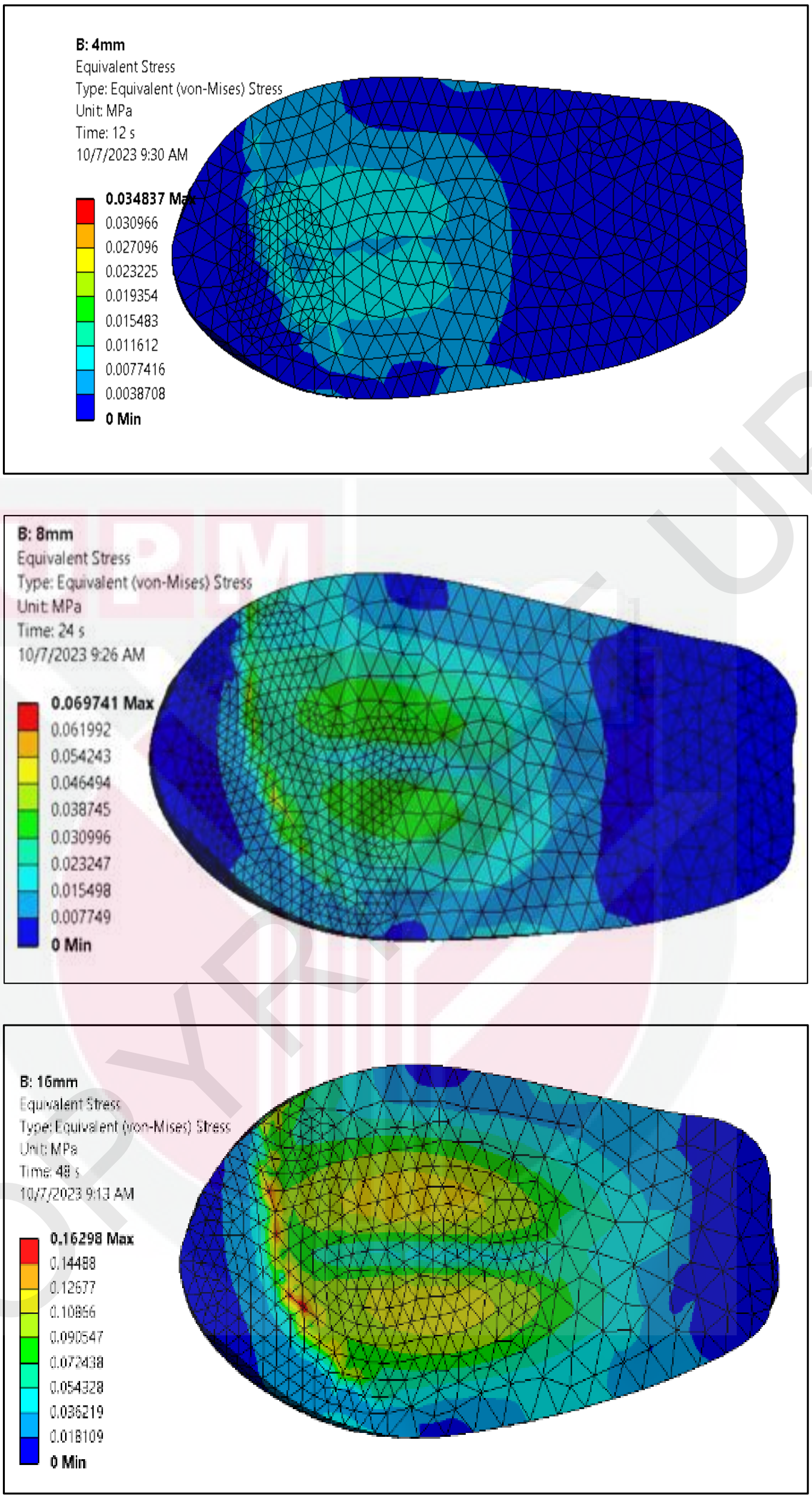

Figure 26 : Variations in the papaya fruit model's von Mises stress distributions as a function of varying compression displacement in the transverse direction. (a) 4 mm displacement along the transverse direction; (b) 8 mm displacement along the transverse direction; (c) 16 mm displacement along the transverse direction

4.3.3 Model Limitations

The FE modelling outcomes presented in this study should be interpreted considering the following limitations:

1. Homogeneous Material Properties: The model assumes homogeneous material properties for the entire fruit, neglecting potential variations in properties within the fruit, such as differences between the skin, flesh, fluid, and seeds.

2. Single Maturity or Ripeness Level: The model only accounts for ripeness index 2. For other stages of ripeness, different model types could present different result.

3. Static Loading: The model is limited to simulating static loading conditions, whereas impact or dynamic loading (vibration) was not considered.

4. Lack of Temperature Effects: Temperature changes can significantly influence the mechanical behaviour of biological materials, including papaya fruit. This is evident in the texture, firmness, and overall mechanical behaviour of the fruit, which are all temperature sensitive. Supporting this, Han et al. (2022) found that increasing the environmental temperature from 5 to 40 °C decreased the elastic modulus of sweet cherries, a property indicative of mechanical behaviour. It is plausible to expect a similar impact on papaya fruit. Future work could consider incorporating temperature effects to enhance the accuracy of the papaya fruit's finite element model. This could involve adjusting model parameters based on temperature or developing a multi-physics model that couples mechanical behaviour with thermal effects. However, this would likely increase the model’s complexity and computational resource requirements.

5. Lack of Detailed Microstructure: The model does not account for the detailed microstructure of papaya tissues, which can significantly impact mechanical behaviour, especially at the cellular level.

6. Computational Resources: Prior to using the half-papaya model, whole-fruit papaya was used for the simulation; the computational time per simulation took up to an average of 12 hours with an error message of incomplete calculation or convergence errors on a 2.5GHz dual core 32GB memory Dell desktop tower. The half-papaya model significantly reduced this time due to the inherent symmetry along the sectioned plane, which optimised computational efficiency (the simulation time per simulation was reduced to less than 2 hours). Further computational time reduction could be reduced by employing more advanced hardware, such as a high-performance computing cluster or graphics processing unit (GPU). Further optimising simulation parameters, such as the mesh size and element type, could also reduce computational time. While a full 3D model would provide a more comprehensive representation of the papaya, it would also significantly increase the computational resources required, potentially negating the efficiency gains achieved with the half-papaya model. Therefore, the decision to use a full 3D model should be carefully weighed against the available computational resources and the level of detail required in the simulation results.

4.4 Summary

In summary, the study focused on mass prediction models and mechanical characterisation of papaya fruit under compression loading. For mass prediction, various models were developed based on the fruit's physical geometric properties, with the power model showing the best performance in single-variable regression models and the OLS model performing best in multiple-variable models. These models provide valuable tools for predicting papaya fruit mass, essential for supply chain operations and handling processes.

The mechanical characterisation involved uniaxial compression and stress relaxation tests, which provided insights into the elastic modulus, failure stress, failure strain, relaxation moduli, and relaxation time of papaya fruit. The results demonstrated that the top section of the papaya fruit exhibited more deformation resistance. In contrast, the cellular composition at the top and middle sections differed from the bottom section, making the bottom section less resistant to deformation. These findings are essential for understanding the mechanical behaviour of papaya fruit, which can influence its handling and transportation.

The results of the papaya fruit's physical and mechanical properties were used to develop an FE model. The results of the FE model show that the viscoelastic model is more appropriate for studying the deformation behaviour of papaya fruit under compressive load. The model was also applied in studying the effect of the loading direction of the fruit, which shows that loading in a transverse direction is more susceptible to damage. Also, there is no significant difference in the simulation results between the scanning and sketching methods used to generate geometry for numerical analysis.

CHAPTER 5

CONCLUSION AND FUTURE RECOMMENDATION

5.1 Conclusion

This study provides valuable insights into papaya fruit's mass prediction and mechanical behaviour under compression loading. The research examines the correlations between the geometric properties of papaya and models for mass prediction based on papaya geometric properties. The power and quadratic models have the highest R^2 = 0.947 and the lowest RMSE = ~ 87 g values in the single-variable regression model for mass modelling using the projected area as a predictor. Meanwhile, the OLS model has the highest R^2 = 0.947 and lowest RMSE = 81.72 value for the multiple-variable models, but the R^2 and RMSE values were comparable for both modelling approaches.

The research used uniaxial compression and stress relaxation tests to describe papaya's elastic and viscoelastic properties along its major axis. The elastic modulus 0.5063 ± 0.19 MPa and failure stress 0.0679 ± 0.02 MPa indicate that papaya fruit is more resistant to deformation at the top section. However, there was no significant variation along the major axis. Similarly, the viscoelastic parameters indicate that papaya's cellular composition differs along its major axis. The bottom section is less resistant to deformation. Understanding the variations in mechanical properties across different fruit sections is crucial for efficient handling and transportation.

The research also used the FE model to study the deformation behaviour of papaya fruit under compressive load. The results of the FE model show that the viscoelastic model is more appropriate for studying the deformation behaviour of papaya fruit under compressive load. The model was also used to study the effect of loading direction on the fruit, which shows that loading in the transverse direction is more susceptible to damage. Also, there is no significant difference in the simulation results between the scanning and sketching methods used to generate geometry for numerical analysis.

Overall, the comprehensive understanding gained from this research can enhance the handling, transportation, and design of systems involving papaya fruit. The findings contribute to the field of food engineering and can be valuable for researchers, agriculturalists, and industries involved in fruit processing and distribution. Further studies could build upon this research by exploring additional factors and optimising material models to improve the accuracy of fruit mechanical simulations.

5.2 Recommendation

Based on the findings and insights gained from this study, here are some future recommendations:

1. Integration of Advanced Techniques: Incorporate advanced technologies such as digital twin framework to incorporate environmental conditions such as temperature and humidity to predict fruit deformation and damage conditions.

2. Multiscale Modelling Approach: A multiscale modelling approach allows for the integration of the mechanical properties of papaya at the cellular level.

3. Studying Different Papaya Fruit Varieties: Extend the study to investigate the mechanical properties of other papaya fruit varieties. Each fruit type may

have unique characteristics, and understanding their behaviour will aid in developing tailored handling methods.

By implementing these recommendations, we can advance fruit modelling and handling practices, reduce postharvest losses, improve fruit quality, and enhance efficiency in the fruit supply chain. Ultimately, these efforts will benefit producers and consumers by ensuring fresher and healthier fruit products.

REFERENCES

Abbaszadeh, R., Rajabipour, A., Sadrnia, H., Mahjoob, M. J., Delshad, M., & Ahmadi, H. (2014). Application of modal analysis to the watermelon through finite element modeling for use in ripeness assessment. *Journal of Food Engineering*, *127*, 80–84.

Abedi, G., & Ahmadi, E. (2013). Design and evaluation a pendulum device to study postharvest mechanical damage in fruits: Bruise modeling of red delicious apple. *Australian Journal of Crop Science*, *7*(7), 962.

Ahmadi, E., Barikloo, H., & Kashfi, M. (2016). Viscoelastic finite element analysis of the dynamic behavior of apple under impact loading with regard to its different layers. *Computers and Electronics in Agriculture*, *121*, 1–11. https://doi.org/10.1016/j.compag.2015.11.017

Ali, A., Muhammad, M. T. M., Sijam, K., & Siddiqui, Y. (2011). Effect of chitosan coatings on the physicochemical characteristics of Eksotika II papaya (Carica papaya L.) fruit during cold storage. *Food Chemistry*, *124*(2), 620–626. https://doi.org/10.1016/J.FOODCHEM.2010.06.085

An, X., Liu, H., Fadiji, T., Li, Z., & Dimitrovski, D. (2022). Prediction of the temperature sensitivity of strawberry drop damage using dynamic finite element method. *Postharvest Biology and Technology*, *190*, 111939. https://doi.org/10.1016/j.postharvbio.2022.111939

Anders, A., Choszcz, D., Markowski, P., Lipiński, A. J., Kaliniewicz, Z., & Ślesicka, E. (2019). Numerical modeling of the shape of agricultural products on the example of cucumber fruits. *Sustainability (Switzerland)*, *11*(10). https://doi.org/10.3390/su11102798

Ansys®. (2023). *Mechanical Application, Release 2023 R1, Help System, Mechanical User's Guide* (2023 R1). ANSYS, Inc.

Arendse, E., Fawole, O. A., & Opara, U. L. (2014). Influence of storage temperature and duration on postharvest physico-chemical and mechanical properties of pomegranate fruit and arils. *CyTA - Journal of Food*, *12*(4), 389–398. https://doi.org/10.1080/19476337.2014.900114

Arrázola, G., Villadiego, F., & Alvis, A. (2021). Mechanical properties and simulation of finite element firmness in Carica papaya L. Tainung F1 cultivated on the high Sinu (Cordoba-Colombia). *Revista Colombiana de Ciencias Hortícolas*, *15*(1). https://doi.org/10.17584/RCCH.2021V15I1.10809/CITED_WORKS.JSON

ASAE. (2008). *Compression Test of Food Materials of Convex Shape* (ASAE S368.4). American Society of Agricultural and Biological Engineers (ASABE). https://books.google.com.my/books?id=xwhPNQAACAAJ

Azene, M., Workneh, T. S., & Woldetsadik, K. (2014). Effect of packaging materials and storage environment on postharvest quality of papaya fruit. *Journal of Food Science and Technology*, *51*(6), 1041–1055. https://doi.org/10.1007/S13197-011-0607-6/TABLES/9

Bargel, H., & Neinhuis, C. (2005). Tomato (Lycopersicon esculentum Mill.) fruit growth and ripening as related to the biomechanical properties of fruit skin and isolated cuticle. *Journal of Experimental Botany*, *56*(413), 1049–1060. https://doi.org/10.1093/JXB/ERI098

Bloch, V., Degani, A., & Bechar, A. (2018). A methodology of orchard architecture design for an optimal harvesting robot. *Biosystems Engineering*, *166*, 126–137. https://doi.org/10.1016/J.BIOSYSTEMSENG.2017.11.006

Bu, L., Chen, C., Hu, G., Zhou, J., Sugirbay, A., & Chen, J. (2021). Investigating the dynamic behavior of an apple branch-stem-fruit model using experimental and simulation analysis. *Computers and Electronics in Agriculture*, *186*, 106224. https://doi.org/10.1016/j.compag.2021.106224

Bu, L., Hu, G., Chen, C., Sugirbay, A., & Chen, J. (2020). Experimental and simulation analysis of optimum picking patterns for robotic apple harvesting. *Scientia Horticulturae*, *261*, 108937. https://doi.org/10.1016/J.SCIENTA.2019.108937

Burubai, W., Akor, A., Igoni, A. H., & Puyate, Y. T. (2007). Some physical properties of African nutmeg (Monodora myristica). *International Agrophysics*, *21*, 123–136.

Cáez-Ramirez, G. R., Téllez-Medina, D. I., & Gutierrez-López, G. F. (2015). Multiscale and nanostructural approach to fruits stability. *Food Engineering Series*, 267–281. https://doi.org/10.1007/978-3-319-13596-0_16/FIGURES/2

Celik, H. K. (2017a). Determination of bruise susceptibility of pears (Ankara variety) to impact load by means of FEM-based explicit dynamics simulation. *Postharvest Biology and Technology*, *128*, 83–97. https://doi.org/10.1016/j.postharvbio.2017.01.015

Celik, H. K. (2017b). Determination of bruise susceptibility of pears (Ankara variety) to impact load by means of FEM-based explicit dynamics simulation. *Postharvest Biology and Technology*, *128*, 83–97. https://doi.org/10.1016/j.postharvbio.2017.01.015

Celik, H. K., Caglayan, N., & Rennie, A. E. W. (2017). Nonlinear FEM based high-speed shell shattering simulation for shelled edible agricultural products: Pecan fruit shattering. *Journal of Food Process Engineering*, *40*(5). https://doi.org/10.1111/jfpe.12520

Celik, H. K., Rennie, A. E. W., & Akinci, I. (2017). Reverse engineering approach for precise measurement of the physical attributes related to the geometric features of agricultural products. *Journal of Food Measurement and*

Characterization, *11*(1), 75–84. https://doi.org/10.1007/s11694-016-9373-5

Celik, H. K., Ustun, H., Erkan, M., Rennie, A. E. W., & Akinci, I. (2021). Effects of bruising of 'Pink Lady' apple under impact loading in drop test on firmness, colour and gas exchange of fruit during long term storage. *Postharvest Biology and Technology*, *179*, 111561. https://doi.org/10.1016/j.postharvbio.2021.111561

Cerri, M., & Reale, L. (2020). Anatomical traits of the principal fruits: An overview. *Scientia Horticulturae*, *270*, 109390. https://doi.org/10.1016/J.SCIENTA.2020.109390

Chai, T., & Draxler, R. R. (2014). Root mean square error (RMSE) or mean absolute error (MAE)? -Arguments against avoiding RMSE in the literature. *Geoscientific Model Development*, *7*(3), 1247–1250. https://doi.org/10.5194/GMD-7-1247-2014

Chen, H., & Baerdemaeker, J. De. (1993). Finite-element-based Modal Analysis of Fruit Firmness. *Transactions of the ASAE*, *36*(6), 1827–1833. https://doi.org/10.13031/2013.28529

Cheng, C. L., Shalabh, & Garg, G. (2014). Coefficient of determination for multiple measurement error models. *Journal of Multivariate Analysis*, *126*, 137–152. https://doi.org/10.1016/J.JMVA.2014.01.006

Coelho, A. L. de F., Santos, F. L., Pinto, F. A. C., & De Queiroz, D. M. (2015). Determinação das propriedades geométricas, físicas e mecânicas do sistema fruto-pedúnculo-ramo do cafeeiro. *Revista Brasileira de Engenharia Agrícola e Ambiental*, *19*(3), 286–292. https://doi.org/10.1590/1807-1929/AGRIAMBI.V19N3P286-292

Coelho, A. L. de F., Santos, F. L., Queiroz, D. M. de, & Pinto, F. de A. de C. (2016). Dynamic behavior of the coffee fruit-stem-branch system using stochastic finite element method. ID - 20163126519. *Coffee Science*, *11*(1), 1–10. http://www.coffeescience.ufla.br/index.php/Coffeescience/article/view/942/pdf_1

Datta, A. K. (2016). Toward computer-aided food engineering: Mechanistic frameworks for evolution of product, quality and safety during processing. *Journal of Food Engineering*, *176*, 9–27. https://doi.org/10.1016/j.jfoodeng.2015.10.010

Datta, A., Nicolaï, B., Vitrac, O., Verboven, P., Erdogdu, F., Marra, F., Sarghini, F., & Koh, C. (2022). Computer-aided food engineering. *Nature Food*, *3*(11), 894–904. https://doi.org/10.1038/s43016-022-00617-5

Defraeye, T., Shrivastava, C., Berry, T., Verboven, P., Onwude, D., Schudel, S., Bühlmann, A., Cronje, P., & Rossi, R. M. (2021). Digital twins are coming: Will we need them in supply chains of fresh horticultural produce? *Trends in Food Science & Technology*, *109*, 245–258. https://doi.org/10.1016/J.TIFS.2021.01.025

Dintwa, E., Van Zeebroeck, M., Ramon, H., & Tijskens, E. (2008). Finite element analysis of the dynamic collision of apple fruit. *Postharvest Biology and Technology*, *49*(2), 260–276. https://doi.org/10.1016/j.postharvbio.2008.01.012

Domnguez, E., Espaa, L., Lpez-Casado, G., Cuartero, J., & Heredia, A. (2009). Biomechanics of isolated tomato (Solanum lycopersicum) fruit cuticles during ripening: the role of flavonoids. *Functional Plant Biology : FPB*, *36*(7), 613–620. https://doi.org/10.1071/FP09039

Du, D., Wang, B., Wang, J., Yao, F., & Hong, X. (2019). Prediction of bruise susceptibility of harvested kiwifruit (Actinidia chinensis) using finite element method. *Postharvest Biology and Technology*, *152*, 36–44. https://doi.org/10.1016/j.postharvbio.2019.02.013

Du, D., Wang, J., Wang, B., & Yao, F. (2019). Application of finite element method to estimate the bruise damage of kiwifruit under drop impact loading. *2019 Boston, Massachusetts July 7- July 10, 2019*. https://doi.org/10.13031/aim.201900242

Erdogdu, F., Datta, A., Vitrac, O., Marra, F., Verboven, P., Sarghini, F., & Nicolai, B. (2022). Mathematical modeling—Computer-aided food engineering. *Food Engineering Innovations Across the Food Supply Chain*, 277–290. https://doi.org/10.1016/B978-0-12-821292-9.00007-8

Fadiji, T., Berry, T., Coetzee, C. J., & Opara, L. (2017). Investigating the mechanical properties of paperboard packaging material for handling fresh produce under different environmental conditions: Experimental analysis and finite element modelling. *Journal of Applied Packaging Research*, *9*(2), 3.

Fadiji, T., Coetzee, C., Chen, L., Chukwu, O., & Opara, U. L. (2016). Susceptibility of apples to bruising inside ventilated corrugated paperboard packages during simulated transport damage. *Postharvest Biology and Technology*, *118*, 111–119. https://doi.org/10.1016/J.POSTHARVBIO.2016.04.001

Fadiji, T., Coetzee, C. J., Berry, T. M., Ambaw, A., & Opara, U. L. (2018). The efficacy of finite element analysis (FEA) as a design tool for food packaging: A review. *Biosystems Engineering*, *174*, 20–40. https://doi.org/10.1016/j.biosystemseng.2018.06.015

Fadiji, T., Coetzee, C., Pathare, P., & Opara, U. L. (2016). Susceptibility to impact damage of apples inside ventilated corrugated paperboard packages: Effects of package design. *Postharvest Biology and Technology*, *111*, 286–296. https://doi.org/10.1016/J.POSTHARVBIO.2015.09.023

FAOSTAT. (2023). *FAOSTAT statistical database*. Food and Agriculture Organization of the United Nations. https://www.fao.org/faostat/en/#data/QV

Fernández-Muñoz, R., Heredia, A., & Domínguez, E. (2022). The role of cuticle in fruit shelf-life. *Current Opinion in Biotechnology*, *78*. https://doi.org/10.1016/J.COPBIO.2022.102802

Finney, E. E. (1971). Random vibration techniques for non-destructive evaluation of peach firmness. *Journal of Agricultural Engineering Research*, *16*(1), 81–87. https://doi.org/10.1016/S0021-8634(71)80007-0

Francis, L. F. (2016). Solid Processes. *Materials Processing: A Unified Approach to Processing of Metals, Ceramics and Polymers*, 251–342. https://doi.org/10.1016/B978-0-12-385132-1.00004-5

Fu, L., Peng, J., Nan, Q., He, D., Yang, Y., & Cui, Y. (2016). Simulation of vibration harvesting mechanism for sea buckthorn. *Engineering in Agriculture, Environment and Food*, *9*(1), 101–108. https://doi.org/10.1016/j.eaef.2015.08.003

Gajanana, T. M., Sudha, M., Saxena, A. K., & Dakshinamoorthy, V. (2010). Post harvest handling, marketing and assessment of losses in papaya. *Acta Horticulturae*, *851*, 519–526. https://doi.org/10.17660/ACTAHORTIC.2010.851.79

Gao, Y., Song, C., Rao, X., & Ying, Y. (2018). Image processing-aided FEA for monitoring dynamic response of potato tubers to impact loading. *Computers and Electronics in Agriculture*, *151*, 21–30. https://doi.org/10.1016/j.compag.2018.05.027

Ghasemi, A., & Zahediasl, S. (2012). Normality Tests for Statistical Analysis: A Guide for Non-Statisticians. *International Journal of Endocrinology and Metabolism*, *10*(2), 486. https://doi.org/10.5812/IJEM.3505

Goñi, S. M., Purlis, E., & Salvadori, V. O. (2007). Three-dimensional reconstruction of irregular foodstuffs. *Journal of Food Engineering*, *82*(4), 536–547. https://doi.org/10.1016/J.JFOODENG.2007.03.021

Gupta, S. K., Ehsani, R., & Kim, N. H. (2016). Optimization of a Citrus Canopy Shaker Harvesting System: Mechanistic Tree Damage and Fruit Detachment Models. *Transactions of the ASABE*, *59*(4), 761–776. https://doi.org/10.13031/trans.59.10819

Hahn, G. J. (1973). The coefficient of determination exposed. *Chemtech*, *3*(10), 609–612.

Han, X., An, X., Fadiji, T., Li, Z., & Khojastehpour, M. (2022). Textural thermo-mechanical properties of sweet cherry for postharvest damage analysis. *Journal of Texture Studies*, *53*(4), 453–464. https://doi.org/10.1111/JTXS.12661

He, L., Wu, C., Du, X., Ye, B., & Tong, J. (2015). Dynamic simulation of the Chinese hickory tree under multi-directional forced vibration. *2015 ASABE International Meeting*, *4*, 2701–2708. https://doi.org/10.13031/aim.20152189003

Hernández, L. F., & Bellés, P. M. (2003). A 3-D finite element analysis of the sunflower (Helianthus annuus L.) fruit under impact: A useful approach for the understanding and improvement of its hullability. *Institute of Physics Conference Series*, *180*, 253–263.

Hertog, M. L. A. T. M. (2016). Modeling Fruit Quality. *Reference Module in Food Science*. https://doi.org/10.1016/B978-0-08-100596-5.03292-3

Ho, Q. T., Carmeliet, J., Datta, A. K., Defraeye, T., Delele, M. A., Herremans, E., Opara, L., Ramon, H., Tijskens, E., Van Der Sman, R., Van Liedekerke, P., Verboven, P., & Nicolaï, B. M. (2013). Multiscale modeling in food engineering. *Journal of Food Engineering*, *114*(3), 279–291. https://doi.org/10.1016/J.JFOODENG.2012.08.019

Horbens, M., Branke, D., Gärtner, R., Voigt, A., Stenger, F., & Neinhuis, C. (2015). Multi-scale simulation of plant stem reinforcement by brachysclereids: A case study in apple fruit peduncles. *Journal of Structural Biology*, *192*(1), 116–126. https://doi.org/10.1016/J.JSB.2015.08.002

IndexBox. (n.d.). *Malaysia - Papayas - Market Analysis, Forecast, Size, Trends and Insights*. Retrieved March 5, 2024, from https://www.indexbox.io/search/production-papaya-malaysia/

Júnior, F., De, L., De Gonzaga, L., Moreira Da Silva, F., Ferreira, D. D., Simão, S. D., Carvalho De Souza, G., & Ferreira, L. K. (2018). Characterization of the coffee fruit detachment force in crop subjected to mechanized harvesting. *Coffee Science - ISSN 1984-3909*, *13*(1), 71–79. http://www.coffeescience.ufla.br/index.php/Coffeescience/article/view/1379

Kechinski, C. P., Montero, C. R. S., Guimarães, P. V. R., Noreña, C. P. Z., Marczak, L. D. F., Tessaro, I. C., & Bender, R. J. (2012). Effects of ozonized water and heat treatment on the papaya fruit epidermis. *Food and Bioproducts Processing*, *90*(2), 118–122. https://doi.org/10.1016/J.FBP.2011.01.005

Khoshnam, F., Tabatabaeefar, A., Varnamkhasti, M. G., & Borghei, A. (2007). Mass modeling of pomegranate (Punica granatum L.) fruit with some physical characteristics. *Scientia Horticulturae*, *114*(1), 21–26. https://doi.org/10.1016/J.SCIENTA.2007.05.008

KIM, G.-W., KIM, M.-S., SAGARA, Y., BAE, Y.-H., LEE, I.-B., DO, G.-S., LEE, S.-H., & KANG, S.-W. (2008). Determination of the Viscoelastic Properties of Apple Flesh under Quasi-Static Compression Based on Finite Element Method Optimization. *Food Science and Technology Research*, *14*(3), 221–231. https://doi.org/10.3136/fstr.14.221

Komarnicki, P., Stopa, R., Szyjewicz, D., Kuta, Ł., & Klimza, T. (2017). Influence of Contact Surface Type on the Mechanical Damages of Apples Under Impact Loads. *Food and Bioprocess Technology*, *10*(8), 1479–1494. https://doi.org/10.1007/S11947-017-1918-Z/FIGURES/9

Kwok, C. Y., & Liang, S. S. (2019). *Biology of Papaya (Carica papaya L.* Department of Biosafety Ministry of Water, Land and Natural Resources. https://www.biosafety.gov.my/wp-content/uploads/2021/08/Papaya-Carica-papaya-L..pdf

Li, Z., Andrews, J., & Wang, Y. (2017). Mathematical modelling of mechanical damage to tomato fruits. *Postharvest Biology and Technology*, *126*, 50–56. https://doi.org/10.1016/j.postharvbio.2016.12.001

Li, Z., & Thomas, C. (2016). Multiscale Biomechanics of Tomato Fruits: A Review. *Critical Reviews in Food Science and Nutrition*, *56*(7), 1222–1230. https://doi.org/10.1080/10408398.2012.759902

Li, Z., Yang, H., Li, P., Liu, J., Wang, J., & Xu, Y. (2013). Fruit biomechanics based on anatomy: a review. *International Agrophysics*, *27*(1). https://doi.org/10.2478/v10247-012-0073-z

Liu, W., Liu, T., Zeng, T., Ma, R., Cheng, Y., Zheng, Y., Qiu, J., & Qi, L. (2023). Prediction of internal mechanical damage in pineapple compression using finite element method based on Hooke's and Hertz's laws. *Scientia Horticulturae*, *308*, 111592. https://doi.org/10.1016/j.scienta.2022.111592

Lorestani, A. N., & Tabatabaeefar, A. (2006). Modelling the mass of kiwi fruit by geometrical attributes. *International Agrophysics*, *20*(2), 135–139. http://www.international-agrophysics.org/Modelling-the-mass-of-kiwi-fruit-by-geometrical-attributes,106594,0,2.html

Mahawar, M. K., Bibwe, B., Jalgaonkar, K., & Ghodki, B. M. (2019). Mass modeling of kinnow mandarin based on some physical attributes. *Journal of Food Process Engineering*, *42*(5), e13079. https://doi.org/10.1111/JFPE.13079

Mansuri, S. M., Gautam, P. V., Jain, D., Nickhil, C., & Pramendra. (2022). Computer vision model for estimating the mass and volume of freshly harvested Thai apple ber (Ziziphus mauritiana L.) and its variation with storage days. *Scientia Horticulturae*, *305*, 111436. https://doi.org/10.1016/j.scienta.2022.111436

Maringgal, B., Hashim, N., Amin Tawakkal, I. S. M., Muda Mohamed, M. T., Hazwan Hamzah, M., Ali, M. M., & Abd Razak, M. F. H. (2020). Kinetics of quality changes in papayas (Carica papaya L.) coated with Malaysian stingless bee honey. *Scientia Horticulturae*, *267*, 109321. https://doi.org/10.1016/J.SCIENTA.2020.109321

Martinez-Romero, D., Serrano, M., Carbonell, A., Castillo, S., Riquelme, F., & Valero, D. (2004). *MECHANICAL DAMAGE DURING FRUIT POST-HARVEST HANDLING: TECHNICAL AND PHYSIOLOGICAL IMPLICATIONS*.

Meisami-asl, E., Rafiee, S., Keyhani, A., & Tabatabaeefar, A. (2009). Some Physical Properties of Apple cv. 'Golab.' *Agricultural Engineering International: CIGR Journal*. https://cigrjournal.org/index.php/Ejounral/article/view/1124

Melesse, T. Y., Bollo, M., Pasquale, V. Di, Centro, F., & Riemma, S. (2022). Machine Learning-Based Digital Twin for Monitoring Fruit Quality Evolution. *Procedia Computer Science*, *200*, 13–20.

https://doi.org/10.1016/J.PROCS.2022.01.200

Miraei Ashtiani, S. H., Baradaran Motie, J., Emadi, B., & Aghkhani, M. H. (2014). Models for predicting the mass of lime fruits by some engineering properties. *Journal of Food Science and Technology*, *51*(11), 3411–3417. https://doi.org/10.1007/s13197-012-0862-1

Miraei Ashtiani, S.-H., Sadrnia, H., Mohammadinezhad, H., Aghkhani, M. H., Khojastehpour, M., & Abbaspour-Fard, M. H. (2019a). FEM-based simulation of the mechanical behavior of grapefruit under compressive loading. *Scientia Horticulturae*, *245*, 39–46. https://doi.org/10.1016/j.scienta.2018.10.006

Miraei Ashtiani, S.-H., Sadrnia, H., Mohammadinezhad, H., Aghkhani, M. H., Khojastehpour, M., & Abbaspour-Fard, M. H. (2019b). FEM-based simulation of the mechanical behavior of grapefruit under compressive loading. *Scientia Horticulturae*, *245*, 39–46. https://doi.org/10.1016/j.scienta.2018.10.006

Mirzabe, A. H., Khazaei, J., Chegini, G., & Nejad, M. H. A. P. R. (2013). Determination of some physical properties of virgin olive fruits. *Agricultural Engineering International: The CIGR Journal*.

Mohsenin, N. N. (1970). *Physical Properties of Plant and Animal Materials: Structure, physical characteristics, and mechanical properties*. Gordon and Breach. https://books.google.com.my/books?id=YX9FAQAAIAAJ

Murakonda, S., Patel, G., & Dwivedi, M. (2022). Characterization of engineering properties and modeling mass and fruit fraction of wood apple (Limonia acidissima) fruit for post-harvest processing. *Journal of the Saudi Society of Agricultural Sciences*, *21*(4), 267–277. https://doi.org/10.1016/J.JSSAS.2021.09.005

MyPF. (2022, September 26). *6 locally produced food items to help lower your grocery costs*. https://www.freemalaysiatoday.com/category/leisure/money/2022/09/26/6-locally-produced-food-items-to-help-lower-your-grocery-costs/

Namdari Gharaghani, B., & Maghsoudi, H. (2018). Free fall analysis of orange fruit using numerical and experimental methods. *International Journal of Food Properties*, *21*(1), 484–495. https://doi.org/10.1080/10942912.2018.1446148

Namdari Gharaghani, B., Maghsoudi, H., & Mohammadi, M. (2020). Ripeness detection of orange fruit using experimental and finite element modal analysis. *Scientia Horticulturae*, *261*, 108958. https://doi.org/10.1016/J.SCIENTA.2019.108958

Nations, F. and A. O. of the U. (n.d.). *FAOSTAT statistical database*. [Rome] : FAO, 2021. https://search.library.wisc.edu/catalog/999890171702121

Nian, Y., Wang, N., Li, R., Shao, Y., & Li, W. (2022). Cold shock treatment alleviates chilling injury in papaya fruit during storage by improving antioxidant capacity and related gene expression. *Scientia Horticulturae*, *294*, 110784. https://doi.org/10.1016/J.SCIENTA.2021.110784

Niu, Z., Xu, Z., Deng, J., Zhang, J., Pan, S., & Mu, H. (2022). Optimal vibration parameters for olive harvesting from finite element analysis and vibration tests. *Biosystems Engineering*, *215*, 228–238. https://doi.org/10.1016/j.biosystemseng.2022.01.002

Nyalala, I., Okinda, C., Nyalala, L., Makange, N., Chao, Q., Chao, L., Yousaf, K., & Chen, K. (2019). Tomato volume and mass estimation using computer vision and machine learning algorithms: Cherry tomato model. *Journal of Food Engineering*, *263*, 288–298. https://doi.org/10.1016/J.JFOODENG.2019.07.012

Onwude, D., Bahrami, F., Shrivastava, C., Berry, T., Cronje, P., North, J., Kirsten, N., Schudel, S., Crenna, E., Shoji, K., & Defraeye, T. (2022). Physics-driven digital twins to quantify the impact of pre- and postharvest variability on the end quality evolution of orange fruit. *Resources, Conservation and Recycling*, *186*, 106585. https://doi.org/10.1016/J.RESCONREC.2022.106585

Opara, U. L., & Fadiji, T. (2018). Compression damage susceptibility of apple fruit packed inside ventilated corrugated paperboard package. *Scientia Horticulturae*, *227*, 154–161. https://doi.org/10.1016/J.SCIENTA.2017.09.043

Panda, S., & Sethy, P. K. (2017). POST-HARVEST GRADING OF CARICA PAPAYA FRUIT USING IMAGE SEGMENTATION AND SOFT COMPUTING. *International Journal of Advanced Research in Computer Science*, *8*(7).

Paull, R. E. (1993). Pineapple and papaya. *Biochemistry of Fruit Ripening*, 291–323. https://doi.org/10.1007/978-94-011-1584-1_10

Pedregosa, F., Varoquaux, G., Gramfort, A., Michel V. and Thirion, B., Grisel, O., Blondel, M., Prettenhofer P. and Weiss, R., Dubourg, V., Vanderplas, J., Passos, A., Cournapeau, D., Brucher, M., Perrot, M., & Duchesnay, E. (2011). Scikit-learn: Machine Learning in Python. *Journal of Machine Learning Research*, *12*, 2825–2830.

Prasad, K., & Paul, J. R. (2021). Postharvest Losses of Papaya and Practice for Management. *Food Sci. Rep.*, *2*(1), 7.

Proulx, É., Cecilia, M., Nunes, N., Emond, J., & Brecht, J. (2005). *Quality attributes limiting papaya postharvest life at chilling and non-chilling temperatures*.

Prusky, D., Alkan, N., Mengiste, T., & Fluhr, R. (2013). Quiescent and Necrotrophic Lifestyle Choice During Postharvest Disease Development. *Https://Doi.Org/10.1146/Annurev-Phyto-082712-102349*, *51*, 155–176. https://doi.org/10.1146/ANNUREV-PHYTO-082712-102349

Rangel, J. P., Queiroz, D. M. de, Pinto, F. de A. de C., Teixeira, C. C., Santos, F. L., & Valente, D. S. M. (2020). Dynamic behavior of the macauba palm (Acrocomia aculeata) fruit-rachilla system using the stochastic finite element method. *Acta Scientiarum. Agronomy*, *43*, e48565. https://doi.org/10.4025/actasciagron.v43i1.48565

Rashvand, M., Akbarnia, A., Abbaszadeh, R., Karimi, D., & Jafari, A. (2021). Measurement bruise volume of olive during impact test using FEM and quality evaluation of extracted olive oil. *Food Science & Nutrition*, *9*(10), 5493–5508. https://doi.org/10.1002/fsn3.2508

Rashvand, M., Altieri, G., Genovese, F., Li, Z., & Di Renzo, G. C. (2022). Numerical simulation as a tool for predicting mechanical damage in fresh fruit. *Postharvest Biology and Technology*, *187*, 111875. https://doi.org/10.1016/J.POSTHARVBIO.2022.111875

Rios, J. C., Robledo, F., Schreiber, L., Zeisler, V., Lang, E., Carrasco, B., & Silva, H. (2015). Association between the concentration of n-alkanes and tolerance to cracking in commercial varieties of sweet cherry fruits. *Scientia Horticulturae*, *197*, 57–65. https://doi.org/10.1016/J.SCIENTA.2015.10.037

Sadrnia, H., Rajabipour, A., Jafari, A., Javadi, A., Mostofi, Y., Kafashan, J., Dintwa, E., & De Baerdemaeker, J. (2008). Internal bruising prediction in watermelon compression using nonlinear models. *Journal of Food Engineering*, *86*(2), 272–280. https://doi.org/10.1016/J.JFOODENG.2007.10.007

Sahin, S., & Sumnu, S. G. (2006). Rheological Properties of Foods. In *Physical Properties of Foods* (pp. 39–105). Springer New York. https://doi.org/10.1007/0-387-30808-3_2

Sahu, R. M. K. F. M. (2018). Engineering physical properties of papaya (Carica papaya L) at different ripening stages. *International Journal of Chemical Studies (IJCS)*, *6*(6), 1945–1952.

Salarikia, A., Miraei Ashtiani, S.-H., Golzarian, M. R., & Mohammadinezhad, H. (2017). Finite element analysis of the dynamic behavior of pear under impact loading. *Information Processing in Agriculture*, *4*(1), 64–77. https://doi.org/10.1016/j.inpa.2016.12.003

Sanchez, N., Gutiérrez-López, G. F., & Cáez-Ramírez, G. (2020). Correlation among PME activity, viscoelastic, and structural parameters for Carica papaya edible tissue along ripening. *Journal of Food Science*, *85*(6), 1805–1814. https://doi.org/10.1111/1750-3841.15130

Santos Pereira, L. F., Barbon, S., Valous, N. A., & Barbin, D. F. (2018). Predicting the ripening of papaya fruit with digital imaging and random forests. *Computers and Electronics in Agriculture*, *145*, 76–82. https://doi.org/10.1016/j.compag.2017.12.029

Sarris, Alexander., & Food and Agriculture Organization of the United Nations. (2003). *Medium-term prospects for agricultural commodities : projections to* *the year 2010*. 181.

Savary, S., Ficke, A., Aubertot, J. N., & Hollier, C. (2012). Crop losses due to diseases and their implications for global food production losses and food security. *Food Security*, *4*(4), 519–537. https://doi.org/10.1007/S12571-012-0200-5/METRICS

Sawicka, B. (2019). Post-harvest Losses of Agricultural Produce. *Zero Hunger. Encyclopedia of the UN's Sustainable Development Goals*. https://doi.org/10.1007/978-3-319-69626-3

Seema, Kumar, A., & Gill, G. S. (2015). Automatic Fruit Grading and Classification System Using Computer Vision: A Review. *Proceedings - 2015 2nd IEEE International Conference on Advances in Computing and Communication Engineering, ICACCE 2015*, 598–603. https://doi.org/10.1109/ICACCE.2015.15

Sekeli, R., Hamid, M. H., Razak, R. A., Wee, C. Y., & Ong-Abdullah, J. (2018). Malaysian carica papaya l. var. eksotika: current research strategies fronting challenges. *Frontiers in Plant Science*, *9*, 1380. https://doi.org/10.3389/FPLS.2018.01380/BIBTEX

Sew, Y. S., Sarip, J., Vellupillai, M., & Bakar, U. K. A. (2015). Isolation of fruit ripening genes from Carica papaya var. Eksotika 1 cDNA libraries (Pemencilan gen pemasakan Carica papaya var. Eksotika 1 daripada perpustakaan cDNA). *Journal of Tropical Agriculture and Food Science*, *39*, 203–211.

Seyedabadi, E., Khojastehpour, M., & Sadrnia, H. (2015). Predicting Cantaloupe Bruising Using Non-Linear Finite Element Method. *International Journal of Food Properties*, *18*(9), 2015–2025. https://doi.org/10.1080/10942912.2014.951892

Seyedabadi, E., Khojastehpour, M., Sadrnia, H., & Saiedirad, M. H. (2011). Mass modeling of cantaloupe based on geometric attributes: A case study for Tile Magasi and Tile Shahri. *Scientia Horticulturae*, *130*(1), 54–59. https://doi.org/10.1016/J.SCIENTA.2011.06.003

Shahgholi, G., Latifi, M., & Jahanbakhshi, A. (2020). Potato creep analysis during storage using experimental measurement and finite element method (<scp>FEM</scp>). *Journal of Food Process Engineering*, *43*(11), e13522. https://doi.org/10.1111/jfpe.13522

Shoji, K., Schudel, S., Shrivastava, C., Onwude, D., & Defraeye, T. (2022). Optimizing the postharvest supply chain of imported fresh produce with physics-based digital twins. *Journal of Food Engineering*, *329*, 111077. https://doi.org/10.1016/J.JFOODENG.2022.111077

Sivakumar, D., & Wall, M. M. (2012). Papaya Fruit Quality Management during the Postharvest Supply Chain. *Http://Dx.Doi.Org/10.1080/87559129.2012.692138*, *29*(1), 24–48.

https://doi.org/10.1080/87559129.2012.692138

Srimartpirom, M., Rakkrai, C., Phankum, S., Intarakamhang, R., Sonsiri, C., Buchatian, P., Phanglerk, P., Jinnalite, P., Khongthawie, S., Unahawutti, U., & Follett, P. A. (2023). Vapor heat treatment for quarantine control of the oriental fruit fly (Diptera: Tephritidae) in papaya fruit from Thailand. *Journal of Asia-Pacific Entomology*, *26*(2). https://doi.org/10.1016/j.aspen.2023.102049

Stopa, R., Szyjewicz, D., Komarnicki, P., & Kuta, Ł. (2018). Determining the resistance to mechanical damage of apples under impact loads. *Postharvest Biology and Technology*, *146*, 79–89. https://doi.org/10.1016/J.POSTHARVBIO.2018.08.016

Sultan, S., Rangaraju, V., Nambi, E., & Chandrasekar, V. (2018). Mathematical modeling of physical properties of banana fruit for machine vision systems using image processing method. *Journal of Advanced Research in Dynamical and Control Systems*, *10*, 617.

Tang, X., Ren, J., Liu, C., & Xiao, D. (2011). Simulation of vibration harvesting mechanism for wolfberry. *American Society of Agricultural and Biological Engineers Annual International Meeting 2011, ASABE 2011*, *5*, 4096–4110.

Terao, D., de Lima Nechet, K., Shiraishi Frighetto, R. T., & Cerqueira Sasaki, F. F. (2019). Ozonated water combined with heat treatment to control the stem-end rot of papaya. *Scientia Horticulturae*, *257*, 108722. https://doi.org/10.1016/J.SCIENTA.2019.108722

Topuz, A., Topakci, M., Canakci, M., Akinci, I., & Ozdemir, F. (2005). Physical and nutritional properties of four orange varieties. *Journal of Food Engineering*, *66*(4), 519–523. https://doi.org/10.1016/J.JFOODENG.2004.04.024

Tridge. (n.d.). *Trends of Fresh Papaya production in Malaysia* . Retrieved March 5, 2024, from https://www.tridge.com/intelligences/papaya/MY/production.

Tsubaki, S., Ozaki, Y., Yonemori, K., & Azuma, J. I. (2012). Mechanical properties of fruit-cuticular membranes isolated from 27 cultivars of Diospyros kaki Thunb. *Food Chemistry*, *132*(4), 2135–2139. https://doi.org/10.1016/J.FOODCHEM.2011.12.039

Umulis, D. M., & Othmer, H. G. (2012). The importance of geometry in mathematical models of developing systems. *Current Opinion in Genetics & Development*, *22*(6), 547–552. https://doi.org/10.1016/J.GDE.2012.09.007

Van Zeebroeck, M., Tijskens, E., Dintwa, E., Kafashan, J., Loodts, J., De Baerdemaeker, J., & Ramon, H. (2006). The discrete element method (DEM) to simulate fruit impact damage during transport and handling: Model building and validation of DEM to predict bruise damage of apples. *Postharvest Biology and Technology*, *41*(1), 85–91. https://doi.org/10.1016/J.POSTHARVBIO.2006.02.007

Vázquez García, E., Mata Vázquez, H., Ariza Flores, R., Santamaría Basulto, F., & Alia Tejacal, I. (2013). Comportamiento mecánico de frutos de papaya bajo compresión axial* Mechanical behavior of papaya fruits under axial compression. *Revista Mexicana de Ciencias Agrícolas*, *4*, 1223–1235.

Vilaplana, R., Chicaiza, G., Vaca, C., & Valencia-Chamorro, S. (2020). Combination of hot water treatment and chitosan coating to control anthracnose in papaya (Carica papaya L.) during the postharvest period. *Crop Protection*, *128*, 105007. https://doi.org/10.1016/J.CROPRO.2019.105007

Villibor, G. P., Santos, F. L., de Queiroz, D. M., Khoury Junior, J. K., & Pinto, F. de A. de C. (2019). Dynamic behavior of coffee fruit-stem system using modeling of flexible bodies. *Computers and Electronics in Agriculture*, *166*, 105009. https://doi.org/10.1016/J.COMPAG.2019.105009

Wang, D., de Boer, G., Neville, A., & Ghanbarzadeh, A. (2022). A Review on Modelling of Viscoelastic Contact Problems. *Lubricants 2022, Vol. 10, Page 358*, *10*(12), 358. https://doi.org/10.3390/LUBRICANTS10120358

Wang, J. (2004). Mechanical Properties of Pear as a Function of Location and Orientation. *International Journal of Food Properties*, *7*(2), 155–164. https://doi.org/10.1081/JFP-120025392

Wang, W., Lu, H., Zhang, S., & Yang, Z. (2019). Damage caused by multiple impacts of litchi fruits during vibration harvesting. *Computers and Electronics in Agriculture*, *162*, 732–738. https://doi.org/10.1016/j.compag.2019.04.037

Wriggers, P., & Avci, B. (2020). Discrete Element Methods: Basics and Applications in Engineering. *CISM International Centre for Mechanical Sciences, Courses and Lectures*, *599*, 1–30. https://doi.org/10.1007/978-3-030-37518-8_1/COVER

Yousefi, S., Farsi, H., & Kheiralipour, K. (2016). Drop test of pear fruit: Experimental measurement and finite element modelling. *Biosystems Engineering*, *147*, 17–25. https://doi.org/10.1016/j.biosystemseng.2016.03.004

Zhang, S., Wang, W., Wang, Y., Fu, H., & Yang, Z. (2021). Improved prediction of litchi impact characteristics with an energy dissipation model. *Postharvest Biology and Technology*, *176*, 111508. https://doi.org/10.1016/J.POSTHARVBIO.2021.111508

Zhao, J., Ma, T., Inagaki, T., Chen, Q., Gao, Z., Sun, L., Cai, H., Chen, C., Li, C., Zhang, S., Tsuchikawa, S., & Chen, J. (2021). Finite Element Method Simulations and Experiments of Detachments of Lycium barbarum L. *Forests*, *12*(6), 699. https://doi.org/10.3390/f12060699

Zhao, J., Sugirbay, A., Chen, Y., Zhang, S., Liu, F., Bu, L., Chen, Y., Wang, Z., & Chen, J. (2019). FEM explicit dynamics simulation and NIR hyperspectral reflectance imaging for determination of impact bruises of Lycium barbarum L. *Postharvest Biology and Technology*, *155*, 102–110. https://doi.org/10.1016/J.POSTHARVBIO.2019.05.024

Zheng, Z., Chen, J., Tian, W., Zhang, C., & An, Z. (2021). Finite element analysis of blueberry stack damage. *Journal of Food Process Engineering*, *44*(11), e13840. https://doi.org/10.1111/JFPE.13840

Zhou, Y., Hu, L., Chen, Y., Liao, L., Li, R., Wang, H., Mo, Y., Lin, L., & Liu, K. (2022). The combined effect of ascorbic acid and chitosan coating on postharvest quality and cell wall metabolism of papaya fruits. *LWT*, *171*, 114134. https://doi.org/10.1016/J.LWT.2022.114134

Zienkiewicz, O., Taylor, R., & Zhu, J. Z. (2013). The Finite Element Method: its Basis and Fundamentals: Seventh Edition. *The Finite Element Method: Its Basis and Fundamentals: Seventh Edition*, 1–714. https://doi.org/10.1016/C2009-0-24909-9

Zulkifli, N., Hashim, N., Harith, H. H., & Mohamad Shukery, M. F. (2020). Finite element modelling for fruit stress analysis - A review. *Trends in Food Science and Technology*, *97*, 29–37. https://doi.org/10.1016/j.tifs.2019.12.029

Zulkifli, N., Hashim, N., Harith, H. H., Mohamad Shukery, M. F., Onwude, D. I., & Sairi, M. (2021). Finite element modelling for predicting the puncture responses in Papayas. *Foods*, *10*(2). https://doi.org/10.3390/foods10020442

APPENDICES

Appendix A

Statistical Analysis Code Snippet

```
# %% [markdown]
# # Libraries

# %%
# Import libraries needed for analysis
import matplotlib.pyplot as plt
import numpy as np
import pandas as pd
import seaborn as sns
from scipy import optimize
import scipy.stats as stats
from sklearn import linear_model
from sklearn import svm
from sklearn.metrics import r2_score, mean_squared_error
from sklearn.model_selection import train_test_split
plt.style.use('seaborn-paper')
plt.rcParams['figure.dpi'] = 600


# %%
# import data

df = pd.read_csv('dim_data.csv')
df.head()

# %%
df['a (cm)'] = df['a'] / 10
df['b (cm)'] = df['b'] / 10
df['c (cm)'] = df['c'] / 10
df.drop(['a', 'b', 'c'], axis=1, inplace=True)
# calculate mean diameter
df['Mean diameter (cm)'] = np.cbrt(df['a (cm)'] * df['b (cm)'] * df['c
(cm)'])

# calculate the density of fruit
df['Surface area (cm\u00b2)'] = np.pi * np.square(df['Mean diameter
(cm)'])
df['Sphericity'] = df['Mean diameter (cm)'] / df['a (cm)']
df['Projected area (cm\u00b2)'] = (np.pi * df['b (cm)'] * df['a
(cm)']) / 4
```

```
summary_physical = df.agg(['mean', 'std', 'max', 'min',
'count']).round(3)
display(summary_physical)

# %%
# Compute the correlation matrix
corr = df.corr()

# Generate a mask for the upper triangle
mask = np.triu(np.ones_like(corr.abs(), dtype=bool))

# Set up the matplotlib figure
f, ax = plt.subplots(figsize=(11, 9))

# Generate a custom diverging colormap

sns.heatmap(corr.abs(), annot=True, linewidths=.5, ax=ax, mask=mask)
# cmap = sns.diverging_palette(230, 20, as_cmap=True)

# # Draw the heatmap with the mask and correct aspect ratio
# sns.heatmap(corr, mask=mask, cmap=cmap, vmax=.3, center=0,
#             square=True, linewidths=.5, cbar_kws={"shrink": .5},
annot=True)

# %% [markdown]
# ## Normality test

# %%
shapiro_stat, p_value = stats.shapiro(df['Mass (g)'])
print("shapiro statistics", shapiro_stat)
print("p-value", p_value)

parameters = list(df.columns)
norm_df = {'Parameters': [], 'shapiro statistics': [], 'p-value': []}
for i in parameters:
    shapiro_stat, p_value = stats.shapiro(df[i])
    norm_df['Parameters'].append(i)
    norm_df['shapiro statistics'].append(shapiro_stat)
    norm_df['p-value'].append(p_value)
    print(f"shapiro stat {i}", shapiro_stat)
    print(f"p-value {i}", p_value)


# %%
norm_df = pd.DataFrame(norm_df)
norm_df.to_excel('normality.xlsx')
norm_df
```

```
# %% [markdown]
# ## Modeling
# The model will be is used is deined based on the following equation
# ![model](models.png)
#
#

# %%
# separating features and labels
X, y = df.iloc[:, 1:].values, df.iloc[:, 0].values
# Split data 70-30% into training and test set
X_train, X_test, y_train, y_test = train_test_split(X, y,
test_size=0.30, random_state=0)

print('The number of features(variables):
{}'.format(X_train.shape[1]))
print('Training set: %d rows\nTest set: %d rows' % (X_train.shape[0],
X_test.shape[0]))

# %% [markdown]
# ### Model Defination

# %%
def linear_model1(x, a, b):
    M = b * x + a
    return M

def quadratic_model(x, a, b, c):
    M = (c * x**2) + (b *x) + a
    return M

def scurve_model(x, a, b):
    M = (b/x) + a
    return M

def power_model(x, a, b):
    M = a * x**b
    return M


# %%
var = df.columns
dependant_var = var[0]
independant_var = var[1:]

print(f'independant variable are {independant_var}')
print(f'Dependant variable is {dependant_var}')
```

```
# %% [markdown]
# ## Single variable modelling

# %% [markdown]
# #### Linear Model

# %%
md = {'linear': [], 'quadratic':[], 'scurve':[], 'power':[]}

# %%
# Linear Model
model_params = {'a':[],'b': [], 'r-square':[], 'rmse':[]}

for i in range(7):
    fig = plt.figure(figsize=(6, 4))
    ax= fig.gca()
    l_popt, l_pcov = optimize.curve_fit(linear_model1, X_train[:,i],
y_train, method='dogbox')
    # print(f'The value of the model constant a ={l_popt[0]} and
b={l_popt[1]} for variable {independant_var[i]}')
    model_params['a'].append(l_popt[0])
    model_params['b'].append(l_popt[1])

    lin_model = linear_model1(X_test[:, i], *l_popt)

    #Plot predicted vs actual
    plt.scatter(y_test, lin_model, c='r')
    # Overlay the regression line
    z = np.polyfit(y_test, lin_model, 1)
    p = np.poly1d(z)
    plt.plot(y_test, p(y_test), '-b')
    # Anotate plot
    plt.xlabel(f'Actual Values')
    plt.ylabel('Predicted Values')
    plt.title(f'{independant_var[i]}')
    # Add model to dictionary md
    md['linear'].append([lin_model])



    # R-squared calculation
    r_square_lin = r2_score(y_test, lin_model)
    # print(f'R_square = {r_square_lin}')
    model_params['r-square'].append(r_square_lin)

    # # Chi-square calculation
    # chi_square_lin = stats.chisquare(df[dependant_var], lin_model)
    # model_params['chi_square'].append(np.round(chi_square_lin[0]))
```

```
    # RMSE calculation
    rmse_lin = np.sqrt(mean_squared_error( y_test, lin_model))
    # print(f'RMSE = {rmse_lin}')
    model_params['rmse'].append(rmse_lin)

# print(model_params)
model_params_df = pd.DataFrame(model_params, index=independant_var)
model_params_df = np.round(model_params_df, 4)
display(model_params_df)
model_params_df.to_csv('linear_model_params.csv')



# %% [markdown]
# #### Quadratic Model

# %%
# Quadratic Model

quad_model_params = {'a': [], 'b': [], 'c': [], 'r-square':[],
'rmse':[]}
for i in range(7):
    fig = plt.figure(figsize=(6, 4))
    ax= fig.gca()
    quad_popt, quad_pcov = optimize.curve_fit(quadratic_model,
X_train[:,i], y_train, method='dogbox')
    # print(f'The value of the model constant a ={quad_popt[0]} and
b={quad_popt[1]} for variable {independant_var[i]}')
    quad_model_params['a'].append(quad_popt[0])
    quad_model_params['b'].append(quad_popt[1])
    quad_model_params['c'].append(quad_popt[2])


    quad_model = quadratic_model(X_test[:, i], *quad_popt)

    #Plot predicted vs actual
    plt.scatter(y_test, quad_model, c='r')
    # Overlay the regression line
    z = np.polyfit(y_test, quad_model, 1)
    p = np.poly1d(z)
    plt.plot(y_test, p(y_test), '-b')
    # Anotate plot
    plt.xlabel('Actual Values')
    plt.ylabel('Predicted Values')
    plt.title(f'{independant_var[i]} ')
    # R-squared calculation
    r_square_quad = r2_score(y_test, quad_model)
    # print(f'R_square = {r_square_quad}')
```

```
    quad_model_params['r-square'].append(r_square_quad)

     # Add model to dictionary md
    md['quadratic'].append([quad_model])

    # # Chi-square calculation
    # chi_square_quad = stats.chisquare(df[dependant_var], quad_model)
    # model_params['chi_square'].append(np.round(chi_square_quad[0]))

    # RMSE calculation
    rmse_quad = np.sqrt(mean_squared_error(y_test, quad_model))
    # print(f'RMSE = {rmse_quad}')
    quad_model_params['rmse'].append(rmse_quad)



# print(model_params)
quad_model_params_df = pd.DataFrame(quad_model_params,
index=independant_var)
quad_model_params_df = np.round(quad_model_params_df, 4)
display(quad_model_params_df)
quad_model_params_df.to_csv('quad_model_params.csv')



# %% [markdown]
# #### S-curve Model

# %%
# S-curve Model
scurve_model_params = {'a': [], 'b': [], 'r-square':[],  'rmse':[]}
for i in range(7):
    fig = plt.figure(figsize=(6, 4))
    ax= fig.gca()
    scurve_popt, scurve_pcov = optimize.curve_fit(scurve_model,
X_train[:, i], y_train, method='dogbox')
    # print(f'The value of the model constant a ={scurve_popt[0]} and
b={scurve_popt[1]} for variable {independant_var[i]}')
    scurve_model_params['a'].append(scurve_popt[0])
    scurve_model_params['b'].append(scurve_popt[1])


    model_scurve = scurve_model(X_test[:, i], *scurve_popt)
    #Plot predicted vs actual
    plt.plot(y_test, model_scurve, 'or')
    # Overlay the regression line
    z = np.polyfit(y_test, model_scurve, 1)
```

```
    p = np.poly1d(z)
    plt.plot(y_test, p(y_test), '-b')
    # Anotate plot
    plt.xlabel('Actual Values')
    plt.ylabel('Predicted Values')
    plt.title(f'{independant_var[i]} ')
    plt.xticks = 25
    plt.yticks = 25
    # R-squared calculation
    r_square_scurve = r2_score(y_test, model_scurve)
    # print(f'R_square = {r_square_scurve}')
    scurve_model_params['r-square'].append(r_square_scurve)

    # # Chi-square calculation
    # chi_square_scurve = stats.chisquare(df[dependant_var],
model_scurve)
    #
scurve_model_params['chi_square'].append(np.round(chi_square_scurve[0]
))


    # RMSE calculation
    rmse_scurve = np.sqrt(mean_squared_error(y_test, model_scurve))
    # print(f'RMSE = {rmse_scurve}')
    scurve_model_params['rmse'].append(rmse_scurve)

      # Add model to dictionary md
    md['scurve'].append(model_scurve)

# print(model_params)
scurve_model_params_df = pd.DataFrame(scurve_model_params,
index=independant_var)
scurve_model_params_df = np.round(scurve_model_params_df, 4)
display(scurve_model_params_df)
scurve_model_params_df.to_csv('scurve_model_params.csv')

# %% [markdown]
# #### Power Model

# %%
# Power Model
power_model_params = {'a': [], 'c': [], 'r-square':[],  'rmse':[]}
for i in range(len(independant_var)):
    fig = plt.figure(figsize=(6, 4))
    ax= fig.gca()
    power_popt, power_pcov = optimize.curve_fit(power_model,
X_train[:, i], y_train, method='dogbox')
```

```
    # print(f'The value of the model constant a ={power_popt[0]} and
b={power_popt[1]} for variable {independant_var[i]}')
    power_model_params['a'].append(power_popt[0])
    power_model_params['c'].append(power_popt[1])
    # power_model_params['c'].append(power_popt[2])

    model_power = power_model(X_test[:, i], *power_popt)
    #Plot predicted vs actual
    plt.scatter(y_test, model_power, c='r')
    # Overlay the regression line
    z = np.polyfit(y_test, model_power, 1)
    p = np.poly1d(z)
    plt.plot(y_test, p(y_test), '-b')
    # Anotate plot
    plt.xlabel('Actual Values')
    plt.ylabel('Predicted Values')
    plt.title(f'{independant_var[i]} ')
    # R-squared calculation
    r_square_power = r2_score(y_test, model_power)
    # print(f'R_square = {r_square_power}')
    power_model_params['r-square'].append(r_square_power)

    # Chi-square calculation
    # chi_square_power = stats.chisquare(df[dependant_var],
model_power)
    #
power_model_params['chi_square'].append(np.round(chi_square_power[0]))

    # RMSE calculation
    rmse_power = np.sqrt(mean_squared_error(y_test, model_power))
    # print(f'RMSE = {rmse_power}')
    power_model_params['rmse'].append(rmse_power)
      # Add model to dictionary md
    md['power'].append(model_power)

# print('/n')
# print(power_model_params)

power_model_params_df = pd.DataFrame(power_model_params,
index=independant_var)
power_model_params_df = np.round(power_model_params_df, 4)
display(power_model_params_df)
power_model_params_df.to_csv('power_model_params.csv')


# %% [markdown]
# #### Lasso
#
```

```
# %%
# Lasso Regression Model
reg_lasso = linear_model.Lasso(alpha=0.9)
lasso_model_params = {'r-square':[],  'rmse':[]}
for i in range(len(independant_var)):
  reg_lasso.fit(X_train[:, i].reshape(-1, 1), y_train)

  # predict
  lasso_prediction = reg_lasso.predict(X_test[:, i].reshape(-1, 1))
  # Plot predicted vs actual
  fig = plt.figure(figsize=(6, 4))
  ax= fig.gca()
  plt.scatter(y_test, lasso_prediction, c='r')
    # Overlay the regression line
  z = np.polyfit(y_test, lasso_prediction, 1)
  p = np.poly1d(z)
  plt.plot(y_test, p(y_test), '-b')
    # Anotate plot
  plt.xlabel('Actual Values')
  plt.ylabel('Predicted Values')
  plt.title(f'{independant_var[i]} ')
    # R-squared calculation
  r_square_lasso = r2_score(y_test, lasso_prediction)
  print(f'R_square = {r_square_lasso}')
    # RMSE calculation
  rmse_lasso = np.sqrt(mean_squared_error(y_test, lasso_prediction))
  print(f'RMSE = {rmse_lasso}')
  lasso_model_params['r-square'].append(r_square_lasso)
  lasso_model_params['rmse'].append(rmse_lasso)

lasso_model_params_df = pd.DataFrame(lasso_model_params,
index=independant_var)
lasso_model_params_df = np.round(lasso_model_params_df, 2)
display(lasso_model_params_df)
lasso_model_params_df.to_csv('lasso_model_params.csv')

# print('/n')
# print(power_model_params)

# %% [markdown]
# #### SVR

# %%
# SV Regression Model
reg_svm = svm.SVR(kernel='linear')
svm_model_params = {'r-square':[],  'rmse':[]}
for i in range(len(independant_var)):
  reg_svm.fit(X_train[:, i].reshape(-1, 1), y_train)
```

```
  # predict
  svm_prediction = reg_svm.predict(X_test[:, i].reshape(-1, 1))
  # Plot predicted vs actual
  fig = plt.figure(figsize=(6, 4))
  ax= fig.gca()
  plt.scatter(y_test, svm_prediction, c='r')
    # Overlay the regression line
  z = np.polyfit(y_test, svm_prediction, 1)
  p = np.poly1d(z)
  plt.plot(y_test, p(y_test), '-b')
    # Anotate plot
  plt.xlabel('Actual Values')
  plt.ylabel('Predicted Values')
  plt.title(f'{independant_var[i]} ')
    # R-squared calculation
  r_square_svm = r2_score(y_test, svm_prediction)
  print(f'R_square = {r_square_svm}')
    # RMSE calculation
  rmse_svm = np.sqrt(mean_squared_error(y_test, svm_prediction))
  print(f'RMSE = {rmse_svm}')
  svm_model_params['r-square'].append(r_square_svm)
  svm_model_params['rmse'].append(rmse_svm)

svm_model_params_df = pd.DataFrame(svm_model_params,
index=independant_var)
svm_model_params_df = np.round(svm_model_params_df, 2)
display(svm_model_params_df)
svm_model_params_df.to_csv('svm_model_params.csv')

# print('/n')
# print(power_model_params)

# %% [markdown]
# ## Multiple variable

# %% [markdown]
# #### Linear Model

# %%
# fit model
reg = linear_model.LinearRegression()
reg.fit(X_train, y_train)
print('coefficients of the multiple regression {} and intercept:
{}'.format(reg.coef_, reg.intercept_))
reg_model = pd.DataFrame({'coefficeint': reg.coef_, 'intercept':
reg.intercept_})
reg_model.to_csv('reg_model.csv')
reg_model
```

```
# %%
# use the model to predict
reg_prediction = reg.predict(X_test)
reg_r2 = r2_score(y_test, reg_prediction)
reg_rmse =  np.sqrt(mean_squared_error(y_test, reg_prediction))
print('The R\u00b2 value: {}'.format(reg_r2))
print('The root mean squared error: {}'.format(reg_rmse))


# %% [markdown]
# #### Lasso

# %%
reg_lasso = linear_model.Lasso(alpha = 0.9)
reg_lasso.fit(X_train, y_train)

# predict
lasso_prediction = reg_lasso.predict(X_test)
lasso_r2 = r2_score(y_test, lasso_prediction)
lasso_rmse = np.sqrt(mean_squared_error(y_test, lasso_prediction))
print('The R\u00b2 value: {}'.format(lasso_r2))
print('The root mean squared error: {}'.format(lasso_rmse))


# %% [markdown]
# #### Support vector regression

# %%
reg_svm = svm.SVR(kernel='linear')
reg_svm.fit(X_train, y_train)

#prediction
svm_prediction = reg_svm.predict(X_test)
svm_r2 = r2_score(y_test, svm_prediction)
svm_rmse = np.sqrt(mean_squared_error(y_test, svm_prediction))
print('The R\u00b2 value: {}'.format(svm_r2))
print('The root mean squared error: {}'.format(svm_rmse))
```

Appendix B

Stack Damage Calculation

To determine how many papaya fruits will cause damage with a given yield stress, we can calculate the maximum force that the average papaya can withstand before experiencing damage and then divide it by the average weight of the papaya.

1. Convert the yield stress to Pascals (Pa):
   Yield stress = 0.0616 MPa = 61,600 Pa (refer to Table 12; Section 4.3.2.1).

2. Calculate the maximum force a papaya can withstand before damage using the yield stress and the cross-sectional area of the papaya. We will assume a simple cylindrical shape for the papaya for this calculation.

$$Cross - sectional\ area\ (A) = \pi * (radius)^2$$
$$Papaya\ diameter\ (approximate) = 100\ mm$$
$$= 0.1\ meters\ (assuming\ an\ average\ size)$$
$$Papaya\ radius\ (r) = 0.1\ meters\ /\ 2 = 0.05\ meters$$
$$A = \pi * (0.05\ meters)^2 = \pi * 0.0025\ square\ meters \approx 0.00785\ square\ meters$$
$$Maximum\ force\ (F) = Yield\ stress\ (\sigma) * Cross - sectional\ area\ (A)$$
$$F = 61{,}600\ Pa * 0.00785\ square\ meters \approx 483.64\ N$$

3. Now, we can calculate how many papaya fruits can be stacked vertically such that the total force applied to the bottom fruit does not exceed the maximum force (F).

$$Average\ mass\ of\ a\ papaya = 1298.68\ g = 1.29868\ kg$$
$$Gravity\ (g) = 9.81\ m/s^2\ (acceleration\ due\ to\ gravity)$$
$$Force\ due\ to\ the\ weight\ of\ one\ papaya\ (W) = Mass\ (m) * Gravity\ (g)$$
$$W = 1.29868\ kg * 9.81\ m/s^2 \approx 12.77\ N$$
$$Number\ of\ papayas\ that\ can\ be\ stacked\ (N) = \frac{F\ (maximum\ force)}{W\ (force\ due\ to\ one\ papaya)}$$
$$N \approx 483.64\ N\ /\ 12.77\ N \approx 37.91$$

So, approximately 37 papaya fruits can be stacked vertically before the force applied to the bottom fruit exceeds the maximum force it can withstand without damage (given the yield stress of 0.0616 MPa). Beyond this height, the bottom fruit may experience damage.

Appendix C

Geometry Modelling Methods Data

The result of the scanned model and outlined model were compared using t-test as discussed in section 4.3.2.1

Strain	Scanned model stress results	Outlined model stress results
3%	0.027937	0.029308
7%	0.038961	0.040092
10%	0.048149	0.049082
13%	0.057775	0.058499
15%	0.066445	0.06698
18%	0.07568	0.076016
21%	0.084296	0.084445
24%	0.093576	0.093523
27%	0.101988	0.101753
29%	0.109291	0.108898
31%	0.117316	0.116749
33%	0.12372	0.123014
35%	0.129358	0.128529
38%	0.139686	0.138634
41%	0.149265	0.148005
45%	0.159505	0.158023
49%	0.171708	0.169962
54%	0.190456	0.188303
58%	0.202138	0.199732

LIST OF PUBLICATIONS

Aina, A. M., Harith, H., Hashim, N., & Shukery, M. F. M. (2024). The influence of papaya shape on its mass model and mechanical properties. Journal of Food Process Engineering, 47(5), e14627. https://doi.org/10.1111/jfpe.1462

Aina, A. M., Hazreen Harith, Norhashila Hashim, Mohamad Firdza Mohamad Shukery (2023, August). Modelling of Mass and Mechanical Properties of Papaya for Optimal Handling in Supply Chain Operation [Poster presentation]. 6th International Conference on Agricultural and Food Engineering (CAFEi2023, Selangor.).